TAL TECH

DOCTORAL THESIS

Abrasive Wear Resistant Composite Hardfacings with *Ex-situ* and *In-situ* Synthesized Carbide Reinforcement

Dmytro Tkachivskyi

TALLINN UNIVERSITY OF TECHNOLOGY
DOCTORAL THESIS
41/2021

Abrasive Wear Resistant Composite Hardfacings with *Ex-situ* and *In-situ* Synthesized Carbide Reinforcement

DMYTRO TKACHIVSKYI

**TAL
TECH**
PRESS

TALLINN UNIVERSITY OF TECHNOLOGY
School of Engineering
Department of Mechanical and Industrial Engineering
This dissertation was accepted for the defence of the degree 08/06/2021

Supervisor: Prof. Em. Priit Kulu
                         School of Engineering
                         Tallinn University of Technology
                         Tallinn, Estonia

Co-supervisor: *PhD* Andrei Surženkov
                         School of Engineering
                         Tallinn University of Technology
                         Tallinn, Estonia

Opponents: *PhD* Arkadi Zikin
                         Laser Centre of Competence
                         Oerlikon Metco AG
                         Pfäffikon SZ, Switzerland

                         PhD Alexander Ryabchikov
                         Institute of Forestry and Rural Engineering
                         Estonian University of Life Sciences
                         Tartu, Estonia

Defence of the thesis: 24/08/2021, Tallinn

Declaration:
Hereby I declare that this doctoral thesis, my original investigation and achievement, submitted for the doctoral degree at Tallinn University of Technology has not been submitted for doctoral or equivalent academic degree.

Dmytro Tkachivskyi

                                  _____
                                                         signature

Abrasiivkulumiskindlad komposiitpinded *ex-situ* ja *in-situ* sünteesitud karbiidkõvafaasiga

DMYTRO TKACHIVSKYI

Contents

List of Publications

The list of author's peer-reviewed publications, referred to in the text as Papers I-IV, on the basis of which the thesis has been prepared:

I **D. Tkachivskyi**, K. Juhani, A. Surženkov, P. Kulu, M. Viljus, R. Traksmaa, V. Jankauskas, R. Leišys, Production of Thermal Spray Cr_3C_2-Ni Powders by Mechanically Activated Synthesis, *Key Engineering Materials*, 2019, **799**, 31-36; doi: 10.4028/www.scientific.net/KEM.799.31

II R. Bendikiene, A. Ciuplys, S. M. Jankus, A. Surzhenkov, **D. Tkachivskyi**, K. Juhani, M. Viljus, R. Traksmaa, M. Antonov, P. Kulu, Study of submerged and plasma arc welded composite hardfacings with a novel Cr_3C_2–Ni reinforcement, *Proceedings of the Estonian Academy of Sciences*, 2019, **68**, 150-157; doi: 10.3176/proc.2019.2.06

III **D. Tkachivskyi**, K. Juhani, A. Surženkov, P. Kulu, T. Tesař, R. Mušálek, F. Lukáč, J. Antoš, M. Vostřák, M. Antonov, D. Goljandin, HVOF Sprayed Fe-Based Wear-Resistant Coatings with Carbide Reinforcement, Synthesized In Situ and by Mechanically Activated Synthesis, *Coatings*, 2020, **10**, 1092; doi: 10.3390/coatings10111092

IV **D. Tkachivskyi**, M. Viljus, R. Traksmaa, M. Antonov, A. Surzhenkov, K. Juhani, P. Kulu, Comparative Study of Plasma Cladded Fe-Based Composite Hardfacings with In Situ Synthesized Cr and Ti Carbide Reinforcement, *Solid State Phenomena*, 2021, **320**, 83-89; doi: 10.4028/www.scientific.net/SSP.320.83

Author's Contribution to the Publications

Contribution to the papers in this thesis is:

I   Preparation of Cr_3C_2-Ni powder for HVOFS *via* mechanically activated synthesis, its characterization and analysis of sprayed coating properties, performing the ARWW test, writing of paper

II Cr_3C_2-Ni powder manufacturing for PTAW hardfacing preparation of specimens (preparation of microsections), microstructure analysis, ARWW test

III Preparation of TiC-NiMo powder for HVOFS *via* mechanically activated synthesis, preparation of specimens (preparation of microsections), microstructure analysis, Vickers hardness measurements, ARWW and AEW tests, writing of paper

IV   Preparation of Ti, TiO_2 and Cr-containing powder mixtures for subsequent PTAW *in-situ* synthesis of hard phase, performance of experimental part – preparation of specimens (preparation of microsections), microstructure analysis, Vickers hardness measurements, writing of paper

Introduction

Half of all cases of faulty machine behavior are attributed to the mechanical wear of machine parts (Noria Corporation, 2018). It has been found that abrasion is the most common cause (~50%) of mechanical wear (Eyre, 1976). Loss of material due to wear has proved to be one of the biggest problems in areas such as the automotive industry (internal combustion engines, exhaust valves), oil extraction (piston rods), aviation (jet engine components), civil engineering (concrete transporting conveyors, hydraulic turbines), recycling (hydroelectric valves, dust collectors), marine engineering (propeller blades) (Davis, 2001). In order to lessen wear effects, the surface of newly-manufactured parts is strengthened by different surface treatment methods, one of which is hardfacing. Similarly, the restoring of already damaged parts by hardfacing of specially designed composition onto their surface is often a cheaper alternative to the complete replacement.

From a variety of hardfacing techniques, the focus of this work was on the following two: high velocity oxy fuel spraying (HVOFS) (Chávez, et al., 2018) and plasma transferred arc welding (PTAW) (García-Vázquez, et al., 2014). These methods are used both for restoration and for manufacturing wear resistant hardfacings that prevent damage of surface. HVOFS utilizes hot gaseous combustion products for applying powders onto the substrate, while PTAW uses electric current for melting powder particles to form hardfacing deposits. These two intrinsically different technologies were paired in the scope of this research because they offer an opportunity to produce a wide range of wear resistant hardfacings from different feedstock powders.

One of the advantages of HVOFS is in producing extremely dense hardfacings with low porosity. In terms of feedstock materials, HVOFS requires rather fine powders whose grain size is ranging from 20–90 μm. Produced hardfacings usually are 150–400 μm thick. The drawback of this approach is the cohesion between inter-splat interfaces in the deposits and between the hardfacing and the substrate. On the other hand, the material selection for PTAW is very wide. Indeed, according to (Bach, et al., 2004) high carbide containing powdery consumables can be deposited only by means of plasma technology. It is capable of working with coarser powders ranging from 150–300 μm of grain size and provides hardfacings with thickness up to 5 mm. However, using PTAW is often coupled with tremendous amount of heat passed onto the substrate, which may cause its deformation and structural changes.

Considering the choice of composite powders for use with the aforementioned methods, the ceramic-metal composite (CMC) powders (cermets) seem to be the most feasible option. They form hardfacings with soft metal matrix, which provides overall ductility and is capable of withstanding an impact wear while hard carbide reinforcement makes the hardfacing resistant to abrasive wear (Wang, et al., 2019) (Bendikiene, et al., 2020). Due to the superb qualities of tungsten carbide (WC), it is thought to be the best raw material for developing wear resistant hardfacings. However, its constantly increasing price stimulates the search for cheaper alternatives, for example titanium carbide (TiC) and chromium carbide (Cr_3C_2). TiC- and Cr_3C_2-based cermets with cobalt (Co), nickel (Ni), nickel-molybdenum (NiMo) matrix coupled with NiCrSiB self-fluxing alloys are commonly used in this domain as quality replacement of expensive WC-based composites (Surzhenkov, et al., 2015).

The cost of feedstock material has a significant impact on the price of a sprayed hardfacing. Sarjas et al. (2014) showed that in the case of HVOFS, the cost of the sprayed

powder makes up 75% of the final cost of a hardfacing. Therefore, it is necessary to utilize cost-saving feedstock matrix materials (Fe-based instead of Ni-based), develop shorter technological routes and compare their effectiveness to existing approaches.

In this work, the technological route chosen for the preparation of conventional TiC-NiMo and Cr_3C_2-Ni cermet powders was mechanically activated synthesis (MAS) (Juhani, 2009). Though rather long, it is an effective way to manufacture feedstock materials for the HVOFS or PTAW process. At the same time, the *in-situ* synthesis of carbides in the deposition process is hypothesized to become a shorter and cheaper alternative to MAS. Unlike the former, it utilizes synthesis of the ceramic phase from elemental powders during the hardfacing process. Stainless steel (AISI 316L) was used as the matrix forming constituent in most of the experiments to evaluate its influence on the quality of final hardfacings.

Hypothesis of the study:

- *In-situ* synthesis of carbide reinforcement provides a metallic-ceramic composite hardfacing with an abrasive wear resistance, which is comparative to one of the MMC hardfacing with the analogous reinforcement added *ex-situ*.
- Introduction of a ductile Fe-based alloy as a matrix-forming material for metallic-ceramic composites can increase their wear resistance to the same level or even outperform Ni-based analogs with the same amount of reinforcing phase.

The main objectives of the study were as follows: utilizing HVOFS and PTAW deposition technologies, to manufacture wear resistant Fe-based metal matrix composite (MMC) harfacings with MAS (*ex-situ* added) and *in-situ* synthesized reinforcement and to compare their wear resistant properties. Special focus was placed on developing experimental hardfacings with *in-situ* synthesized reinforcement to be wear resistant under the abrasion and/or abrasion-erosion (impact angles 30° and 90°) wear conditions.

The novelty of the presented work lies in three aspects: 1) technological – optimization of the manufacturing process of TiC-NiMo and Cr_3C_2-Ni cermet powders by excluding the disintegrator milling stage; 2) scientific – development of cermet hardfacings with *in-situ* synthesized carbide reinforcement and comparison to analogous hardfacings with *ex-situ* added reinforcement; 3) practical – comparison of the wear resistance of hardfacings developed by the HVOFS and PTAW deposition techniques.

The materials of the doctoral thesis research were presented at the conferences (Modern Materials and Manufacturing 2019 (joint event of the 12th International DAAAM Baltic Conference and 27th International Baltic Conference BALTMATTRIB 2019), the 28th International Baltic Conference Materials Engineering and Modern Manufacturing) and published in the international journals (Proceedings of the Estonian Academy of Sciences; Journal of Materials Research and Technology; Coatings) and conference proceedings (Key Engineering Materials and Solid State Phenomena).

Abbreviations

AEW	Abrasive Erosion Wear
ARWW	Abrasive Rubber Wheel Wear
ASTM	American Society for Testing and Materials
CMC	Ceramic-Metal Composite
EDS	Energy-Dispersive (X-Ray) Spectroscopy
HVOFS	High Velocity Oxy-Fuel Spraying
KTU	Kaunas University of Technology
MAS	Mechanically Activated Synthesis
MMC	Metal Matrix Composite
PM	Powder Metallurgy
PTAW	Plasma Transferred Arc Welding
SAW	Submerged Arc Welding
SEM	Scanning Electron Microscopy
SS	Stainless Steel
TalTech	Tallinn University of Technology
XRD	X-Ray Diffraction

1 Review of literature

1.1 Metal matrix composites

Metal matrix composites are a class of compound materials consisting of metal alloys with embedded particulate (AlMangour, et al., 2018), whisker (nano-scale) (Qu, et al., 2018) or fiber (micro-scale) (Ozerov, et al., 2017) reinforcement. The common matrix material is either aluminum (Al), copper (Cu), magnesium (Mg), titanium (Ti), cobalt (Co) or cobalt-nickel (Co-Ni); the reinforcement is either another metal or ceramic material, such as tungsten carbide (WC), alumina (Al_2O_3), silicon carbide (SiC), zirconia (ZrO_2), titanium nitride (TiN), titanium carbide (TiC), cubic boron nitride (CBN) etc. Certain composites (e.g., Al-based) are lightweight and the initial demand for them was formed by spacecraft, aviation and automotive industries (Kumar Koli, et al., 2015). Figure 1.1 depicts some of the possible applications for MMCs.

(a)   (b)
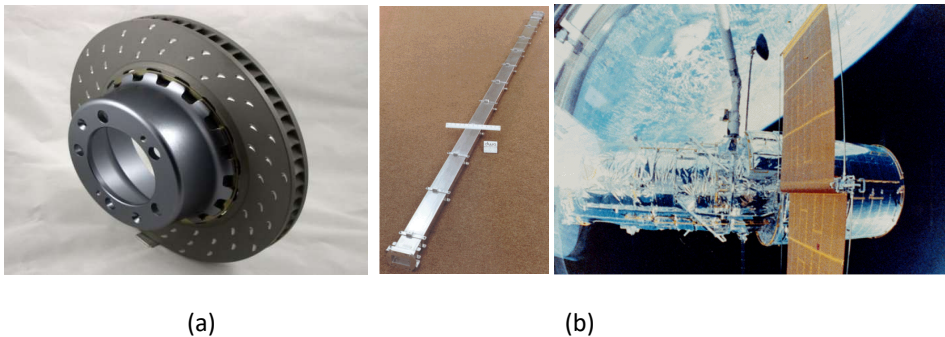
Figure 1.1 Examples of MMC applications: (a) in the production of breaking discs in the automotive sector (All Answers Ltd., 2017); (b) in the aerospace industry, manufacturing high-gain antenna for the Hubble Space Telescope (left – before integration, right – after deployment on the telescope) (Rawal, 2001).

In addition, MMCs are beneficial in tribology as wear resistant materials (Mohapatra, et al., 2020, Dev Srivyas & Charoo, 2018, Narayanasamy, et al., 2018). Metal matrix composites reinforced by ceramic particles are deservedly appreciated due to their enhanced mechanical properties. It has been shown by several researchers (Liang, et al., 2018, Kim, et al., 2017) that addition of different amounts of ceramic particles (30–90%) facilitates an increase in overall hardness of a material to 795–1813 HV30 range.

In order to produce a bulk MMC specifically tailored to withstand mechanical wear, the methods of powder metallurgy (PM) are often employed, using the "solid state manufacturing" approach (Fig. 1.2): feedstock powders are mixed or mechanically alloyed in an attritor during some period of time (usually 4–72 h), after which they are compacted and/or sintered in the vacuum under different temperatures (600–1450 °C) to form bulk agglomerates or powders (Juhani, 2009). The bulk agglomerates are usually produced as ready-to-use parts or their constituents *via* PM methods. Likewise, the MMC powders for thermal spray are often manufactured utilizing the PM technologies, supplemented by, e.g., mechanical milling of agglomerates. However, unlike the latter, they must be subsequently applied to the wearing-out surface by means of surface treatment (hardfacing) techniques.
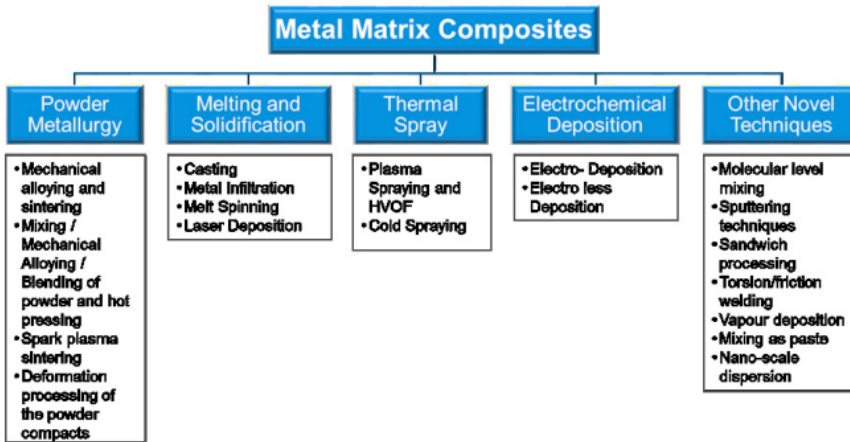
Figure 1.2 Metal matrix composite powder and bulk manufacturing methods (Behera, et al., 2019).

The MMC material for tribological applications is usually manufactured out of the following metals: iron (Fe), cobalt (Co), copper (Cu), aluminum (Al), nickel (Ni), nickel-chromium (NiCr), molybdenum (Mo), and nickel-molybdenum (NiMo) (Karaoglanli, et al., 2017, Vashishtha, et al., 2017, Rao, et al., 2016, Yung, et al., 2017). The most common reinforcements used in such systems are alumina (Al_2O_3), silica-based (SiC), tungsten-based (WC; WB), chromium-based (Cr_3C_2) or titanium-based (TiC, TiN, TiB) ceramic compounds. Together they form another class of materials called ceramic-metallic composites.

1.1.1 Ceramic-metallic composites (cermets)

Ceramic-metallic composites or cermets possess superior properties compared to either of their constituents. They are designed to be resistant to mechanical wear due to the presence of hard ceramic particles and to have simultaneous plastic properties granted by the presence of the metallic phase. As can be seen from Fig. 1.3, cermets are rather well-balanced with regard to hardness and toughness. The field of cermets ranges from almost pure metal to almost 100% ceramic.
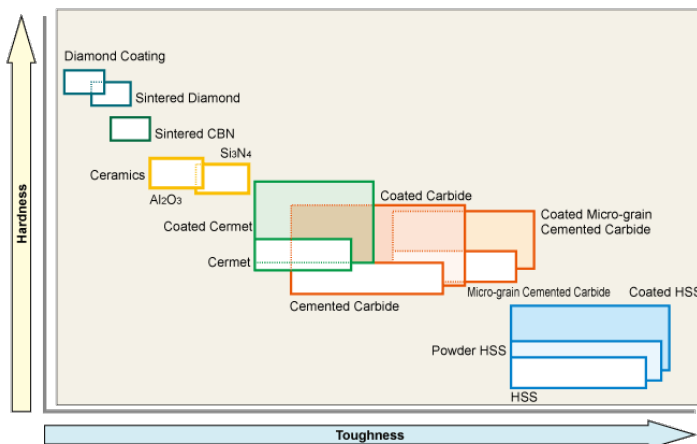
Figure 1.3 Properties of cermets in comparison with different material subsets (Mitsubishi Materials, 2020).

Therefore, for a more precise subdivision, a distinction is made between infracermets and ultracermets. They are called infracermets (metallic phase 85 vol.%) if ceramic inclusions enhance the properties of the metallic phase; they are called ultracermets (ceramic phase 85 vol.%) if a metal is an auxiliary phase (Franke, 2019).

Metals that do not form carbides or have limited carbon dissolution (Ni, NiMo, Co, Fe) are utilized for the production of carbide-based cermets (Young, 2016, Engelberg, 2010). Figure 1.4 shows a typical structure of vacuum sintered TiC-NiMo cermet compact.
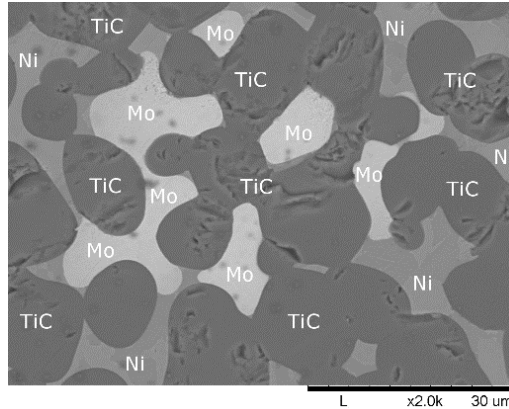
Figure 1.4 The microgrpah of the internal structure of TiC-NiMo compact sintered in vacuum.

Choice of the feedstock components for cermet production is dictated by the principles of their chemical, physical and technological compatibility (Fayyaz, Muhamad, & Sulong, 2018, Lombardi, et al., 1997):

- there is no chemical interaction between ceramic and metal components;
- there is no mutual dissolution when materials are heated and they match each other in terms of necessary physical properties (coefficient of thermal expansion, modulus of elasticity, etc.);
- there is no big difference in sintering temperatures of ceramic and metal components, their density and wettability.

1.1.2 *Ex-situ* and *in-situ* synthesis of cermet reinforcement

The methods for synthesizing composite materials are broadly divided into the use of *in-situ* and *ex-situ* processes. In an *in-situ* process, the reinforcing phase of the material is formed within the matrix phase during the synthesis. Conversely, in an *ex-situ* process, the reinforcing phase is produced by a separate process and subsequently added to the matrix phase during the synthesis of the composite material (Aikin Jr, 1997).

Particularly, the *in-situ* synthesis of cermets has an advantage over the *ex-situ* synthesis by excluding probable oxidation and/or contamination originated from the pre-synthesized (*ex-situ*) phase, therefore, increasing the quality of the matrix-reinforcement interface. The *in-situ* approach does not require the complexity of *ex-situ* method per se. Instead, the synthesis takes place during manufacturing of a cermet (Fig. 1.5b). Potentially, it is a cheap and fast way to obtain wear-resistant composites.
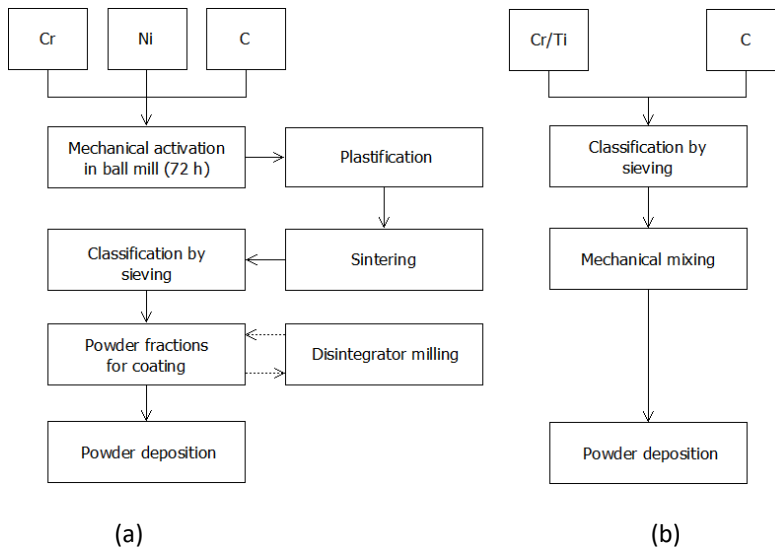
Figure 1.5 Technological routes of cermet production: (a) ex-situ (Sarjas, 2016); (b) in-situ.

Many researchers have successfully achieved the *in-situ* synthesis of the hard ceramic phase, using various deposition techniques: induction cladding (Yu, et al., 2017), laser melting (Khalili, et al., 2016), welding (Wang, et al., 2007, Emamianet et al., 2012, Gallo, et al., 2013), and thermal spray (Liu & Huang, 2005, Sun, et al., 2019) techniques. The result of these studies was deposits with hardness ranging 600–2800 HV30 and possessing remarkable wear resistance (about 3–6 times higher than reference steel, etc.). Furthermore, it has been reported that the wear rate of the *in-situ* synthesized composite was 35% less than the wear rate from an analogous material produced by the *ex-situ* method (Zhang, et al., 2017).

Producing Cr_3C_2-Ni cermet powder and coatings thereof using an *ex-situ* technological route, which includes mechanical activation of feedstock powders in a ball mill with subsequent reactive sintering and deposition, was reported by (Sarjas, et al., 2016). This process is known as the mechanically activated synthesis (MAS). Mechanical activation in the first stage allows further usage of lower sintering temperatures. The hardness of the resulted material after deposition was ~715 HV1. The abrasive wear resistance was generally the same as that of the reference, except for the abrasive-erosive wear under 90° impact angle. The presence of only 20% of ductile metallic phase in the studied composition resulted in 3.4 times more material loss compared to steel C45. It is evident that for manufacturing of cermet-based materials resistant to the impact wear, the amount of metallic matrix must be substantially increased.

Cermets as a whole are also used as a reinforcing phase for fabricating more complex systems, so-called dual-reinforced composites. For instance, a steel matrix can be dually reinforced *in-situ* with TiC-TiB_2 particles by means of argon arc cladding (AAC) (Wang, et al., 2008). In this research, the average microhardness of cladded Fe/TiC-TiB$_2$ hardfacing was nearly 800 HV0.5. To compare their mechanical properties, an attempt to manufacture Ti-4Al-2Fe/TiB (conventional cermet) and Ti-4Al-2Fe/TiB/TiC (dual-reinforced) bulk composites was made by (Chaudhari & Bauri, 2018) *via* spark plasma sintering (SPS). In their study, under the same conditions, the hardness of Ti-4Al-2Fe/TiB-TiC and

Ti-4Al-2Fe/TiB was found to be 2039 HV30 and ~714 HV30, respectively. Meanwhile, the wear rate of the former was 10 times lower than the latter. This signifies an excellent applicability of dual-reinforced composites to the tasks that involve sliding wear.

The impact wear resistance, on the other hand, requires materials with dual-matrix design. For instance, (Wu, et al., 2017) have reported fabrication of Ni-based composite of such type by adding 4 and 8 wt.%Mo to the commercial powder 88Ni60-2C-10TiN. As a result, hardness in the deposited dual-matrix composite increased by nearly 17%, from 1010 to 1220 HV0.2, and the wear rate decreased by 50% during the pin-on-disc wear test.

Due to high cost and toxicity of widespread matrix materials (Co and Ni) in composites, alternatives are extensively searched. Kübarsepp & Juhani, 2020 reported an increasing amount of publications focused on development of Fe-based MMCs. At their early implementation as reinforcement, Fe and its alloys were largely disregarded because of mechanical properties – hardmetals with Fe-based reinforcement were found inferior to those with Co and Ni. However, Fe-alloys have advantages over Co and Ni, such as low cost, potential to heat treatment and high strength (Kübarsepp & Juhani, 2020).

Figure 1.6 illustrates the difference in price between steel and Ni throughout several years. Despite the fact that historically steel has always had lower price, it demonstrates a steady decrease (525 *vs.* 511 U.S. dollars per metric tonn) over a 3-year span, whereas price for Ni has raised by roughly 34% (11335.77 *vs.* 15239.36 U.S. dollars per metric tonn) over the same period. This testifies in favor of Fe-based alloys as a more attractive replacement for Ni.
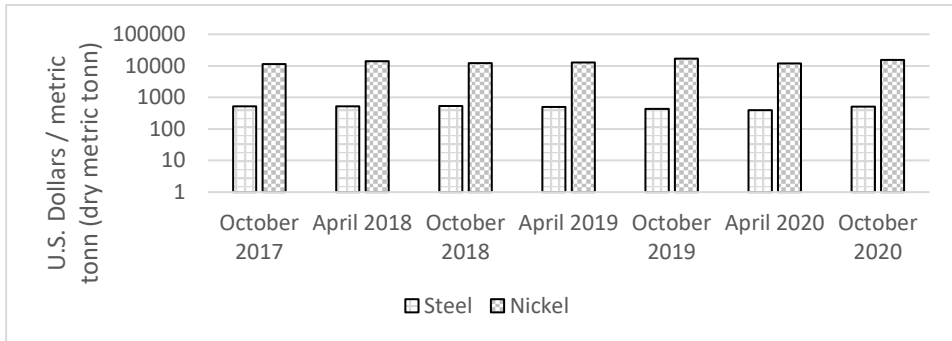
Figure 1.6 Price comparison of steel (SteelBenchmarker™, 2020) and nickel (Dow & Macadangdang, 2020) feedstock over a 3-year span.

The interest in powder metallurgy in the *in-situ* synthesis is dictated by a shorter and cheaper production procedure of cermet-based coatings or hardfacings it offers (Fig. 1.5). To the author's best knowledge, no comparative analysis has been done between wear resistant HVOFS coatings and PTAW hardfacings based on *ex-situ* and *in-situ* manufactured cermet powders. Therefore, this thesis research concentrates on the development and comparison of Fe-based carbide-reinforced composite coatings/hardfacings using *ex-situ* and *in-situ* approaches.

1.2 Hardfacing technologies

The technical excellency of equipment is one the most important preconditions for a stable and reliable production cycle. It is quite common practice in industrial facilities of any kind to shut down the whole production line or unit for maintenance of parts that are subjected to wear. The number of such stops and detrimental consequences they cause is significantly lower when the components with wear-resistant coatings manufactured by hardfacing are used (Laskowski, 2017, Lazić, et al., 2018, Ferdinandov & Gospodinov, 2020).

Hardfacing is a general term of a cost-efficient approach for extending the service life of component surfaces by wear-resistant materials. They are mainly used for refurbishing of damaged and worn-out parts. However, pre-service treatment of new components is also common practice. In general, hardfacing provides the following benefits:

- less frequent part replacement;
- productivity increase due to fewer maintenance stops;
- use of cheaper base materials (substrates);
- reduction of general production cost.

The following materials can be used as base materials: nickel-based and copper-based alloys, carbon and alloy steels, stainless steel, cast iron, and manganese steel (Pradeep, et al., 2010). Depending on the task, hardfacing is done by buildup or weld overlay methods. Buildup is used for shape restoration of the worn-out parts while weld overlay is applied to surfaces of new components. In both cases, metal is deposited onto the base material as a solid surface or in a pattern (Fig. 1.7).

| (a) | (b) | (c) | (d) |
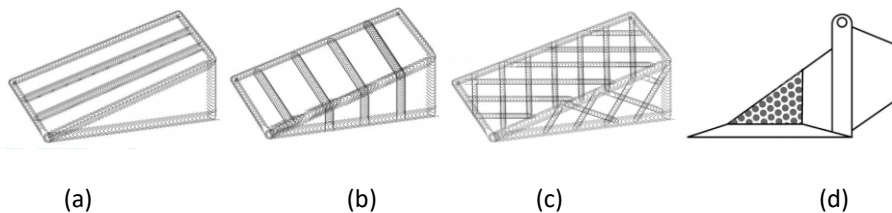
Figure 1.7 Hardfacing patterns: (a) parallel beads; (b) beads at right angle; (c) waffle pattern; (d) dot pattern (Postle Industries, Inc., 2020).

The economic importance of hardfacing derives from the feasibility of selectively applying expensive materials chosen for their properties, and depositing them onto a common inexpensive base metal where they are required for best performance of their specialized function (Sexton, 2015).

1.2.1 Thermal spray technologies

Recent definition of hardfacing has been complemented by the thermal spray family: "Hardfacing is the deposition of thick coatings of hard, wear-resistant materials on a worn or new component surface that is subject to wear in service. Thermal spraying, spray-fuse and welding processes are generally used to apply the hardfacing layer" (The Welding Insitute, TWI, 2020). In order to avoid confusion in terminology,

the products of thermal spray deposition in the next chapters of this study will be referred to as "coatings".

Thermal spraying is a process of constructing a coating using high temperature gas stream with heated and accelerated particles of sprayed material. These particles bond with the substrate or the previously sprayed layer of the coating due to welding or mechanical adhesion. The essence of the process lies in utilizing high temperatures when melting, wetting, adhesion or sintering happens, turning mechanical conglomerate into uniform substance.

The advantages of thermal spraying are (Davis, 2004):

- minimal thermal degradation of the substrate (substrate temperature is usually below 150 °C);
- wide range of feedstock materials (metals, alloys, cermets, plastics, their combination);
- low processing cost;
- wide range of coating thickness.

The common feature for all thermal spraying techniques is heating of the coated material, its spraying and acceleration in a hot gas stream (Fig. 1.8).

(a)   (b)
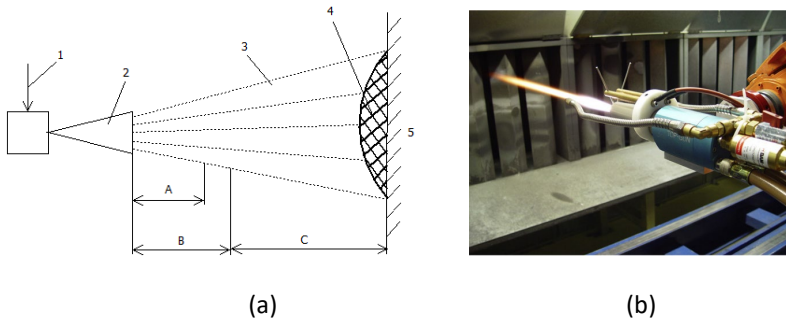
Figure 1.8 Thermal spraying: (a) schematics of conventional (Anciferov, et al., 1987); (b) spraying equipment, operated at Fraunhofer IWS, Dresden, Germany (Berger, 2015).

In Fig. 1.8a the sprayed material (1) is loaded into a high-temperature heat source (2) and it is heated during traveling within a distance (A). Simultaneously, particles spread on the distance (A) and accelerate in the gas stream on the distance (B) (usually B > A). Further, on the distance (C), particles (3) travel directly to the substrate (5) and form the coating (4) on its surface.

Small size of the particles makes thermal spraying applicable for tasks where low heat input on the substrate is critical. During spraying, the structure of the coating can be adjusted to any type. It consists of heavily-deformed splats that are interconnected along the contact surfaces (Fig. 1.9). These splats are characterized by diameter D_x and surface F_x (Anciferov, et al., 1987):

$$F_x = \frac{\pi D_x^2}{4}$$

(1.1)
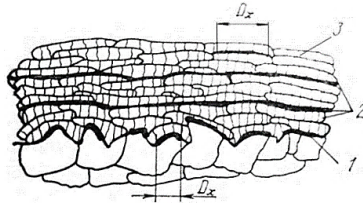
Figure 1.9 Schematic representation of the structure (Anciferov, et al., 1987).

In Fig. 1.9 the substrate-coating interface (1) defines the strength of adhesion between the substrate material and the sprayed coating. The interlayer interface (2) inside the coating is a result of delay between spraying sets. The properties of the coating are mostly dictated by the inter-splats cohesion (3).

The size range of particles applicable for thermal spraying is 20–60 μm and thickness of the resulting coating usually fluctuates in the range 50–1,000 μm (Davis, 2004). The microstructure of a typical thermally sprayed coating is presented in Fig. 1.10. On the right hand figure of the Fig. 1.10 the magnified part of the coating is shown.
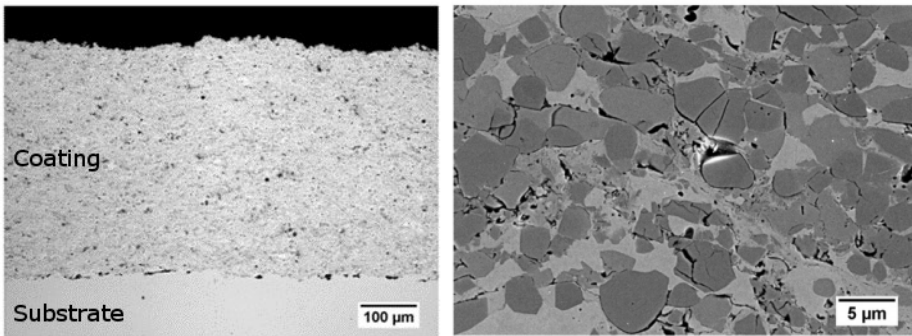
Figure 1.10 Micrographs of a Cr_3C_2-NiCr coating produced by thermal spraying (Berger, 2015).

Thermal energy for spraying may be generated chemically, through the combustion of fuels with oxygen or air, or through the electrical heating of industrial gases (Davis, 2004). Table 1.1 contains the division of thermal spraying techniques based on the nature of used energy.

Table 1.1. Thermal spraying techniques propelled by the energy of different nature.

Type of energy	Process
Thermal	Flame Spray (FS)
	High Velocity Oxy/Air Fuel Spray (HVOFS/HVAFS)
	Detonation Gun Spray (DGS)
Electrical	Wire Arc Spray (WAS)
	Vacuum Plasma Spray (VPS)
	Air Plasma Spray (APS)
	Radiofrequency Plasma Spray (RFS)

Berger, 2015 defines high velocity oxy-fuel spraying (HVOFS) as current state-of-the art technology for hardmetal coating preparation. Moreover, he calls it a two-stage shaping technology, in which the first stage consists of the powder preparation and the second stage is the spray process. With regard to all existing thermal spraying techniques, HVOFS holds its place as shown in Fig. 1.11.
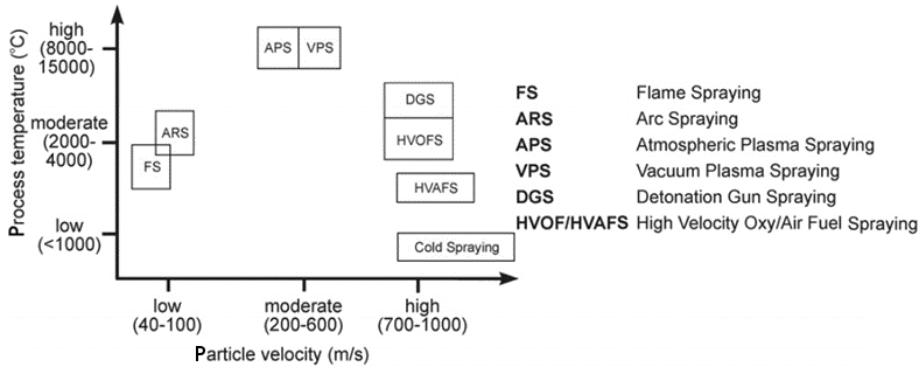
Figure 1.11 Schematic presentation of the combination of process temperature and velocity for the different thermal spray processes (Berger, 2015).

It is clearly seen that HVOFS equipment operates in the mid-range temperature level, which excludes substrate overheating; the high kinetic energy of sprayed particles provides an excellent intersplat cohesion and homogeneity of the coating. As a result, HVOFS is capable of producing ceramic-reinforced coatings with an excellent hardness of 800–900 HV0.3 for TiC-25NiCr and TiC-40NiCr deposits (Bolelli, et al., 2020) and about 960–1010 HV for TiC-30FeCr and TiB$_2$-30FeCr compositions (Jones, et al., 2001).

More complex dual-matrix systems discussed above were studied by (Surzhenkov, et al., 2013). Their work focuses on the mechanical properties of HVOFS composite from the FeCrSiB matrix reinforced with either TiC-NiMo or Cr$_3$C$_2$-Ni cermets. The matrix-to-reinforcement ratio was 3:1 and 7:3, respectively. Both dual-matrix composites even though they possessed the same microhardness of around 850 HV0.1, demonstrated 80% difference in the wear rate. It was lower in the Cr$_3$C$_2$-Ni reinforced coating due to smaller presence of metallic Ni (versus NiMo phase of the counterpart), which made it more resistant to ball-on-plate sliding wear testing. The main disadvantage of material choice of that study is the cost of feedstock materials. Alternatively, the HVOFS with the induced *in-situ* synthesis of the carbide phase could potentially decrease the cost of the production process.

1.2.2 Weld cladding technologies

Cladding is a process of combining two or more different materials to enhance the properties of one of the constituents or protect it from wear. In this study, weld cladding is considered as a partial case of cladding. Depending on the application, it might be also known as hardfacing or weld overlay. Therefore, the products of weld cladding in the following chapters of this thesis study will be referred to as "hardfacings".

Unlike thermal spray processes, hardfacing requires the surface to be melted to form a metallurgical interface. As a result, hardfacing is deposited on larger components that are not deformed by the heat of application (Davis, 2004).

Weld overlay cladding techniques were originally developed at Strachan & Henshaw, Bristol, to defend the (Navy) components subjected to extreme pressure and shock loading. These clad components came in contact with sea water, but needed less maintenance (Saha & Das, 2016). Typical thickness of welded hardfacings fluctuates between 2 and 20 mm. Table 1.2 summarizes the most common weld overlay cladding techniques.

Table 1.2. Types of weld cladding (Sexton, 2015).

Category	Process
Arc welding	Flux core arc welding (FCAW)
	Gas metal arc welding (GMAW/MIG)
	Gas tungsten arc welding (GTAW/TIG)
	Plasma arc welding (PAW/PTAW)
	Shielded metal arc welding (SMAW)
	Submerged arc welding (SAW)
Torch welding	Oxy/fuel gas welding (OFW)
Other welding	Electron beam welding (EBW)
	Electroslag welding (ESW)
	Laser beam welding (LBW)

The main requirements for weld overlay are the following:

- the heat impact on the base metal should be minimal;
- the dilution of the base metal with hardfacing should be minimal;
- the residual stress and deformation of the base metal in heat affected zone (HAZ) should be minimal;
- the part tolerances for further machining should be maintained.

The common feature of all the aforementioned welding techniques is that they operate on the heat from the electric arc generated between the electrode and the workpiece. However, each of those processes was developed as a response to different industrial demands and, thus, they comprise certain differences in design. For instance, in the FCAW process, shielding is provided due to the decomposition of the flux contained at the surface of the consumable wire electrode; a modified form FCAW-S has a metal self-shielded electrode, which makes it suitable for outdoor welding/cladding. Essentially, the GMAW technology is the same as FCAW only with addition of shielding gas (Ar, CO_2) and continuous metal wire filament. Unlike, in FCAW and GMAW where a consumable electrode is used, GTAW comprises a non-consumable electrode for igniting the electrical arc. Here a larger number of hardfacing alloys is available for selection due to higher operating temperatures. SAW utilizes granular flux as a replacement for shielding gas. It fills and covers molten pool and thermally insulates deposits, protecting them from rapid cooling and oxidation.

The PTAW process is often considered to be a thermal spray process, but historically, it is a weld overlay process. In this process, an electric arc is struck between the workpiece and the tungsten cathode, creating an electric arc. This arc is confined in a

restricting orifice, and a plasma formed as the gas flowing through an annular orifice is ionized. The material to be coated is in powder form and is fed into the ionized gas stream. Because the arc is rooted on the workpiece, a diffusion bond layer is generated at the interfaces that consists of both the substrate material and the coating material. A protective auxiliary shielding gas can be used if needed. A second power supply is connected between the workpiece and the restricting orifice to help ignite the initial arc and add additional energy to the electric arc (Davis, 2004). Figure 1.12 shows a general look of the PTAW unit and a schematic representation of the welding torch.

| (a) | (b) |
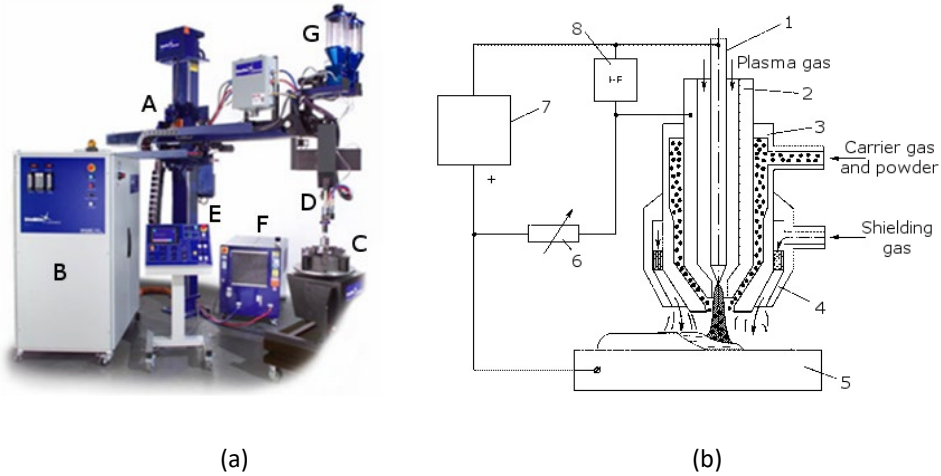
Figure 1.12 PTA welding: (a) generic plant (Kennametal Inc., 2013); (b) schematic illustration of torch (Arcraftplasma, 2016). Equipment (a): A - stand, B - digital welding system set, C - rotary table, D - welding torch system, E - control panel, F - cooling unit, G - powder feeders. Equipment (b): 1 - electrode, 2 - plasma nozzle, 3 - powder feed nozzle, 4 - shielding nozzle, 5 - work piece, 6 - ballast resistance, 7 - power source, 8 - power supply.

The PTAW utilizes feedstock powders ranging in size from 150 to 410 µm and is capable of producing 2.5 mm thick hardfacings (Zikin, et al., 2012, 2012a). Figure 1.13 illustrates typical morphology of the feedstock powder and hardfacing microstructure deposited by the PTAW technology.

| (a) | (b) |
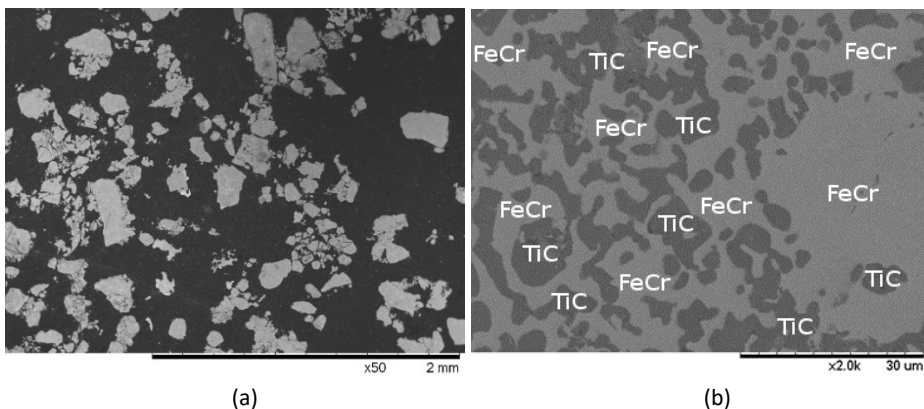
Figure 1.13 Micrographs of (a) TiC-NiMo feedstock powder for PTAW; (b) TiC-FeCr composite hardfacing deposited by PTAW.

Some authors report the hardness value of PTA cladded FeCrSiB/WC-Co hardfacings to be as high as 1425 HV1 (Simson, et al., 2018). The abrasive sliding wear rate of hardfacings in their study was comparably low compared to that of 30WC-Ni observed by (Deng, et al., 2015) under similar test conditions. Interestingly, when (Yuan & Zhuguo, 2014) used the PTAW cladding of similar FeCrNiBSi hardfacing with Cr_3C_2 powder as reinforcement, hardness as high as 1145 HV0.5 was achieved with an initial powder ratio of 5:5 and 875 HV0.5 with an initial powder ratio of 1:5. The previous studies where Cr powder was used as a precursor for the *in-situ* synthesis of chromium carbide hard phase reported an average value of hardness in the pre-surface layers of PTAW deposited hardfacing to be 850–950 HV30 (Liu & Gu, 2006, Liu, et al., 2006).

Excellent examples of dual-matrix composites in the scope of PTAW hardfacing were developed by (Zikin, et al., 2013). It is a thorough study based on the comparison between Cr_3C_2-Ni and TiC-NiMo cermets, each of which was introduced as reinforcement to the NiCrBSi matrix during the PTAW hardfacing. In each case, the matrix-to-reinforcement volumetric ratio was 3:2. This study revealed rather equal value of hardness for both materials (~650 HV10) under temperatures up to 100 °C and nearly 50% lower erosion wear rate of hardfacing containing TiC-NiMo in an analogous temperature range. This difference, most likely, is dictated by the presence of more ductile NiMo matrix in the TiC-NiMo cermet, which makes it more resistant to the impact of abrasive wear. Similar to the analysis of (Surzhenkov, et al., 2013), the main disadvantages of material choice in this study are the feedstock material cost and potentially toxic Ni-based matrix material. The method of the *in-situ* reinforcement synthesis in Fe-based composite hardfacings seems to be an approach free from these limitations.

Figure 1.14 depicts the hardness values and abrasive impact resistance of Ni- and Fe-based hardfacings manufactured in the PTAW process and compared to similar HVOFS coatings. It is apparent that PTAW hardfacings are 4–6 times more resistant to erosion wear and have at least 1.5–2 times higher hardness than the HVOFS counterparts.
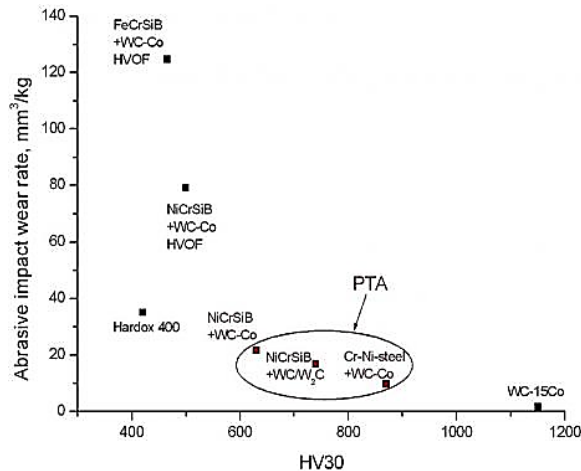
Figure 1.14 Properties of PTAW hardfacings in comparison with HVOFS coatings (Kulu, et al., 2015).

Regarding use of Ti as one of the feedstock powders for reinforcement synthesis, two studies (Corujeira Gallo, et al., 2013, 2013a) addressed the *in-situ* synthesis of TiC in the iron matrix utilizing the PTAW hardfacing. They report similar results, where hardfacing

deposits with the microhardness of 550–600 HV0.1 were obtained. The Fe:Ti volumetric ratio was 7:1, which, likewise, contributed to forming ductile metallic matrix. However, even with only 14 vol.% of TiC present in the hardfacing, its wear rate under abrasive sliding conditions was already nearly 60 times lower than that of the reference material.

PTAW demonstrates potential to be applied in other fields of industry as well. As shown in (Mercado Rojas, et al., 2018), by applying the principles of additive manufacturing, a fine quality weld printed parts with enhanced mechanical properties, low porosity and excellent hardness can be manufactured for the mining, oil and gas industrial sectors. Overall, PTAW is an excellent method for the production of thick wear resistant hardfacings. It greatly complements HVOFS, which usually aims at manufacturing of relatively thin wear resistant coatings.

1.3 Planned activities of the study

In the thesis research, a synergetic effect of joining the *in-situ* synthesis of the hard phase and development of composite coatings and hardfacings for abrasive wear applications is targeted.

To achieve the main objectives, the following activities were planned:

1. Production of MMC powders with preliminary MAS synthesized TiC- and Cr_3C_2 reinforcement for thermal spraying and weld cladding, as well as production of MMC coatings and hardfacings from these powders by the HVOFS and PTAW methods, respectively.
2. Development of deposition (thermal spraying and welding) techniques for eventual production of MMC coatings and hardfacings with *in-situ* synthesized Ti and Cr carbide-based reinforcement.
3. Characterization of the obtained coatings and hardfacings (morphology, structure, hardness) and assessment of their abrasive wear resistance.

2 Experimental

2.1 Hardfacing materials

2.1.1 Cermet powders produced by mechanically activated synthesis

The production of cermet powders by mechanical activation (MAS) consisted of the following steps:

a) milling of mixed feedstock powders in a ball mill with WC-Co lining for 72 h in the presence of isopropanol as wetting agent and WC-Co balls as milling media with balls-to-powder ratio 20:1. The chemical compositions of feedstock powders are given in Table 2.1;

b) plasticizing (3–4 wt.% of paraffin; 60–120 wt.% of wetting agent (isopropyl alcohol), depending on the wettability of precursor powders) and drying of mixture for losing an excessive moisture;

c) vacuum sintering of plastisized mixure under pressure 13–27 Pa for 4–6 h with the formation of the hard carbide phase at 1075 °C for Cr_3C_2-Ni and TiC-NiMo at 1400 °C (Papers I–III).

The optimal heating rates used for the synthesis of Cr_3C_2-Ni were found to be 5 °C/min and 10 °C/min with dwelling times at 600 °C and 950 °C for 30 min and for 15 min at 1075 °C. The cooling was nearly linear with an approximate rate of 6 °C/min. The optimal heating rate for the TiC-NiMo synthesis was 10 °C/min with 60 min dwelling time at 1270 °C and 1400 °C. The approximate cooling rate was 10 °C/min. After sintering, powder compacts were manually crushed, and obtained cermet powders were subjected to sieving for extracting particles of acceptable size: 20–90 µm for HVOFS and 90–300 µm for PTAW. Schematic representation of the MAS process is given in Fig. 2.1.
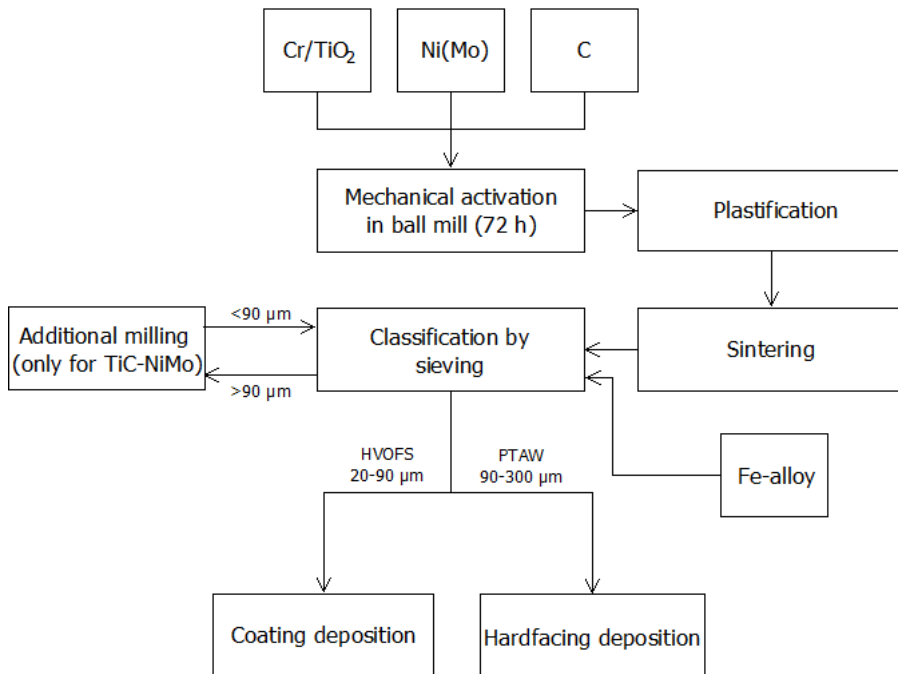
Figure 2.1 Schematic representation of the MAS process (with SS AISI 316L).

Table 2.1. Chemical composition of feedstock MAS powders for HVOFS, PTAW and SAW.

Type of powder	Chemical composition, wt.% / vol.%				
	Cr	TiO_2	C	Ni	Mo
TiC-NiMo	-	64/62.4	16/28.7	13.3/6.2	6.7/2.7
Cr_3C_2-Ni	69.3/58.4	-	10.7/28	20/13.6	-
Particle size, µm	6.65	0.02	6.45	2.4	2.32
Manufacturer	Pacific Particulate Materials Ltd.	Precheza a.s.	Imerys SA	Pacific Particulate Materials Ltd.	

The fraction of TiC-NiMo with particles larger than 90 µm was additionally exposed to dry milling in the aforementioned ball mill for 4 h. Subsequently, in the experiments with HVOFS, the fraction of 20–90 µm or PTAW, the fraction of 90–300 µm of MAS powders were mixed with the commercial Fe-alloy powder stainless steel AISI 316L (Castolin 16316; wt.%: 0.03 C, 17.5 Cr, 13 Ni, 2.7 Mo, bal. Fe) or self-fluxing alloy powder NiCrSiB (Castolin 16221; wt.%: 0.2 C, 4 Cr, 1 B, 2.5 Si, max. 2 Fe, 1 Al, bal. Ni) (Table 2.2).

Table 2.2. Reinforcement-to-matrix ratio of the experimental powders for HVOFS (Paper III), PTAW and SAW (Paper II).

Composition | Deposition method	Ratio, vol.%			
	TiC-NiMo : SS	TiC-NiMo : NiCrSiB	Cr_3C_2-Ni : SS	Cr_3C_2-Ni : NiCrSiB
HVOFS	53 : 47	-	50 : 50	-
PTAW	49 : 51	50 : 50	43 : 57	44 : 56
SAW	-	-	43 : 57	44 : 56

In the experiments with PTAW, cladding powders were transported to the welding pool from separate feeders (Paper II). The presence of Fe-alloy (SS) in the composition was meant to catalyze the forming of a dual-matrix structure. Figure 2.2 depicts the morphology of cermet powder particles mixed with SS.
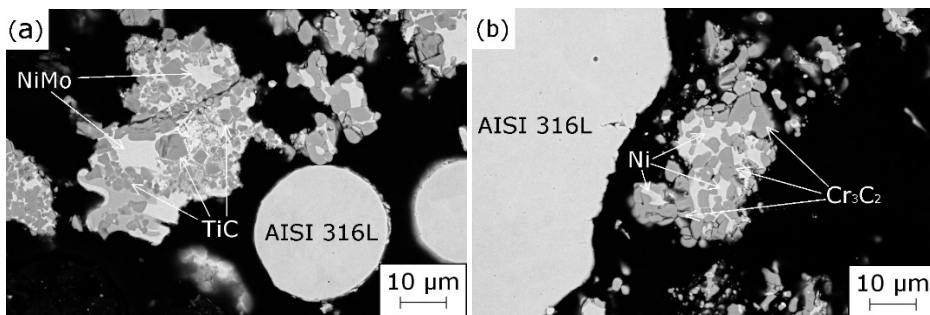
Figure 2.2 The morphology of : a) TiC-NiMo + SS; b) Cr_3C_2-Ni + SS.

2.1.2 Precursor powders for the *in-situ* synthesis of reinforcement

To obtain carbide reinforcement synthesized *in-situ,* the feedstock powders of carbide-forming metals (Cr, Ti), carbon (obtained from disintegrator milling of graphite electrodes), and Fe-alloy SS (Castolin 16316) were manually mixed in certain proportions (Tables 2.3 and 2.4). To comply with the requirements for the particle size of the feedstock material for HVOFS, the separation of 20–90 µm fraction suitable for spraying took place after mixing.

Table 2.3. Feedstock powders for the in-situ synthesis of TiC- (Paper III) and Cr_3C_2-containing reinforcements in the HVOFS process.

Type of powder	Chemical composition, wt.% / vol.%			
	Cr	Ti	C	SS
Ti + C + SS	-	32.8/40	8.2/19.7	59/40.3
Cr + C + SS	29.5/28.7	-	4.5/13.9	66/57.4
Particle size, µm	20–90	20–90	20–90	20–90
Manufacturer	Pacif. Part. Mat. Ltd.	Baoji Z. Met. Mat.CO., Ltd.	Tallinn Univ. Tech.	Castolin Eutectics®

In the case of the PTAW process, adding the plasticizer (3–4 wt.% of paraffin) to the powder mixture created a slurry, which then was uniformly manually laid on the sandblasted substrate and dried at 20 °C in ambient air for 24 hours. Instantly before cladding, the pre-fabricated specimens were pre-heated at 300 °C for 6 h in order to induce the pre-expansion of the substrate and thus to decrease the thermal stresses in the resultant hardfacings. In the case of the HVOFS process, the feedstock powders were fed to the spaying gun instantly from a powder feeder.

Table 2.4. Feedstock powders for the in-situ synthesis of TiC- and Cr_3C_2-containing reinforcement in PTAW (Paper IV).

Type of powder	Chemical composition, wt.% / vol.%				
	Cr	Ti	TiO$_2$	C	SS
TiO$_2$ + C + SS	-	-	40/47.1	10/21.7	50/31.2
Ti + C + SS	-	40/45.6	-	10/22.3	50/32.1
Cr + C + SS	32/29	-	-	8/22.5	60/48.5
Particle size, µm	10–15	60–80	0.1–0.3	5.5–7	10–45
Manufacturer	Pacif. Part. Mat. Ltd.	Baoji Z. Met. Mat.Co., Ltd.	Precheza a.s.	Imerys SA	Castolin Eutectics®

Principal stages for the *in-situ* synthesis of carbide reinforcement in HVOFS and PTAW processes are demonstrated in Fig. 2.3. The morphology of used Ti + C + SS and Cr + C + SS mixtures is shown in Fig. 2.4. The composition TiO$_2$ + C + SS was not subjected to SEM imaging due to the submicron size of TiO$_2$ particles.
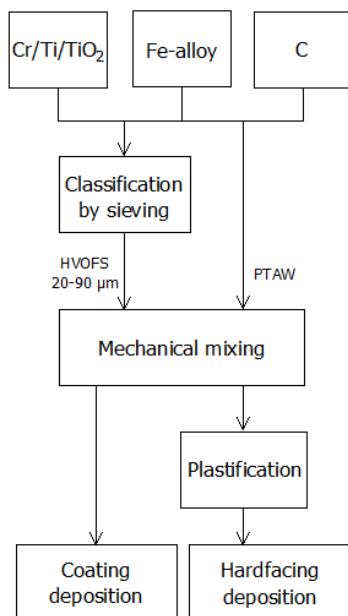
Figure 2.3 Schematic representation of the in-situ synthesis of carbide reinforcement.

The flowability of the developed powder mixtures was assessed using a manual Hall flowmeter funnel (ASTM B213) (ASTM International, 2020). The phase identification was performed through the X-ray diffraction (XRD) method with CuKα radiation (Burker AXS D5005, Germany; Burker D8 Discover, Germany). The particles morphology was analyzed by a scanning electron microscope (SEM) EVO MA-15 (Carl Zeiss, Germany).
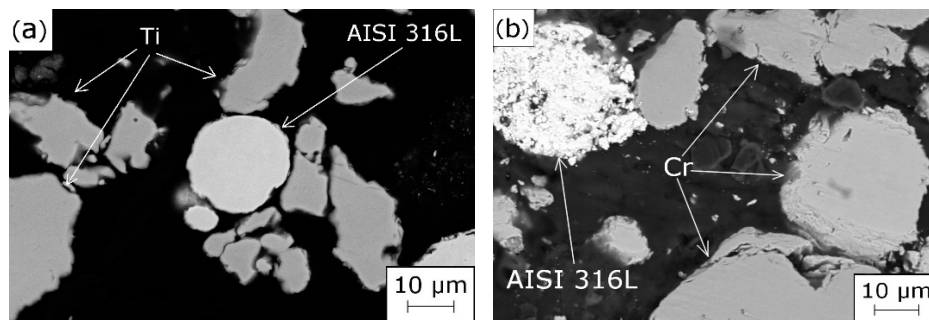
Figure 2.4 The morphology of : a) Ti + C + SS; b) Cr + C + SS.

2.2 Hardfacing technologies

2.2.1 High velocity oxy-fuel spraying

Obtained powders were deposited onto steel C45 and S235 substrates (50 x 25 x 10 mm) by means of HVOFS systems Hipojet 2700 (Metallizing Equipment Co. Pvt. Ltd., India; Paper I) or HP/HVOF Tafa JP-5000® (Praxair Inc., Danbury, CT, USA; Paper III). In each case, substrate materials were preliminarily sandblasted. Table 2.5 contains the parameters of spraying.

Table 2.5. HVOFS parameters (Papers I, III).

Parameter	Value
Oxygen flow rate, l/s	14.5–15
Kerosene flow rate, l/s	0.4–0.47
Carrier gas flow rate, l/s	0.83
Powder feed rate, g/s	1–1.67
Spraying distance, mm	360–380
Number of passes	6–14

The flow rate of combustion gases was found to depend on the average enthalpy of specific powder composition and was derived empirically. Generally, the more homogeneous the powder composition, the more oxygen (and less kerosene) it required in the spraying jet. The rest of parameters had an inverse relationship with the flowability value of the powder (except for the feed rate whose dependence was direct).

2.2.2 Plasma transferred arc welding

PTAW hardfacing with *ex-situ* added MAS reinforcement was performed using the device EuTronic Gap 3001 DC (Castolin Eutectics®) with the process parameters summarized in Table 2.6. As a substrate, the specimens from the structural steel S355 or S235 (50 x 25 x 10 mm) were used. The powder-to-substrate delivering methods varied. The matrix materials were either an austenitic SS powder Castolin 16316 or self-fluxing NiCrSiB alloy powder Castolin 16221. Two separate powder feeders were used, mixing matrix and reinforcement powder in certain proportion and feeding the resulting composition to the plasma torch.

Table 2.6. PTAW parameters (Papers II, IV).

Parameter	Value	
	Paper II	Paper IV
Current, A	95	95
Voltage, V	22–24	22–24
Oscillation frequency, Hz	0.6	0.6
Traverse speed, mm/s	1	0.2
Plasma gas consumption (Ar), l/s	0.025	0.025
Shield gas consumption (Ar), l/s	0.108	0.108
Carrier gas consumption (Ar+H_2) (reinf.), l/s	0.0625	-
Carrier gas consumption (Ar+H_2) (matrix), l/s	0.0458	-
Powder feed rate, g/s	0.035–0.085	0.085

To manufacture hardfacings with the *in-situ* synthesized reinforcement during the PTAW process, the lower value of the traverse speed (Table 2.6) was used (Paper IV) to provide enough time for the synthesis.

2.2.3 Submerged arc welding

Submerged arc welding (SAW) of hardfacing was done at Kaunas University of Technology (KTU) using the Cr_3C_2-Ni cermet powder developed at TalTech, as reinforcing material (Paper II). The matrix materials were an austenitic SS powder Castolin 16316 or self-fluxing NiCrSiB alloy powder Castolin 16221. The deposition process was accomplished

on an Integra 350 Professional (Miller) welding machine utilizing Ø1.2 mm consumable low carbon wire electrode (wt.%: 0.1 C, <0.03 Si, 0.35–0.6 Mn, <0.15 Cr, <0.3 Ni, bal. Fe) and standard flux (wt.%: 38–44 SiO_2, 38–44 MnO, <2.5 MgO, 6–9 CaF_2, <6.5 CaO, <2 Fe_2O_3, <0.15 S, < 0.15 P). The normalized structural steel S355 prisms (6 x 6 x 20 mm) were chosen as substrates. The matrix and the reinforcement powders were manually mixed, pre-laid on the substrate, covered with a powder flux and after that remelted, applying the parameters provided in Table 2.7.

Table 2.7. SAW parameters (Paper II).

Parameter	Value
Current, A	180–200
Voltage, V	22–24
Traverse speed, mm/s	4
Welding wire feed rate, mm/s	7

2.3 Characterization of coatings and hardfacings

2.3.1 Microstructure analysis and phase composition

A microstructural analysis was performed on a scanning electron microscope (SEM) EVO MA-15 (Carl Zeiss, Germany) equipped with energy dispersive X-ray spectroscopy (EDS) detector XFlash® 5010 (Paper I–IV). Specimens' cross-sections were embedded into resin and polished using series of polishing discs with a descending roughness order. The phase compositions were determined by the X-ray diffraction (XRD) method with Cu Kα radiation using the X-ray diffraction device AXS D5005 (Bruker, Germany) with a 0.04° step (Paper I, II), using the X-ray diffraction device D8 Discover (Bruker, Germany) with a 0.025° step (Paper III) or using the X-ray diffraction device SmartLab SE (Rigaku, Japan), equipped with the D/teX Ultra 250 1D detector (Rigaku, Japan) with a 0.01° step (Paper IV). The phase composition of all the materials was determined from the specimen's surface.

2.3.2 Determination of thickness and hardness

The thickness of HVOFS coatings was determined by a coating thickness gage Positector 6000 (DeFelsko, USA) (Paper III). The thickness of PTAW hardfacings was not assessed as its values differed by an order of magnitude from the thickness of HVOFS coatings. The hardness of the obtained coatings and hardfacings was assessed by means of the Vickers testing method according to the standard ISO 6507-1 (International Organization for Standardization, 2018). The load for microindentation was chosen to be 2.94 N (0.3 kgf) and for macroindentation 9.8 N (1 kgf) or 294.3 N (30 kgf). The hardness was measured by a Nexus 4505 hardness tester (Innovatest, Maastricht, The Netherlands), Indentec 5030 SKV (Zwick, Germany) and Micromet 2001 (Buehler, Germany). Dwell time was 10 s. For each material, 10–12 measurements were made and an average value of hardness was calculated. Standard deviation was calculated according to the following formula:

$$S = \sqrt{\frac{\Sigma(x-\bar{x})^2}{N-1}}, \qquad (2.1)$$

where S is the standard deviation, x is each value in the data set, $\bar{x}$ is a mean of all values in the data set, and N is the number of values in the data set.

Additionally, in order to determine the H/E ratio of hardfacings in (Paper IV), a Young's modulus was measured with load 100 N (10.2 kgf) and dwell time 10 s on the device Z2.5 (Zwick, Germany).

2.3.3 Abrasive wear tests

The wear resistance of the manufactured coatings/hardfacings was assessed using two methods: three-body abrasion rubber wheel wear (ARWW) test according to the standard ASTM G65 (ASTM International, 2016) and abrasive-erosive wear (AEW) test using a centrifugal accelerator, which was set up according to the standard GOST 23.201-78 (GOST 23.201-78 Standard, 1987). ARWW tests were originally reported in (Papers I–IV) and the AEW test was reported before only in (Paper III). The test parameters are given in Table 2.8.

Table 2.8. Parameters of the abrasive wear tests of HVOFS coatings and PTAW hardfacings.

Parameter	Test type	
	ARWW	AEW
Load, N	22.6 and 130	-
Linear speed, m/s	2.4	40^1
Impact angle, °	-	30, 90
Wheel diameter, mm	80 and 227	-
Testing temperature, °C	20	20
Abrasive type and size, mm	Silica, 0.2–0.3	Silica, 0.2–0.3
Abrasive amount, kg	1.85	$2+6^2$
Abrasive feed rate, g/s	5–6.5	6.95
Duration of the test, s	300, 600 and 1800	2400

[1] Velocity of abrasive particles; [2] Run-in—2 kg, regular test—6 kg.

Before and after testing, all the samples were ultrasonically cleaned in acetone. The standard deviation was calculated according to Eq. (2.1). In every experiment, run in was done immediately before regular testing. Overall, 3-5 samples of each coating type were tested in the abrasive wear test.

The wear mechanisms of the worn surfaces were assessed by SEM EVO MA-15 (Carl Zeiss, Germany) and TM1000 (Hitachi High-Technologies Europe GmbH, Mannheim, Germany).

The relative wear resistance ε_v was determined according to the following equation:

$$\varepsilon_v = I_v^{H400} / I_v, \qquad (2.2)$$

where I_v^{H400} is the volumetric wear rate of the reference steel Hardox 400; I_v is the same of the tested sample.

3 Composite coatings and hardfacings with cermet MAS reinforcement

3.1 Production of TiC-NiMo and Cr₃C₂-Ni powders by MAS

3.1.1 Optimal titanium-to-carbon and chromium-to-carbon ratio

For the manufacturing of the MAS TiC-NiMo powder, the carboreduction of titanium dioxide (TiO_2) was used. In terms of reactivity, the optimal TiO_2:C weight ratio was empirically derived as 4:1 in (Paper III). Phase analysis of the manufactured Cr_3C_2-Ni and TiC-NiMo powders is presented in Fig, 3.1. TiC-NiMo cermet (Fig. 3.1a) exhibited the presence of two main phases, TiC and $TiNi_3$, while Cr_3C_2-Ni (Fig. 3.1b) revealed the presence of three main phases in the obtained powder: Cr_3C_2, Cr_7C_3 and Ni. The optimal Cr:C weight ratio for the production of the Cr_3C_2-based MAS powder was found to be around 7:1 (Paper I).

(a)   (b)
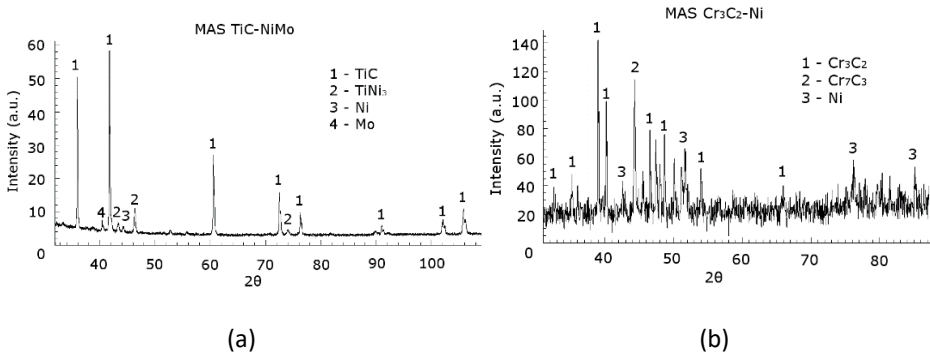
Figure 3.1 XRD pattern of MAS powder: (a) TiC-NiMo; (b) Cr₃C₂-Ni.

3.1.2 Size distribution and flowability

The particle size distributions in the MAS TiC-NiMo and Cr_3C_2-Ni cermet powders are presented in Fig. 3.2. In the TiC-containing powder, the fraction suitable for HVOFS (20–90 μm) yielded 42% from the overall produced quantity of the material, while the amount of the same fraction in the Cr_3C_2-based powder was approximately 10% larger. The fraction suitable for PTAW was 41% in the TiC-NiMo and 21% in the Cr_3C_2-Ni composition.
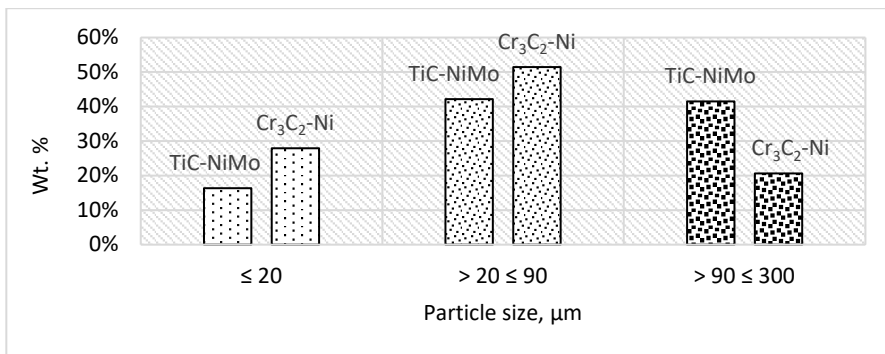
Figure 3.2 Particle size distribution in the MAS TiC- and Cr₃C₂-containing cermet powders.

Due to a higher sintering temperature, the average grain size of the TiC in TiC-NiMo cermet was larger than that of the Cr_3C_2 grain in Cr_3C_2-Ni, respectively (see section 2.1). More intense densification made the coarse fraction (> 90 μm) of TiC-NiMo unsuitable for manual crushing. For this reason, an additional short-term ball milling was used (see section 2.1) with subsequent classification by sieving.

The flowability of pure TiC-NiMo and Cr_3C_2-Ni cermets could not be assessed due to the angular shape of agglomerated particles (see section 2.1). Addition of spherically-shaped SS powder (Castolin) to the composition of each cermet improved their flowability and became measurable (Table 3.1).

Table 3.1. Flowability of the MAS TiC- and Cr_3C_2-containing powders for HVOFS (Paper III).

Composition	Flowability, s
TiC–NiMo + SS	31.9 ± 0.3
Cr_3C_2–Ni + SS	55.7 ± 2.2
SS (Castolin)	15.2 ± 0.1
NiCrSiB (Castolin)	13.6 ± 0.3

3.2 HVOFS coatings with MAS reinforcement

3.2.1 Microstructure and hardness

The HVOFS coating with the MAS TiC-containing reinforcement was found to have good homogeneity (Fig. 3.3a). However, some regions of unmolten SS particles with interfaces can be seen, which influences cohesion. The coating with the MAS Cr_3C_2-containing reinforcement did not acquire desirable homogeneity or thickness (Fig. 3.3b). Here, the cohesion between the cermet particles and stainless steel as well as their adhesion with the substrate was observed to be lower than that of TiC reinforced coating. Moreover, a visible long crack in Fig. 3.3b was apparently formed due to lack of intrinsic ductility of Cr_3C_2-Ni particles as compared to those of TiC-NiMo. This could contribute to the low thickness of the coating by eroding the upper layers away during high kinetic energy spraying.
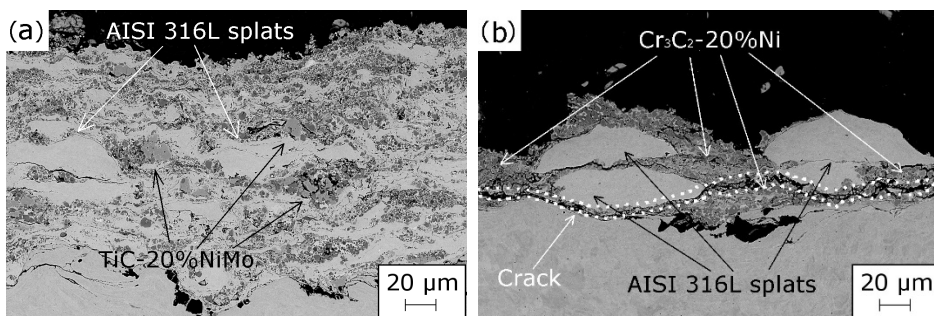
Figure 3.3 Cross-sectional SEM images of HVOFS coatings: (a) with MAS TiC-containing reinforcement; (b) with MAS Cr_3C_2-containing reinforcement.

On the XRD patterns of the HVOFS coating with the MAS TiC-containing reinforcement (Fig. 3.4a), three main phases were identified: TiC, austenite (γ-Fe) and ferrite (α-Fe). XRD analysis of a similar coating but with the MAS Cr_3C_2-containing reinforcement (Fig. 3.4b) indicated the presence of Cr_3C_2, austenite (γ-Fe) and ferrite (α-Fe).

(a)   (b)
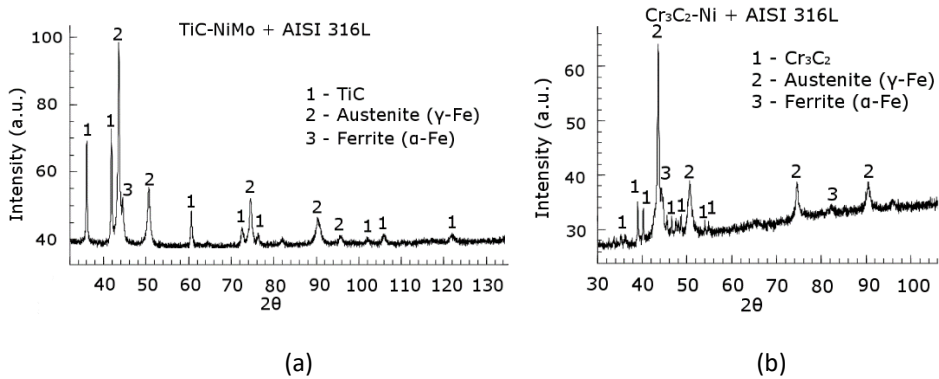
Figure 3.4 XRD patterns of HVOFS coatings: (a) with the MAS TiC-containing reinforcement; (b) with the MAS Cr_3C_2-containing reinforcement.

The thickness and hardness of coatings with the MAS TiC- and Cr_3C_2-containing reinforcements are given in Table 3.2. The testing loads were chosen proportionally to the thicknesses of the coatings.

Experimental composition with the MAS TiC-containing reinforcement, as well as coatings from the reference materials (Cr_3C_2-25NiCr (Amperit 588.074, H.C. Starck)), SS (Castolin 16316)) showed practically identical hardness on the free surface and the cross-section, which indicates their structural uniformity. In contrast, the noticeable gap between the surface and cross-sectional microhardness in the material with the MAS Cr_3C_2-containing reinforcement signifies the lack thereof.

Table 3.2. Average thickness and hardness of the HVOFS coatings and reference materials (Paper III).

Type of coating	Thickness, (µm)	Vickers hardness HV		
		Surface		Cross-Section
		HV1	HV0.3	HV0.3
TiC–NiMo + SS	130 ± 10	4.5 ± 1.0	-	4.5 ± 1.3
Cr_3C_2–Ni + SS	40 ± 20	-	4.9 ± 1.1	2.6 ± 0.8
Cr_3C_2-NiCr (Amperit)	267 ± 4	8.8 ± 1.0	8.2 ± 2.1	9.2 ± 1.6
SS (Castolin)	208 ± 5	3.2 ± 0.4	2.7 ± 1.2	3.1 ± 0.7

3.2.2 Wear resistance and mechanisms

Volumetric abrasive rubber wheel wear rates for experimental coatings reinforced with the TiC- and Cr_3C_2-containing cermets are highlighted in Fig. 3.5. The performance of the coating with the MAS TiC-containing reinforcement (TiC 38 wt.%/49 vol.%) is analogous in terms of the wear rate of the reference material (Cr_3C_2 58 wt.%/65 vol.%) based on the commercial Cr_3C_2-NiCr cermet powder. However, superb abrasive wear resistance can only be achieved *via* homogeneous dispersion of the carbide phase within the metallic matrix, as opposed to how the MAS Cr_3C_2 reinforced coating was formed. For more details see (Paper III).
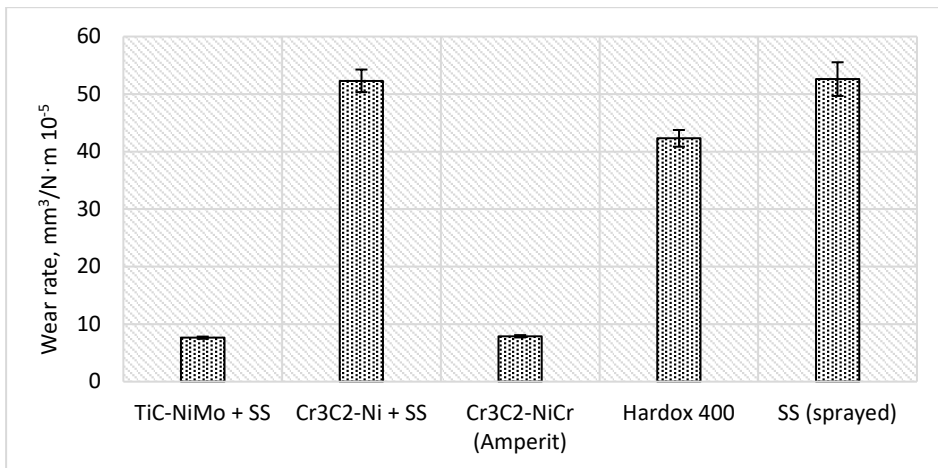
Figure 3.5 ARWW rates of HVOFS coatings with MAS TiC- and Cr_3C_2-containing reinforcement.

The wear resistance of the experimental coatings as well as the reference materials to AEW under 30° and 90° impact angles is shown in Fig. 3.6.
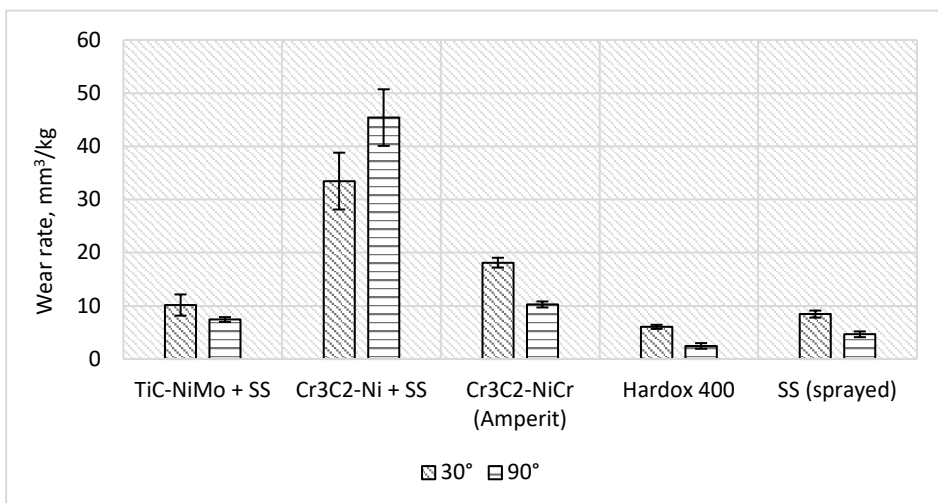
Figure 3.6 AEW rates of HVOFS coatings with the MAS TiC- and Cr_3C_2-containing reinforcement.

Due to the presence of the ductile metallic matrix, the MAS TiC reinforced coating exhibited 38-44% better resistance than the commercial Cr_3C_2-based material (Amperit) but worse than the reference SS powder (sprayed) and the bulk steel Hardox 400. The MAS Cr_3C_2-Ni reinforced coating did not demonstrate competitive wear resistance in abrasive-erosive testing due to its weak intersplat cohesion and low thickness.

The wear mechanisms of the experimental coatings are presented in Fig. 3.7. The common wear mechanism during the performed tests (ARWW and AEW) was microcutting (Paper III). For the coatings with the MAS TiC-containing reinforcement, the wear mechanism was a combination of the microcutting of the softer metallic matrix and the fragmentation of brittle carbide reinforcement. After the abrasion test, the wear

of the steel matrix was more intense compared to the carbide reinforcement (Fig. 3.7a). In some parts, carbide clusters formed surface pits (Fig. 3.7c).

At the composition with the MAS Cr_3C_2-containing reinforcement, the wear was similar to that of the MAS TiC reinforced coating (Fig. 3.7b). Under impact action of erodent particles, it had higher brittleness than its TiC-containing counterpart (Fig. 3.7d).
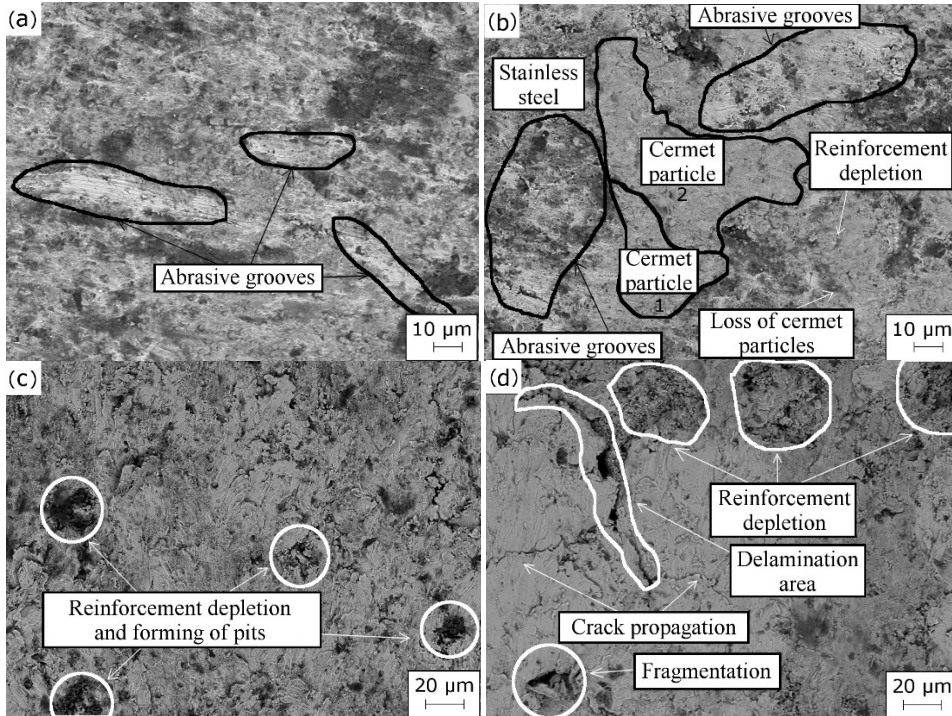
Figure 3.7 Topography of worn HVOFS surfaces after ARWW (a,b) and AEW (c, d): (a) TiC-NiMo + SS; (b) Cr_3C_2-Ni + SS; (c) TiC-NiMo + SS; (d) Cr_3C_2-Ni + SS.

3.3 PTAW and SAW hardfacings with MAS reinforcement

3.3.1 Microstructure and hardness

The microstructure of PTAW hardfacings with the MAS TiC-containing reinforcement is presented in Fig. 3.8.

It is notable that cermet particles are scattered more homogeneously in the Fe-based matrix (Fig. 3.8a) than in the Ni-based one (Fig. 3.8b), which may be related to their different melting temperatures (1400 °C vs. 1200 °C, respectively). The macrohardness of TiC reinforced hardfacings is given in Table 3.3, along with its Cr_3C_2-Ni-based counterparts.
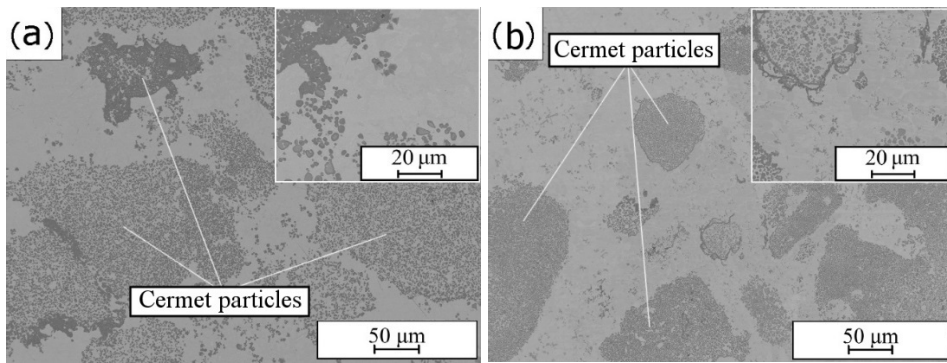
Figure 3.8 Microstructure of hardfacings with the MAS TiC-NiMo-containing reinforcement developed by PTAW: (a) TiC-NiMo + SS; (b) TiC-NiMo + NiCrSiB.

The presence of the following main phases was discovered during the XRD analysis of PTAW hardfacings with the MAS TiC-containing reinforcement: TiC, $Cr_{23}C_6$, nickel molybdenum and nonstoichiometric iron carbide in TiC-NiMo + SS (Fig. 3.9a) and Cr_3Ni, Cr_5B_3 and nonstoichiometric boron silicon carbide in TiC-NiMo + NiCrSiB (Fig. 3.9b). The presence of the TiC phase was not detected in the latter composition.
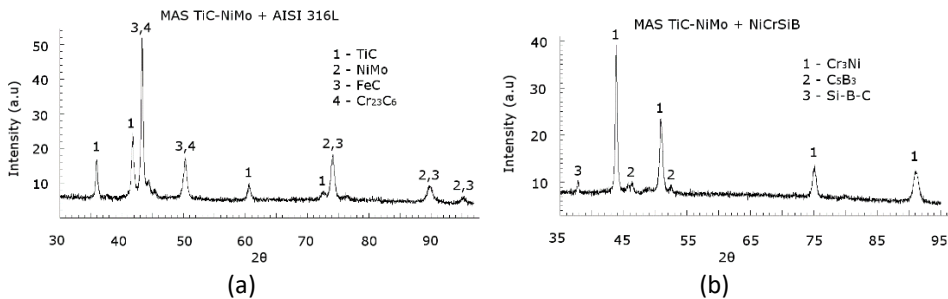
Figure 3.9 XRD patterns of the MAS TiC-containing PTAW hardfacings: (a) with the Fe-based matrix; (b) with the Ni-based matrix.

The microstructure of PTAW and SAW hardfacings with the MAS Cr_3C_2-containing reinforcement is shown in Fig. 3.10. PTAW hardfacings showed a typical structure for this type of claddings (Fig. 3.10a,b); however, the absence of the Cr_3C_2-Ni reinforcement was obvious in SAW hardfacings (Fig. 3.10c,d). Due to higher welding current, and thus the heat input used in SAW, the hard carbide phase dissolved in the hardfacing much more extensively (Paper II).
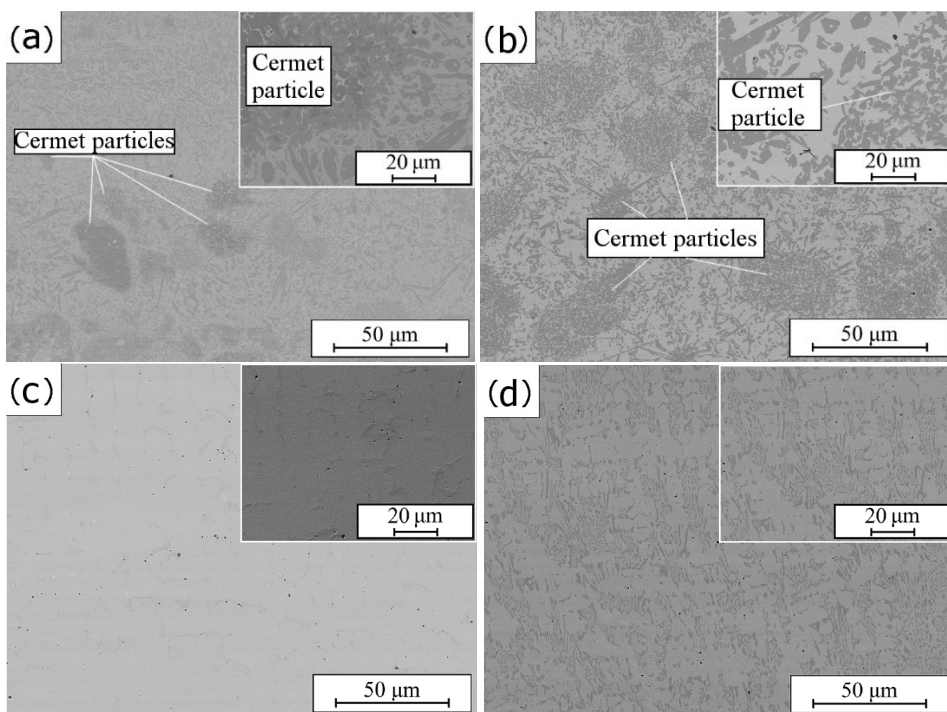
Figure 3.10 Microstructure of hardfacings with the MAS Cr_3C_2-containing reinforcement developed by PTAW (a,b) and SAW (c,d): (a) Cr_3C_2-Ni + SS; (b) Cr_3C_2-Ni + NiCrSiB; (c) Cr_3C_2-Ni + SS; (d) Cr_3C_2-Ni + NiCrSiB.

The phase composition of PTAW hardfacings with the Cr_3C_2-based MAS reinforcement is presented in Fig. 3.11. In the coating with the Fe-based matrix, there were two principal phases of austenite (γ-Fe) and Cr_7C_3 with a small amount of ferrite (α-Fe), while in the structure of the coating with the Ni-based matrix, primary Cr_3C_2 and Ni-based secondary $NiC_{0.22}$ carbides prevailed. SAW hardfacing with the Fe-based matrix comprised mostly solid solution α-Fe(Cr), Ni-rich retained austenite (γ-Fe), and a small amount of secondary carbide Cr_3C. SAW hardfacing with the Ni-based matrix contained predominantly different chromium carbides (CrC and Cr_3C_2) and some amount of austenite (γ-Fe).
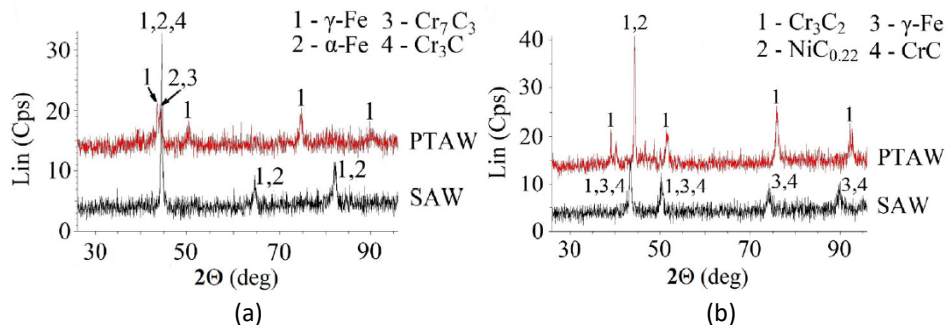
Figure 3.11 XRD patterns of the MAS Cr_3C_2-Ni-containing PTAW and SAW hardfacings: (a) with the Fe-based matrix; (b) with the Ni-based matrix (Paper II).

The macrohardness of PTAW hardfacings with the MAS TiC- and Cr_3C_2-containing reinforcements is given in Table 3.3. In this research, SAW hardfacings will not be further discussed due to their intrinsically inferior microstructure and phase composition with regard to the PTAW counterparts (Figs. 3.10 and 3.11).

Table 3.3. Vickers hardness of PTAW hardfacings and reference materials.

Type of hardfacing	Vickers hardness HV30
TiC–NiMo + SS	5.2 ± 0.4
TiC–NiMo + NiCrSiB	2.3 ± 0.2
Cr_3C_2–Ni + SS	3.8 ± 0.2
Cr_3C_2–Ni + NiCrSiB	4.1 ± 0.2
SS (Castolin)	1.7 ± 0.1
NiCrSiB (Castolin)	3.5 ± 0.3

The probable explanation of the highest increment of macrohardness in hardfacings with the Fe-based matrix is that the retained austenite underwent secondary martensitic transformation (secondary hardening). On the other hand, the drop of macrohardness in the TiC-NiMo + NiCrSiB hardfacing can be explained by the higher dissolution of the TiC-NiMo cermet in the metallic matrix due to their similar melting temperatures (1200–1300 °C) (Limin, et al., 2000, Ayyappan Susila & Arun, 2020).

After the MAS Cr_3C_2-containing reinforcement was introduced to pure SS and NiCrSiB PTAW hardfacings, their macrohardness increased by more than 2–3 times (SS matrix) and by 17% in the Cr_3C_2-Ni + NiCrSiB hardfacing.

3.3.2 Wear resistance and mechanisms

The wear resistance of the developed PTAW hardfacings and reference materials at the abrasive rubber wheel wear (ARWW) test is illustrated in Fig. 3.12.
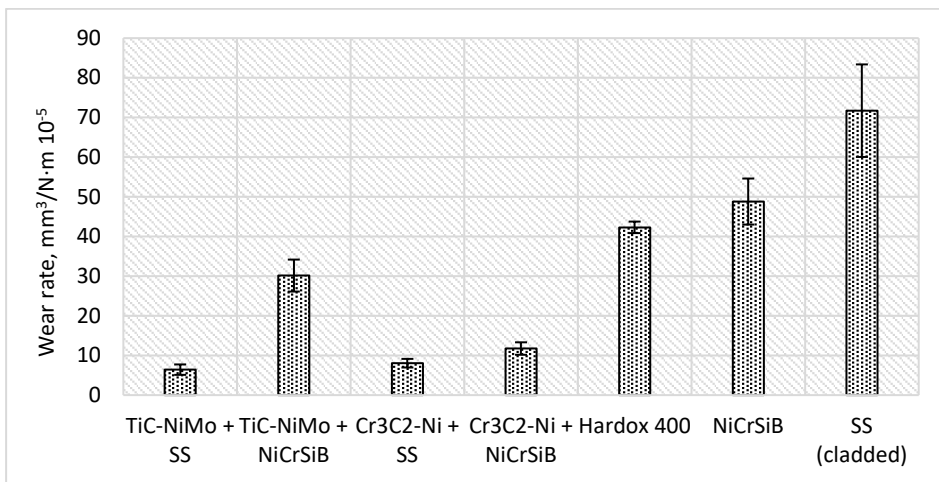
Figure 3.12 ARWW rates of PTAW hardfacings based on different matrix materials (Fe, Ni) and the MAS TiC- and Cr_3C_2-containing reinforcement.

As expected, in the abrasive rubber wheel wear test, the MAS reinforced hardfacings exhibited much lower wear rate than the unreinforced counterparts. Particularly, compositions with the added MAS TiC-containing reinforcement decreased the wear rate by 90% (for the Fe-based matrix) and 40% (for the Ni-based matrix). Despite the decreased macrohardness of the latter, it has demonstrated lower wear rate than the unreinforced hardfacing. The wear rate of the composition with the Ni-based matrix and the MAS Cr_3C_2-containing reinforcement was decreased by three times, while the Fe-based matrix hardfacing dropped its wear rate by nine times. A significant decrease of the latter is in direct correlation with its increased macrohardness (Table 3.3).

Abrasive-erosive wear (AEW) rates of the developed PTAW hardfacings and the reference materials under impact angles 30° and 90° are shown in Fig. 3.13. Experimental hardfacings with the MAS Cr_3C_2-containing reinforcement demonstrated nearly identical wear rate. Strict correlation between macrohardness (Table 3.3) and AEW was observed in the wear experiments under 30° impact angle. Furthermore, in a less intense erosive regime under low impact angle, which is intrinsically similar to the ARWW test, the wear of the experimental hardfacings was lower than that of unreinforced reference hardfacings (Fig. 3.13). Experimental hardfacings with the MAS Cr_3C_2-containing reinforcement demonstrated the same 20% lower absolute wear rate under 90° impact angle than under 30° angle, which is expected from metal-matrix type structures with 56–57 vol.% of the metallic phase.
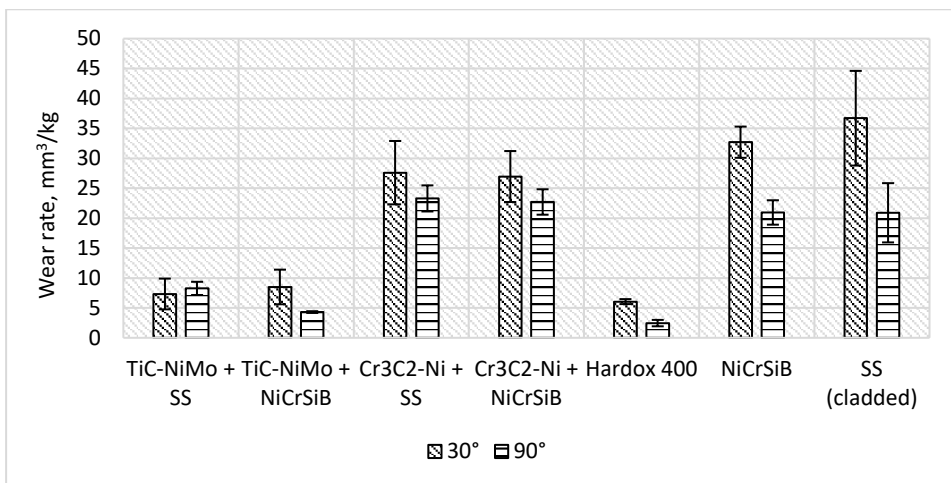
Figure 3.13 AEW rates of PTAW hardfacings based on different matrix materials (Fe, Ni) and MAS TiC- and Cr_3C_2-containing reinforcement.

At the erosive wear regime with a 90° impact angle, the experimentally obtained hardfacings with the MAS Cr_3C_2-containing reinforcement showed higher wear rate than their unreinforced counterparts. The most likely cause was that the the ductility had diminished by the presence of the brittle carbide phase (43–44 vol.%). As a result, the Cr_3C_2-Ni + SS hardfacing possessed the highest wear among the tested materials. All the experimentally developed hardfacings demonstrated the wear rate higher than that of the reference steel Hardox 400.

The worn surfaces of PTAW hardfacings with the MAS TiC- and Cr_3C_2-containing reinforcements after the ARWW test are depicted in Fig. 3.14. Microcutting was the

common wear mechanism for all MAS cermet reinforced hardfacings (Fig. 3.14). The wear mechanism of the TiC-NiMo + SS hardfacing was found to be more distinct than that of TiC-NiMo + NiCrSiB. Figure 3.14a depicts a singular cermet particle that had depleted more than 50% of its volume, whilst a similar cermet particle is seen to be completely holistic in Fig. 3.14b. Nevertheless, on a macroscale, the amount of these carbide clusters in the TiC-NiMo + NiCrSiB hardfacing is incomparably smaller (due to reasons discussed earlier) compared to TiC-NiMo + SS; thus, the overall wear rate of the former turned out to be much higher (Fig. 3.12). The other defects like insignificant cracks were common for both compositions.

Numerous abrasive grooves were spotted on the surface of hardfacings with the Cr_3C_2-based reinforcement, as silica particles were tackled by the soft metallic matrix, while some carbide particles were stripped off the cermets splats (Fig. 3.14c). Nevertheless, the latter remained integral, which signifies good bonding between them and the matrix. No signs of carbide spallation were found on the micrographs of the worn Cr_3C_2-Ni + NiCrSiB hardfacing. However, as compared to the Cr_3C_2-Ni + SS composition, the abrasive grooves were much more distinctive with more silica particles found in the vicinity. This may have decreased its abrasive wear rate, especially considering the explicit plasticity of the Ni-based matrix (Fig. 3.14d).
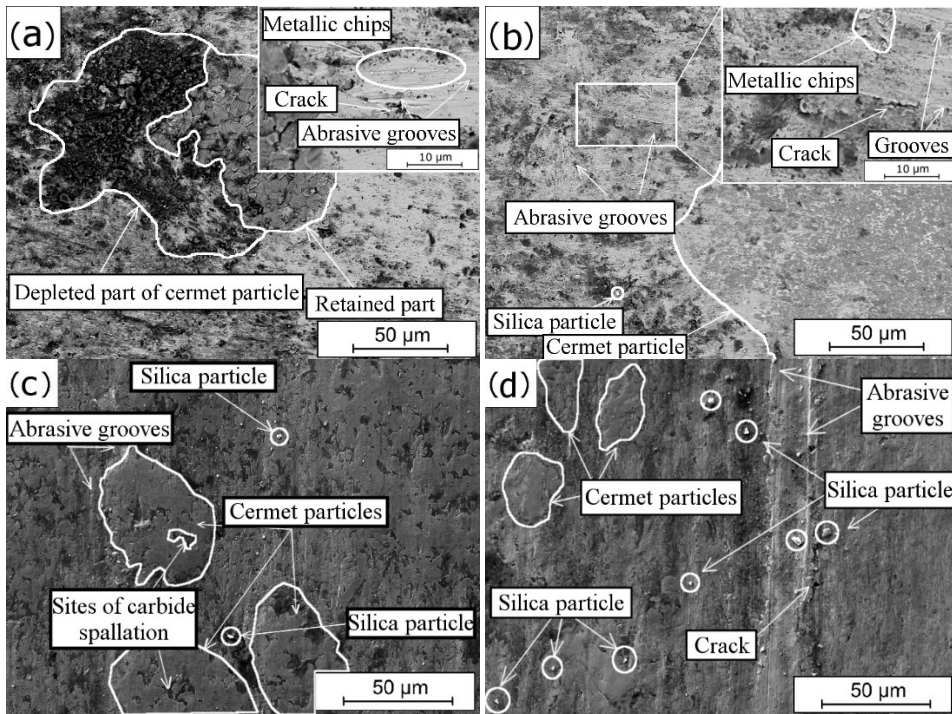
Figure 3.14 Topography of worn PTAW surfaces after ARWW: (a) TiC-NiMo + SS; (b) TiC-NiMo + NiCrSiB; (c) Cr₃C₂-Ni + SS; (d) Cr₃C₂-Ni + NiCrSiB.

The SEM images of AEW worn surfaces of experimental hardfacings with the MAS TiC- and Cr_3C_2-containing reinforcements are depicted in Fig. 3.15. Wear rates under 30° impact angle of almost all experimental hardfacings, except for TiC-NiMo + SS, were

higher than under 90° impact angle. Therefore, in Figure 3.15, the worn surfaces subjected to the abrasive-erosive test under 30° impact angle are depicted.
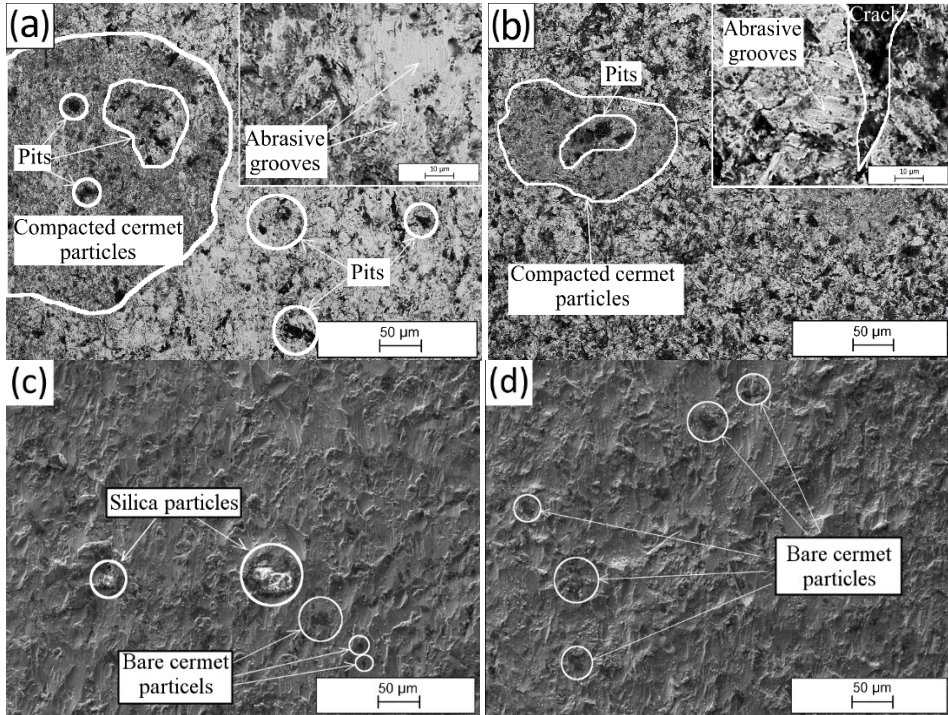
Figure 3.15 Topography of worn PTAW surfaces after AEW (30°): (a) TiC-NiMo + SS; (b) TiC-NiMo + NiCrSiB; (c) Cr_3C_2-Ni + SS; (d) Cr_3C_2-Ni + NiCrSiB.

The AEW mechanism of hardfacings with the TiC-NiMo reinforcement was microcutting, as a multitude of metallic chips were spotted along the abrasive groove lines left by erodent silica particles. However, in the hardfacings, no silica particles were observed to be stuck to the surface. In Fig. 3.15a and 3.15b, compacted carbide regions show visible pits formed due to the depletion of the brittle hard phase. In Fig. 3.15b (insertion),
a significant crack in the matrix material can be noticed. Its direction is perpendicular to the erosive groove lines, which may be a sign of internal stresses in the pre-surface layers of the TiC-NiMo + NiCrSiB hardfacing.

Similar wear products – the metallic chips - were observed on the micrographs of Cr_3C_2-Ni reinforced hardfacings to be present in great numbers on their surfaces, indicating that microcutting was the common wear mechanism (Fig. 3.15c,d). Additionally, some silica particles can be seen stuck to the surface of the Cr_3C_2-Ni + SS hardfacing (Fig. 3.15c). In the hardfacings with the MAS Cr_3C_2-containing reinforcement, some cermet particles scattered on the surface were found bare yet holistic. High impact angle (90°) testing regime imposes certain difficulties regarding observing of worn surfaces by means of SEM imaging. Nevertheless, the dominating wear mechanism at this wear condition was proved to be low-cycle fatigue (Kulu, et al., 2007).

4 Composite coatings and hardfacings with *in-situ* synthesized reinforcement

4.1 HVOFS coatings with *in-situ* synthesized reinforcement

4.1.1 Microstructure and hardness

The microstructure images of HVOFS coatings obtained from the mechanical mixtures Ti + C + SS and Cr + C + SS are presented in Fig. 4.1.
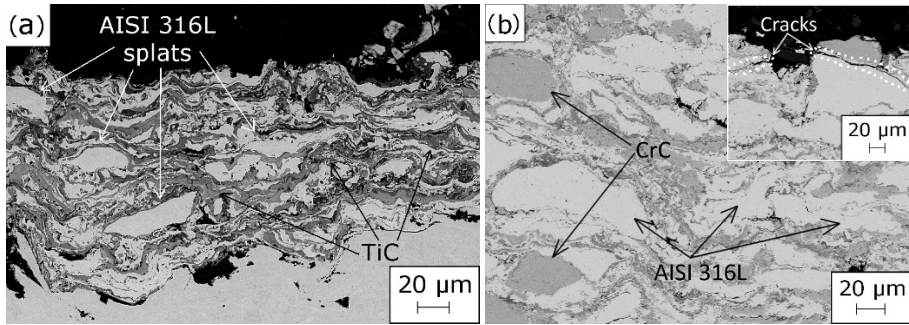
Figure 4.1 Cross-sectional SEM images of HVOFS coatings with in-situ synthesized reinforcement: (a) Ti + C + SS; (b) Cr + C + SS.

Generally, both coatings exhibited similar microstructure with different thickness: 100–130 µm in the TiC-containing coating and 250–280 µm of the CrC-containing coating (Table 4.1). However, the coating with the *in-situ* synthesized TiC reinforcement (Fig. 4.1a) consisted of swirled alternating layers of the Fe-based matrix and the TiC reinforcement with some amount of unmolten stainless steel particles, while the coating with the *in-situ* synthesized CrC reinforcement contained unmolten and slightly deformed Cr particles (Fig. 4.1b). Some cracks were discovered in the pre-surface area of this coating. Their presence indicates the decreased cohesion between the matrix and the reinforcement phases in the upper layers of the coating. The crack-forming mechanism, apparently, is similar to that in the MAS counterpart (see section 3.2).
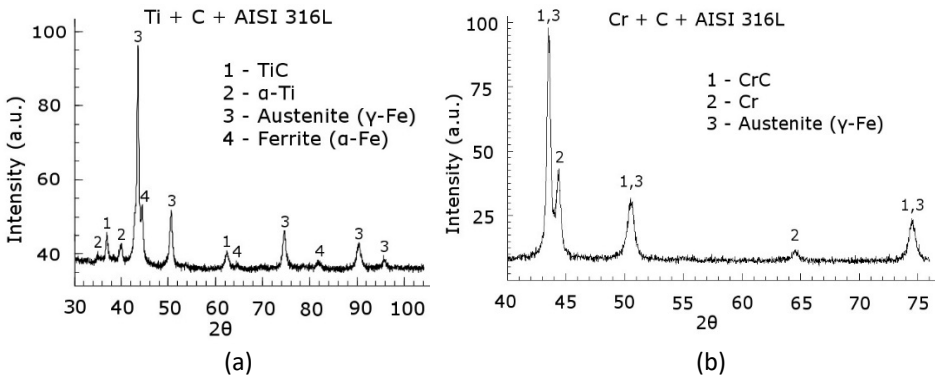
Figure 4.2 XRD patterns of HVOFS coatings with the in-situ synthesized reinforcement: (a) Ti + C + SS; (b) Cr + C + SS.

The X-Ray diffractograms of the coatings discussed above are presented in Fig. 4.2. The phase composition of the TiC-containing coating consisted of four main phases: TiC, α-Ti, austenite (γ-Fe), and ferrite (α-Fe) (Fig. 4.2a). The presence of the α-Ti phase is most likely the result of excessive burning out of carbon meant for bonding with Ti. Three principal phases were discovered in the CrC-containing coating: CrC, pure Cr and austenite (γ-Fe) (Fig. 4.2b). Similarly, during coating deposition, the burning out of carbon led to the abundance of unreacted Cr, which prevents forming of other reinforcement phases (Cr_3C_2, Cr_7C_3, etc.).

The microhardness values of the experimental coatings with the *in-situ* synthesized reinforcement are given in Table 4.1. Coating with the TiC-based reinforcement showed the difference between the microhardness on the surface and the cross-section of about 20%, which may be a sign of compromised structural uniformity. The surface and cross-sectional microhardness of the coating with CrC reinforcement was nearly similar to the microhardness of that obtained from stainless steel. It is caused by little presence of the hard carbide phase in the structure. The noticeable difference between the thickness of the Ti + C + SS and Cr + C + SS coatings apparently originates from the difference in the morphology of sprayed mechanical mixtures (Fig. 2.4), which, in turn, impacts their flowability: 49.2 ± 1 s and 39.1 ± 0.4 s, respectively.

Table 4.1. Average thickness and Vickers hardness of the HVOFS coatings with in-situ synthesized reinforcements (Paper III).

Type of coating	Thickness, (μm)	Vickers hardness HV	
		Surface	Cross-section
		HV1	HV0.3
Ti + C + SS	110 ± 20	4.0 ± 0.6	3.3 ± 0.7
Cr + C + SS	265 ± 15	3.4 ± 0.4	3.3 ± 0.4
Cr_3C_2-NiCr (Amperit)	263 ± 11	8.8 ± 1.0	9.2 ± 1.6
SS (Castolin)	203 ± 13	3.2 ± 0.4	3.1 ± 0.7

4.1.2 Wear resistance and mechanisms

The ARWW volumetric wear rates of coatings with the *in-situ* synthesized reinforcements are presented in Fig. 4.3.
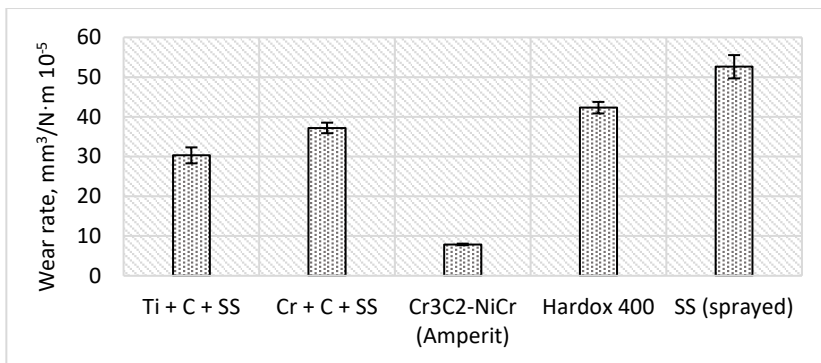
Figure 4.3 Comparison of ARWW rates of HVOFS coatings with the in-situ synthesized reinforcement.

In the abrasive wear testing, the TiC-containing coating demonstrated about 25% higher wear resistance than the CrC-containing counterpart due to higher percentage of the hard carbide phase (TiC 27 wt.%/34 vol.% *vs.* CrC 8 wt.%/9 vol.%) (Paper III). However, as compared to the commercial Cr_3C_2-based cermet coating with 53 wt.%/65 vol.% of hard phase, the experimental coatings with the *in-situ* synthesized reinforcement showed poor performance.
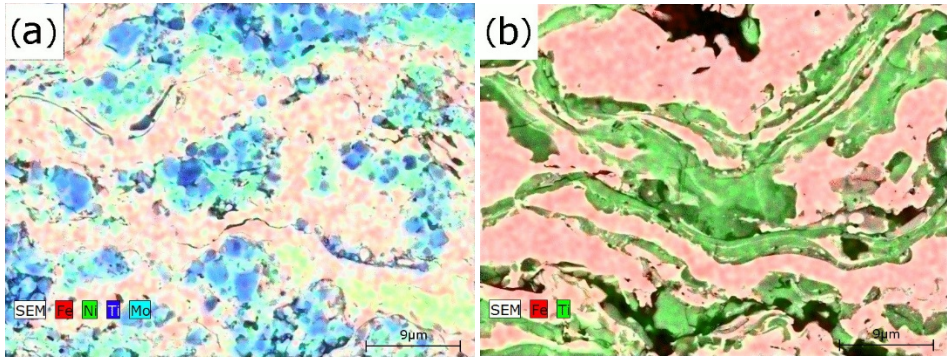
Figure 4.4 EDS maps of TiC-containing HVOFS coatings: (a) MAS TiC-NiMo + SS; (b) Ti + C + SS (Paper III).

MAS coating TiC–NiMo + SS (Fig. 4.4a) has fewer and smaller internal cracks and voids, and the distribution of its carbide particles appears to be more homogeneous than that of the lamellar structure of its counterpart (Fig. 4.4b). It is therefore suggested that these factors make the MAS coating more resistant to material loss under the abrasion.
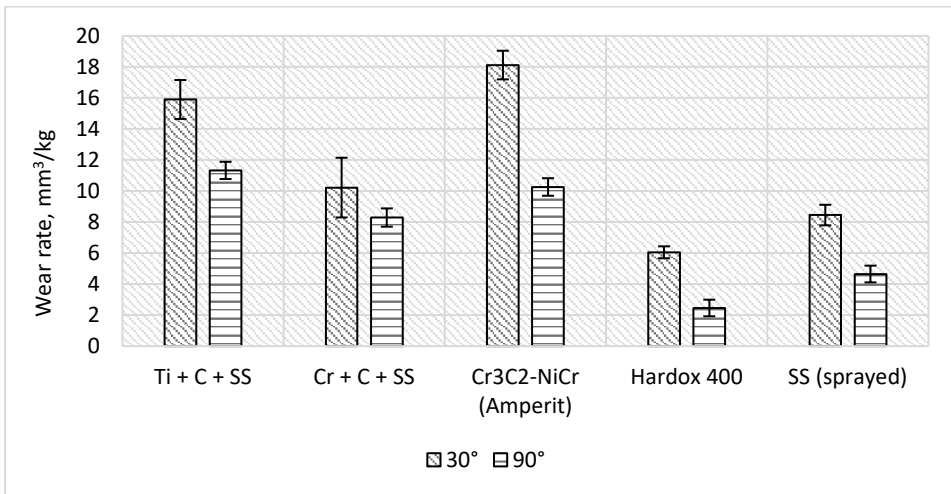
Figure 4.5 Comparison of AEW rates of HVOFS coatings with the in-situ synthesized reinforcement and reference materials.

The wear rates of HVOFS coatings with *in-situ* synthesized after the AEW testing under 30° and 90° impact angles are presented in Fig. 4.5. TiC-containing experimental coating demonstrated better performance than the commercial Cr_3C_2-based coating (Amperit)

under low impact angle, but not under 90° angle. The alienating of the entire layer of the commercial coating (and leaving bare steel substrate exposed to erodent particles) may be the reason why the Cr_3C_2-NiCr (with Cr_3C_2 58 wt.%/ 65 vol.%) commercial coating performed better under direct erodent impact than the experimental coating with only 27 wt.%/34 vol.% of TiC.

At the same time, the volumetric wear of the experimental CrC-containing coating turned out to be lower than that of the aforementioned commercial Cr_3C_2-containing counterpart under both impact angles. Nevertheless, as compared to reference steels SS (sprayed) and Hardox 400, the erosion wear rates of the experimental coatings were still significantly higher.

The wear mechanism of both coatings with the *in-situ* synthesized reinforcement (Fig. 4.6) resembled that of coatings with the MAS reinforcement (see section 3.2). After the ARWW and AEW tests, the rare depleted carbide clusters with scarce regions of delaminated (Fig. 4.6a) or fractured (Fig. 4.6b,c) matrix material were observed. Similar to the coatings with the MAS reinforcement, few silica inclusions were found embedded in the soft metallic matrix. This could slightly influence the post-testing weight results. Infrequent surface pits and cracks formed under the impact of erodent particles on carbide clusters with lower cohesion, while those with higher interparticle connections remained holistic (Fig. 4.6c,d).
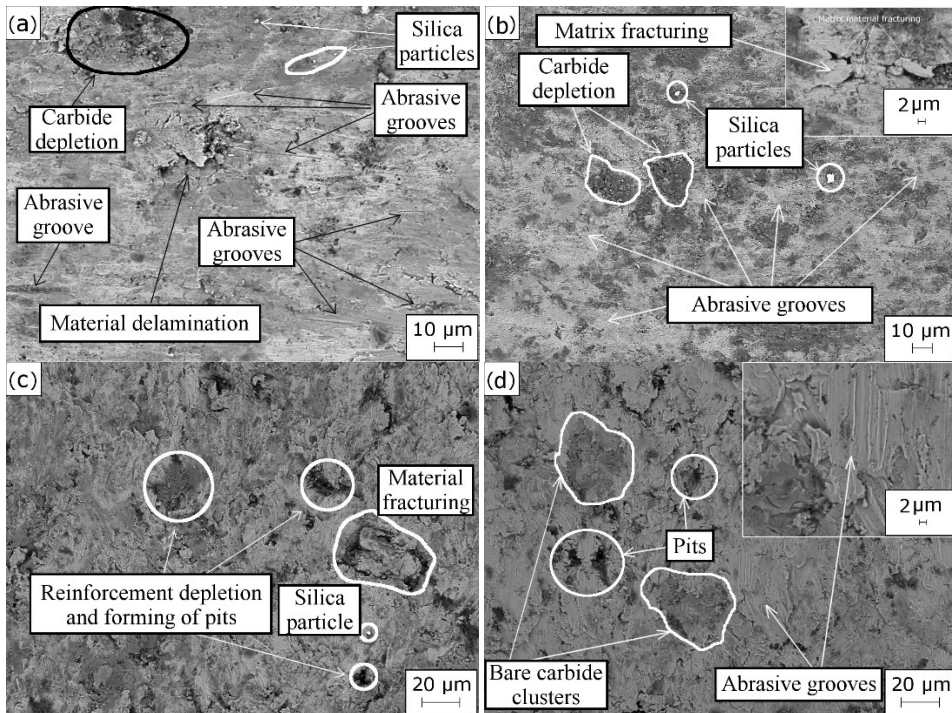
Figure 4.6 Topography of worn HVOFS surfaces after ARWW (a,b) and AEW (c,d): (a) Ti + C + SS; (b) Cr + C + SS; (c) Ti + C + SS; (d) Cr + C + SS.

4.2 PTAW hardfacings with *in-situ* synthesized reinforcement

4.2.1 Microstructure and hardness

The microstructure images of the obtained PTAW hardfacings with the *in-situ* synthesized reinforcement are shown in Fig. 4.7. The TiC reinforced hardfacing showed rather non-homogeneous microstructure with notable carbide-free regions (Fig. 4.7a). Carbon burn out most likely occurred during hardfacing deposition. This is additionally confirmed by gaseous porosity seen on the SEM images. On the contrary, the hardfacing with the chromium carbide (CrC) based reinforcement showed an eutectic structure with evenly distributed carbide grains (Fig. 4.7b). The hardfacing obtained from TiO_2 was observed to have pore-free structure with an insignificant amount of Ti- and Mo-based carbides precipitated at the grain boundaries (Fig. 4.7c). On the unmachined surface of this hardfacing, a plenitude of small-sized (less than 1 μm) carbides was observed (Fig. 4.7d). Therefore, all the carbide phases were likely to have concentrated in the thin upper layer due to their lower density and were afterwards removed by machining. For more detail see (Paper IV).
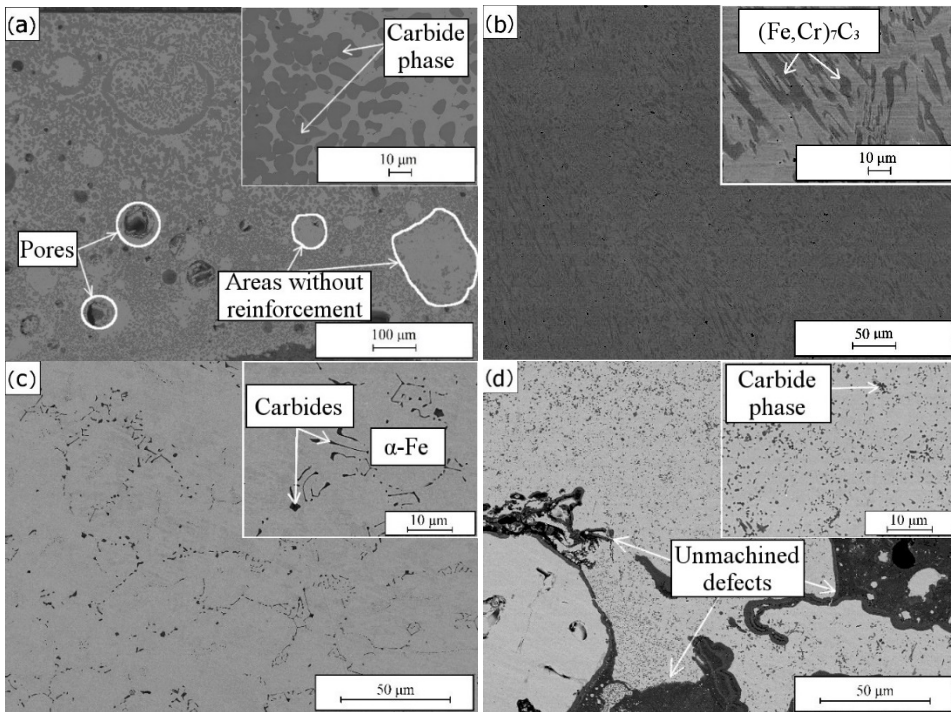
Figure 4.7 Microstructure of PTAW hardfacings with the in-situ synthesized reinforcement: (a) Ti + C + SS; (b) Cr + C + SS; (c) TiO₂ + C + SS; (d) TiO₂ + C + SS (unmachined) (Paper IV).

X-ray diffractograms of hardfacings with the *in-situ* synthesized TiC and CrC reinforcements are shown in Fig. 4.8. The phase analysis of hardfacings from Ti + C + SS and TiO_2 + C + SS mixtures showed some presence of TiC (9.9 wt.%) and (Ti,Mo)C (9.6 wt.%), respectively. However, the microstructure of the machined TiO_2 + C + SS sample comprised no carbide reinforcement phase and is not depicted in Fig. 4.8. The matrix of the Ti + C + SS hardfacing was mostly ferritic-austenitic. The main phases

were TiC, (Ti,Mo)C and chromium iron solid solution (Fig. 4.8a). Meanwhile, the *in-situ* synthesis of the CrC reinforcement (19.8 wt.%/23.5 vol.%) was confirmed during the deposition of Cr + C + SS. Other significant phases were Fe-Mn-C carbides and Ni-Mo-Cr solid solution (Fig. 4.8b). The matrix was austenitic due to remaining carbon after less complete reaction of precursor elements (Cr, C), as compared to Ti + C + SS.
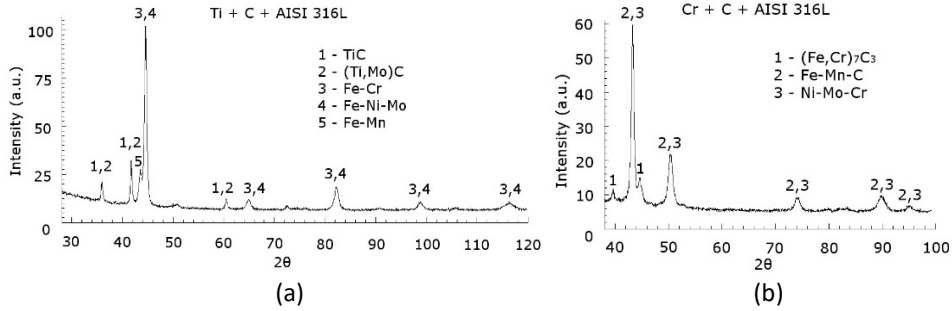
Figure 4.8 XRD patterns of PTAW hardfacings with the in-situ synthesized reinforcement: (a) Ti + C + SS; (b) Cr + C + SS.

Among the obtained hardfacings with the *in-situ* synthesized reinforcements, CrC-contained composition showed the highest hardness (Table 4.2), which was 16% and 60% higher than Ti- and TiO_2-containing counterparts, respectively, and 2.7 times higher than the hardfacing deposited from the unreinforced stainless steel powder. This difference between the welded hardfacings as well as relatively large deviation of the hardness values within the Ti + C + SS composition is apparently linked to the amount of the synthesized hard phase and its distribution across the each particular hardfacing.

Table 4.2. Vickers hardness of the PTAW hardfacings with the in-situ synthesized reinforcements (Paper IV).

Type of hardfacing	Vickers hardness HV30
Ti + C + SS	3.7 ± 0.6
TiO_2 + C + SS	2.7 ± 0.8
Cr + C + SS	4.3 ± 0.1
SS (Castolin)	1.6 ± 0.1

4.2.2 Wear resistance and mechanisms

The ARWW test results of PTAW hardfacings with the *in-situ* synthesized reinforcements and reference materials (cladded SS, Hardox 400) are presented in Fig. 4.9. The CrC-containing hardfacing exhibited slightly better wear resistance than its TiC-containing counterpart and is in direct correlation with the *in-situ* synthesized hard phase amount in these hardfacings. Both of them showed better wear resistance than the reference materials. Expectedly, TiO_2-containing machined hardfacing did not demonstrate any competitive wear resistance due to the concentration of carbides in the removed outer layer.
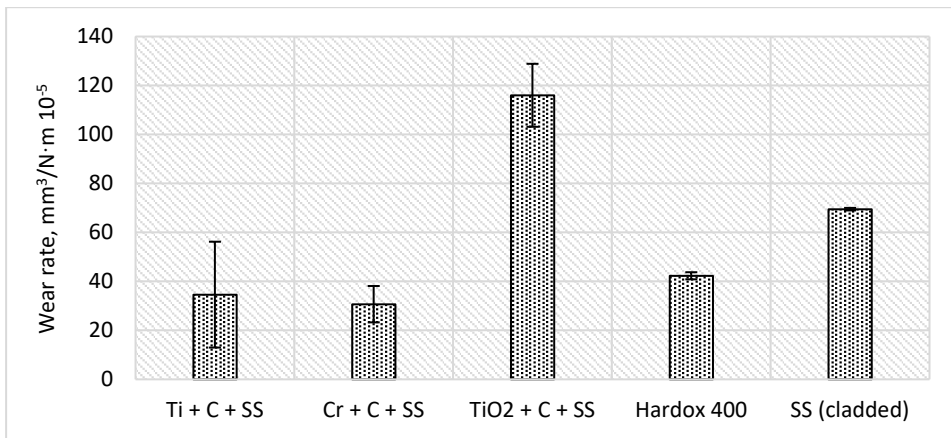
Figure 4.9 ARWW rates of PTAW hardfacings with the in-situ synthesized reinforcement and reference materials.

The results of AEW testing under 30° and 90° impact angles are presented in Fig. 4.10. It can be seen that under low impact angle, in terms of wear resistance, Ti + C + SS composition outperformed commercial reference steel Hardox 400 by around 13 % and exhibited similar wear resistance to the unreinforced SS result. Meanwhile, the Cr + C + SS hardfacing demonstrated slightly higher (~15 %) wear rate than Hardox 400 (30°, 90°) and the same wear rate as the unreinforced SS under 90° impact angle (Fig. 4.10).
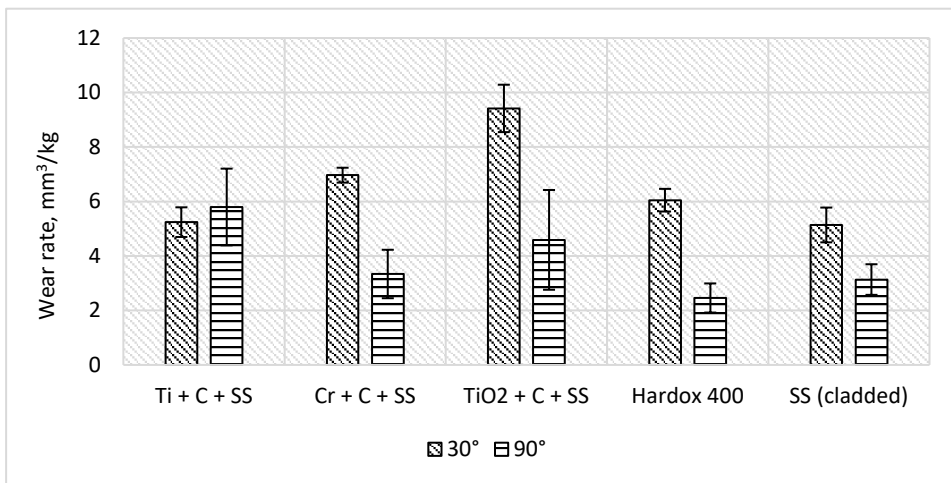
Figure 4.10 AEW rates of PTAW hardfacings with the in-situ synthesized reinforcement and reference materials.

The difference in the wear rates, especially under 90° impact angle, between the TiC- and CrC-containing hardfacings can be explained by the presence of ductile Ni- and Fe-rich solid solutions in the structure of the Cr + C + SS hardfacing. However, it demonstrated a significant gap between the wear rate in 30° and 90° impact angles, whilst Ti + C + SS exhibited practically identical wear resistance under both regimes.

Therefore, the latter is seen as a more well-balanced material, better suited to the abrasive-erosive wear under various conditions. Due to earlier discussed reasons, the demonstrated wear resistance of the TiO_2-containing deposition was not higher than that of bare substrate.

The wear mechanism micrographs of PTAW cladded hardfacings after the ARWW test are presented in Fig. 4.11. The principal wear mechanism of all the studied hardfacings was a combination of microcutting and microploughing. There are some metallic chips and abrasive grooves left by the abrasive particles, which can be seen on each SEM image. However, the grooves were much shallower in the case of the Ti + C + SS (Fig. 4.11a) and Cr + C + SS (Fig. 4.11b) hardfacings. Thus, the wear was less intense as compared to the hardfacing TiO_2 + C + SS. These results correlate with the corresponding phase analysis (Fig. 4.8) and wear rates (Fig. 4.9).
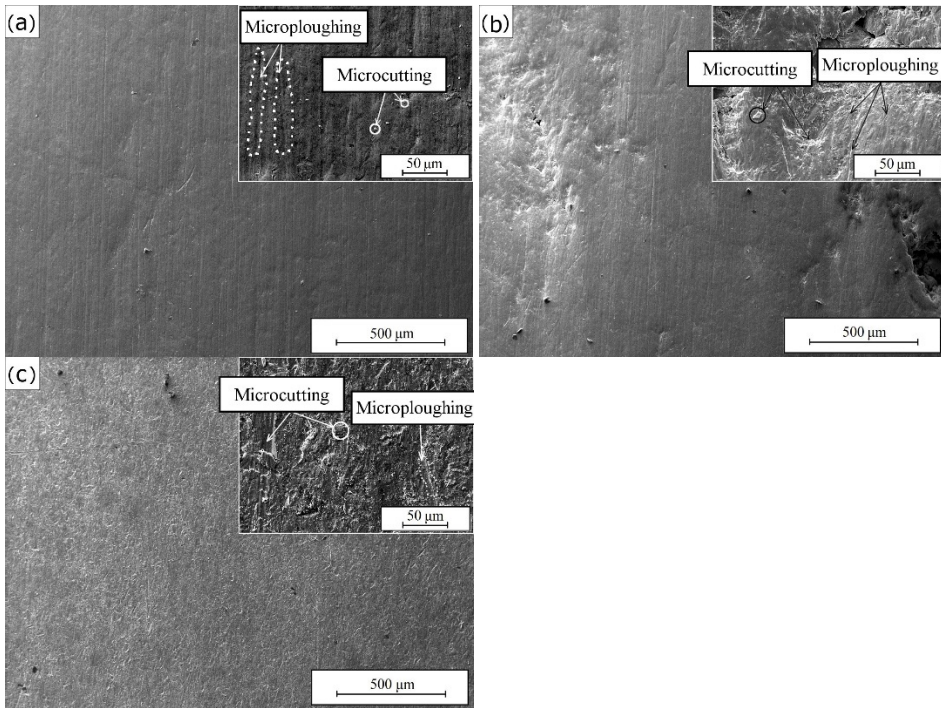
Figure 4.11 Topography of worn PTAW hardfacing surfaces after ARWW: (a) Ti + C + SS; (b) Cr + C + SS; (c) TiO_2 + C + SS (Paper V).

The SEM images of AEW-tested (impact angle 30°) PTAW hardfacings with the *in-situ* synthesized reinforcement are shown in Fig. 4.12. The common wear mechanism for all tested surfaces was microcutting. However, it was more pronounced in the case of CrC- and TiO_2-containing hardfacings, as some metallic particles were found scattered around (Fig. 4.12b,c). The hardfacing with the TiC reinforcement appeared to be less prone to forming defects, which is in strict correlation with the demonstrated wear rates (Fig. 4.10).

The common defects for all tested compositions (Fig. 4.12) were cracking and material depletion (removal). Additionally, on the Cr-based hardfacing, abrasive grooves caused by microploughing were observed (Fig. 4.12b). It is suggested that the depleted or

fractured areas of the tested hardfacings used to be clusters of carbide reinforcement, which were destroyed and alienated upon direct impact of silica particles that in some cases may be seen stuck in the vicinity (Fig. 4.12c).
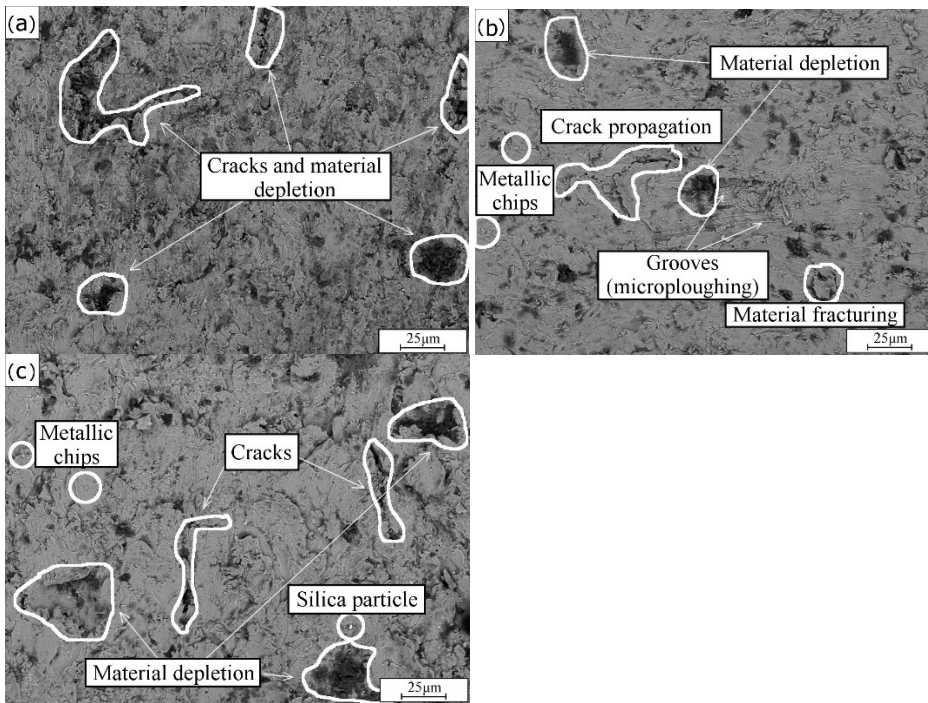
Figure 4.12 Topography of worn PTAW hardfacing surfaces after AEW (30°): (a) Ti + C + SS; (b) Cr + C + SS; (c) TiO$_2$ + C + SS.

5 Comparison of coating and hardfacing wear resistance

5.1 HVOFS coatings with MAS and *in-situ* synthesized reinforcement

Among all experimental coatings in the ARWW test, the MAS TiC-NiMo + SS coating exhibited the lowest wear rate (Fig. 5.1). It is, supposedly, linked to the highest amount of the hard carbide phase (TiC 38 wt.%/49 vol.%) obtained cumulatively after the synthesis of the respective cermet MAS powder and its subsequent high velocity spraying. It was shown that the performance of this composition is analogous to the commercial reference material Cr_3C_2-NiCr with much higher amount of the hard phase (58 wt.%/65 vol.%).
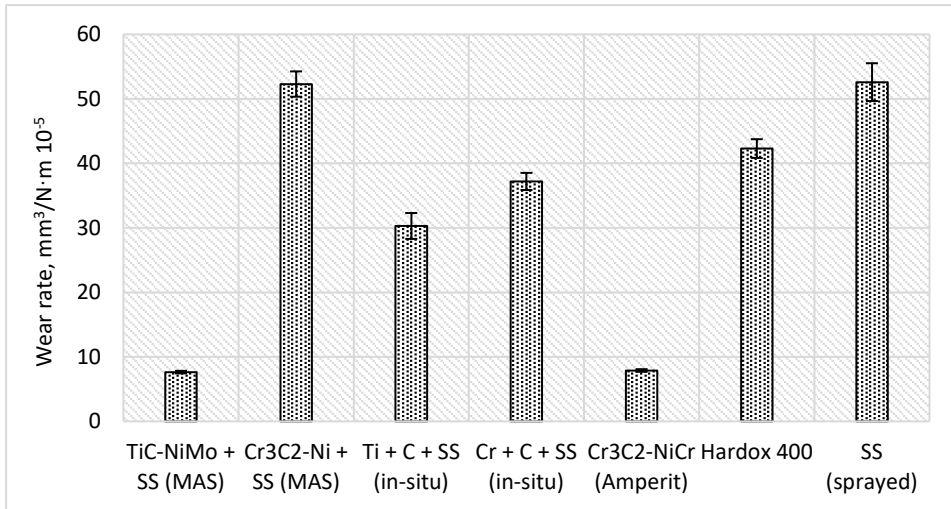
Figure 5.1 Comparison of ARWW rates of HVOFS coatings with the MAS and in-situ synthesized reinforcement.

In AEW testing at the impact angle 30°, MAS TiC-NiMo + SS showed the best performance as well (Fig. 5.2). It is followed by the Ti + C + SS coating with nearly 60% higher wear rate, which was caused by the smaller amount of TiC in its structure (27 wt.%/34 vol.%) (Paper III). The reason is unequal distribution of the metallic phase amount (51 vol.% in MAS TiC-NiMo + SS vs. 66 vol. % in Ti + C + SS), which has considerable influence on the wear resistance under 30° angle.

At normal impact angle (90°), coatings with the highest content of the ductile metallic phase expectedly demonstrated the lowest wear rate. Among the experimental coatings, the closest wear rate to the reference materials was exhibited by the MAS TiC-NiMo + SS and *in-situ* synthesized Cr + C + SS coatings, which both contained significantly lower amount of the hard phase.
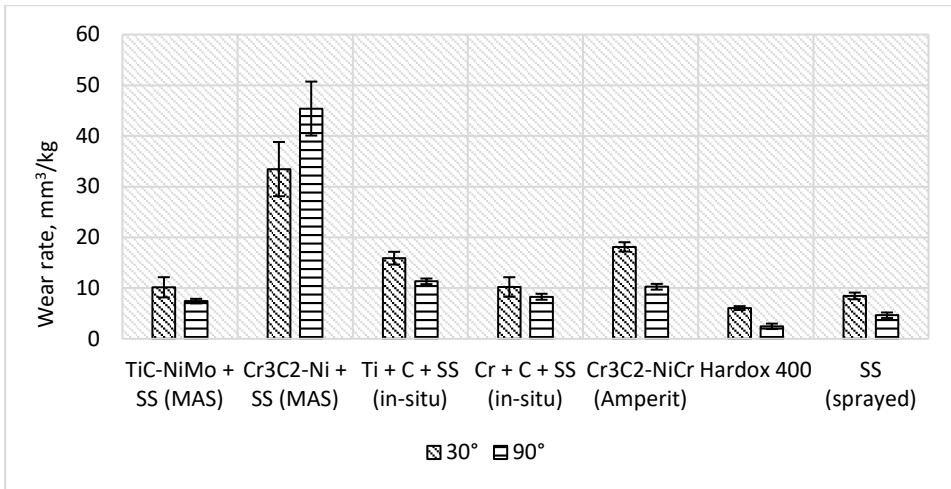
Figure 5.2 Comparison of AEW rates of HVOFS coatings with MAS and in-situ synthesized reinforcement.

5.2 PTAW hardfacings with MAS and *in-situ* synthesized reinforcement

The comparison of wear rates of PTAW MAS hardfacings and hardfacings with *in-situ* synthesized reinforcements are presented in Fig. 5.3. MAS TiC-NiMo + SS and Cr_3C_2-Ni + SS hardfacings demonstrated significantly lower wear rate of the material due to higher carbide content and multiple carbide phases present in the composition (see section 3.3) compared to Ti/Cr/ TiO_2 + C + SS hardfacings (see section 4.2). However, it was achieved using a longer and more expensive fabrication method, which, unlike the *in-situ* synthesis, includes multiple technological stages (see section 2.1).
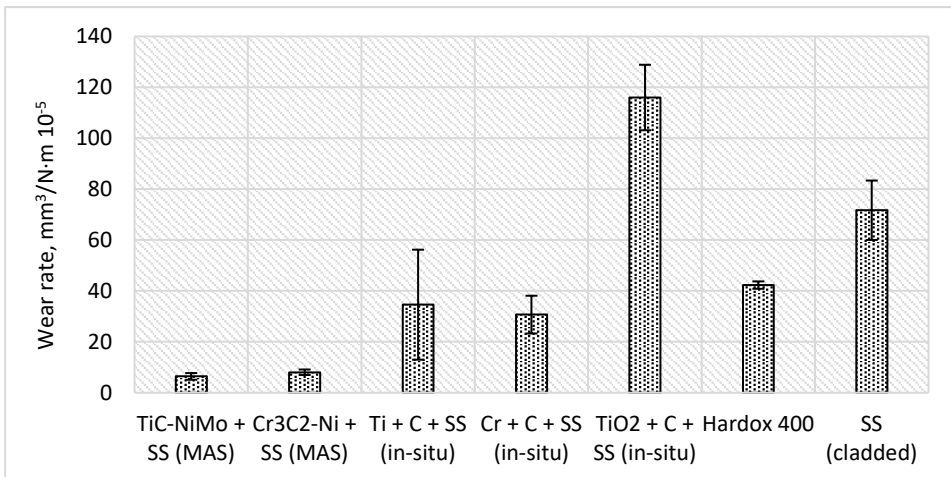
Figure 5.3 ARWW rates of PTAW hardfacings with the MAS and in-situ synthesized reinforcement.

In the abrasive-erosion wear testing under low impact angle (30°), the experimental PTAW hardfacing with the *in-situ* synthesized reinforcement Ti + C + SS revealed the lowest wear rate compared to the MAS TiC-NiMo + SS hardfacing (Fig. 5.4). Under 90° impact angle, the *in-situ* synthesized Cr + C + SS hardfacing demonstrated about 30% higher wear rate than the steel Hardox 400. Other experimental hardfacings with the *in-situ* synthesized reinforcement exhibited higher wear rate than Cr + C + SS. The least wear resistant was the TiC-NiMo + SS MAS hardfacing due to the highest content of brittle phases (Fig. 3.9a): TiC (30 wt.%/38 vol.%) and $Cr_{23}C_6$ (13 wt.%/11 vol.%). The MAS Cr_3C_2-Ni + SS hardfacing exhibited more than 9–11 times higher wear rate than the commercial steel Hardox 400 due to the reasons discussed earlier.
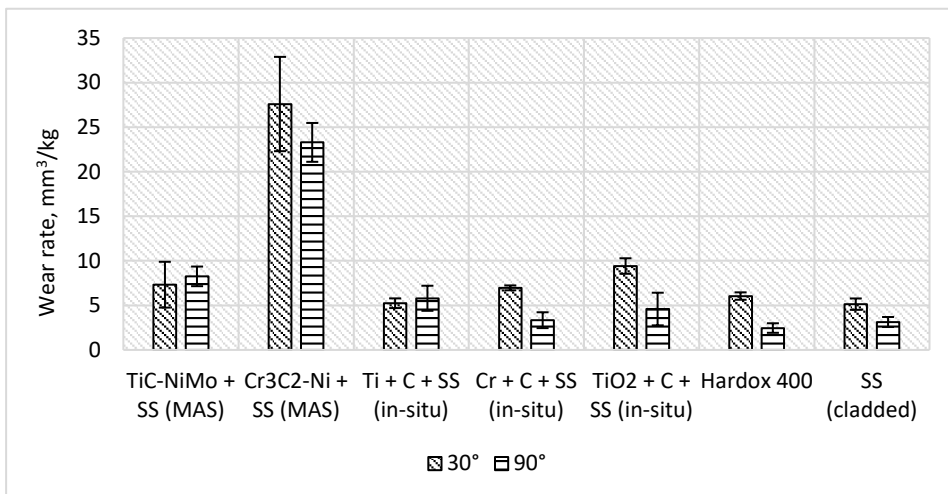
Figure 5.4 AEW rates of PTAW hardfacings with the MAS and in-situ synthesized reinforcement.

The wear rate of the MAS TiC-containing hardfacing higher than that of Hardox 400 in the AEW test is likely to be attributed to the higher matrix-to-reinforcement ratio, which is almost 1:1 (see section 3.3). It signifies the inability of the ductile metallic phase in its current amount to provide enough plasticity. Regarding to the MAS Cr_3C_2-Ni + SS hardfacing, due to the dominant presence of the brittle hard phase, it exhibited 4.5 times higher wear rate than the commercial ductile steel Hardox 400.

On the contrary, hardfacings with the *in-situ* synthesized TiC and CrC reinforcements contained a higher content of the metallic phase. Thus, under 30° impact angle, the TiC-containing hardfacing showed a wear resistance higher or similar to that of the Hardox 400 and SS hardfacing, respectively, while under 90° impact angle, hardfacing with the CrC reinforcement demonstrated a wear rate rather comparable to the SS cladded hardfacing.

5.3 Relative wear resistance

The relative wear of all experimental coatings/hardfacings under ARWW and AEW testing conditions is presented in Table 5.1. The reference material is the commercial steel Hardox 400.

Table 5.1. Relative wear resistance ε_v of experimental coatings/hardfacings under different testing condtions ($\varepsilon<1$ – poor; $\varepsilon>1$ – good).

Type of material ---------- Wear test	Ref. Hardox 400	HVOFS Com. Cr$_3$C$_2$-NiCr Amperit	HVOFS MAS TiC-NiMo + SS	HVOFS MAS Cr$_3$C$_2$-Ni + SS	HVOFS In-situ Ti + C + SS	HVOFS In-situ Cr + C + SS	PTAW MAS TiC-NiMo + SS	PTAW MAS Cr$_3$C$_2$-Ni + SS	PTAW In-situ Ti + C + SS	PTAW In-situ Cr + C + SS	PTAW In-situ TiO$_2$ + C + SS
ARWW	1	5.4	5.5	0.8	1.4	1.1	6.4	5.3	1.2	1.4	0.4
AEW (30°)	1	0.3	0.6	0.2	0.4	0.6	0.8	0.2	1.2	0.9	0.7
AEW (90°)	1	0.2	0.3	0.1	0.2	0.3	0.3	0.1	0.4	0.7	0.5

It can be concluded from Table 5.1 that experimental coatings and hardfacings may be recommended for application in abrasion conditions where they possess the highest relative wear resistance (5–6 times). Meanwhile, it was observed that the developed coatings and hardfacings, generally, were not suitable for erosion, except for PTAW hardfacings with the *in-situ* synthesized TiC and CrC reinforcements, which demonstrated wear resistance comparable to that of the reference materials.

6 Conclusions

In this study, abrasive wear resistant composite hardfacings with the *ex-situ* and *in-situ* synthesized carbide reinforcement were developed by the HVOFS (high velocity oxy-fuel spraying) and PTAW (plasma transferred arc welding) deposition technologies.

- Experimental coatings and hardfacings with the *in-situ* synthesized reinforcement showed 4–5 times greater wear rate in abrasion and similar or slightly lower material loss under the abrasion-erosion (under impact angles 30° and 90°) wear conditions compared to the counterparts with the *ex-situ* added (MAS) cermet reinforcement. This can be explained by domination of metallic phase in the structure of coatings and hardfacings with the *in-situ* synthesized reinforcement due to the excessive carbon burn out. This was the common shortcoming for both HVOFS and PTAW deposition technique whith regard to *in-situ* synthesis of carbide reinforcement.
- PTAW hardfacings with the Fe-based matrix exhibited 1.5-5 times higher wear resistance in abrasion and similar wear rate in the abrasion-erosion (except for TiC-containing composition with 49 vol.% of hard phase under 90° impact angle) wear conditions as compared to analogous hardfacings with the Ni-based matrix. Due to more extensive dissolution of the hard carbide phase, caused by higher operating current, SAW hardfacings did not demonstrate quality phase content and microstructure as compared to the PTAW counterparts and their wear resistance was not further assessed.
- HVOFS coatings and PTAW hardfacings with the *ex-situ* added reinforcement in abrasive wear demonstrated 5–6 times higher wear resistance than the reference steel Hardox 400 and are recommended for application in abrasion conditions.
- PTAW hardfacing with the *in-situ* synthesized TiC reinforcement was the only experimental composition that outperformed the reference steel Hardox 400 by 20% in the abrasive-erosive wear conditions under low (30°) impact angle. Among all the developed compositions, PTAW hardfacing with the *in-situ* synthesized CrC reinforcement showed the best wear resistance under normal (90°) impact angle.
- The wear mechanism dominating among all HVOFS coatings and PTAW hardfacings was the microcutting of the ductile metallic matrix paired with the removal of the brittle carbide phase, except for the PTAW hardfacings with the *in-situ* synthesized reinforcement (Ti/TiO_2/Cr + C + SS), in which microcutting was coupled with the microploughing wear mechanism.

The novelty of the present work can be outlined by:

- The synthesis with the preliminary mechanical activation (mechanically activated synthesis, MAS) of TiC-NiMo and Cr_3C_2-Ni cermet powders was improved to obtain powders for sprayed coatings or welded hardfacings in such

a way that mechanical grinding of the synthesized materials in a disintegrator is no longer necessary;

- Development of composite coatings/hardfacings with *in-situ* formation of hard phase;
- Wear resistance of metal-ceramic coatings/hardfacings with the *in-situ* synthesized titanium and chromium carbide-based reinforcement was compared under the conditions of abrasive and erosive wear;
- The wear resistance between the cermet coatings/hardfacings with the *ex-situ* and *in-situ* synthesized carbide reinforcement was compared under the conditions of abrasive and erosive wear.

In the future work, focus could be on the following:

- Further research and development of Ti- and Cr-containing PTAW hardfacings with *in-situ* synthesized reinforcement, which demonstrated competetive wear resistance in abrasion-erosion;
- Improvement of their abrasion resistance by minimizing the carbon burn out during deposition process.

References

Aikin Jr, R. (1997). The mechanical properties of in-situ composites. *JOM, 49*, 35-39. doi:https://doi.org/10.1007/BF02914400

All Answers Ltd. (2017, 08 31). *Aluminium Based Metal Matrix Composites*. Retrieved 11 19, 2020, from https://www.ukessays.com/essays/engineering/aluminium-based-metal-matrix-6811.php

AlMangour, B., Baek, M.-S., Grzesiak, D., & Lee, K.-A. (2018). Strengthening of stainless steel by titanium carbide addition and grain refinement during selective laser melting. *Materials Science & Engineering A, A 712*, 812-818. doi:https://doi.org/10.1016/j.msea.2017.11.126

Anciferov, V. N., Bobrov, G. V., Druzhinin, L. K., Kiparisov, S. S., Kostikov, V. I., Krupin, V. V., Roman, O. V. (1987). *Powder Metallurgy and Sprayed Coatings: A Textbook for Universities.* Moscow: Mettalurgy.

Arcraftplasma. (2016, 02 19). *What is PTA welding (Plasma Transferred Arc).* Retrieved 12 07, 2020, from http://arcraftplasma.blogspot.com/2016/02/what-is-pta-welding-plasma-transferred_63.html

ASTM International. (2016). ASTM G65-16e1, Standard Test Method for Measuring Abrasion Using the Dry Sand/Rubber. West Conshohocken, PA, USA: ASTM International.

ASTM International. (2020). ASTM B213-20, Standard Test Methods for Flow Rate of Metal Powders Using the Hall. West Conshohocken, PA, USA: ASTM International.

Ayyappan Susila, P., & Arun , A. (2020). Effect of nano-Al_2O_3 addition on the microstructure and erosion wear of HVOF sprayed NiCrSiB coatings. *Materials Research Express* (**7**). doi:https://doi.org/10.1088/2053-1591/ab5bda

Bach, F.-W., Möhwald, K., Laarmaan, A., & Wenz, T. (2004). *Modern Surface Technology.* Weinheim: WILEY-VCH Verlag GmbH & Co. KGaA.

Behera, M., Dougherty, T., & Singamneni, S. (2019). Conventional and Additive Manufacturing with Metal Matrix Composites: A Perspective. *Procedia Manufacturing, 30*, 159-166. doi:https://doi.org/10.1016/j.promfg.2019.02.023

Bendikiene, R., Ciuplys, A., Sertvytis, R., Surzhenkov, A., Tkachivskyi, D., Viljus, M., Kulu, P. (2020). Wear behaviour of Cr_3C_2–Ni cermet reinforced hardfacings. *Journal of Materials Research and Technology, 9*(4), 7068-7078. doi:https://doi.org/10.1016/j.jmrt.2020.05.042

Berger, L.-M. (2015). Application of hardmetals as thermal spray coatings. *Int. Journal of Refractory Metals and Hard Materials, 49*, 350-364. doi:https://doi.org/10.1016/j.ijrmhm.2014.09.029

Bertin, J. (1981). *Graphics and Craphic Information Processing.* Berlin: Walter de Gruiter.

Bolelli, G., Colella, A., Lusvarghi, L., Morelli, S., Puddu, P., Righetti, E., Testa, V. (2020). TiC–NiCr thermal spray coatings as an alternative to WC-CoCr and Cr_3C_2–NiCr. *Wear* (**450-451**). doi:doi.org/10.1016/j.wear.2020.203273

Chaudhari, R., & Bauri, R. (2018). A novel functionally gradient Ti/TiB/TiC hybrid composite with wear resistant surface layer. *Journal of Alloys and Compounds, 744*, 438-444. doi:https://doi.org/10.1016/j.jallcom.2018.02.058

Chávez, C., Dávila, J., Gutierrez, P., Mondragon, J., & Zambrano-Robledo, P. (2018). Tribological and microstructural behaviour in coatings applied using GTAW and HVOF (thermal spraying process) and used to recover AISI/SAE D2 grade tool steels. *Welding International, 32*(10), 660-666. doi:10.1080/09507116.2017.1347347

Corujeira Gallo, S., Alam, N., & O'Donnell, R. (2013). In-situ precipitation of TiC upon PTA hardfacing with grey cast iron and titanium for enhanced wear resistance. *Surface & Coatings Technology, 214*, 63-68. doi:http://dx.doi.org/10.1016/j.surfcoat.2012.11.003

Corujeira Gallo, S., Alam, N., & O'Donnell, R. (2013). In-situ synthesis of titanium carbides in iron alloys using plasma transferredarc welding. *Surface & Coatings Technology, 225*, 79-84. doi:http://dx.doi.org/10.1016/j.surfcoat.2013.03.019

Davis, E. (2004). *Handbook of Thermal Spray Technology.* ASM International.

Davis, J. R. (2001). *Surface Engineering: for corrosion and wear resistance.* ASM International.

Deng, D., Zhang, L., Niu, T., Liu, H., & Zhang, H. (2015). Microstructures and Wear Performance of PTAW Deposited Ni-Based Coatings with Spherical Tungsten Carbide. *Metals, 5*, 1984-1996. doi:doi:10.3390/met5041984

Dev Srivyas, P., & Charoo, M. (2018). Role Of Reinforcements On The Mechanical And Tribological Behavior Of Aluminum Metal Matrix Composites – A Review. *Materials Today: Proceedings, 5*, 20041-20053.

Dow, B., & Macadangdang, M. (2020, 03 11). *World Bank Commodity Price Data (The Pink Sheet).* Retrieved 11 23, 2020, from http://pubdocs.worldbank.org/en/561011486076393416/CMO-Historical-Data-Monthly.xlsx

Emamian, A., Corbin, S., & Khajepour, A. (2012). Tribology characteristics of in-situ laser deposition of Fe-TiC. *Surf. Coat. Technol., 206*, 4495–4501. doi:https://doi.org/10.1016/j.surfcoat.2012.01.051

Engelberg, D. (2010). 2.06 - Intergranular Corrosion. In B. Cottis, M. Graham, R. Lindsay, S. Lyon, T. Richardson, D. Scantlebury, & H. Stott (Eds.), *Shreir's Corrosion* (pp. 810-827). Manchester: Elsevier. doi:https://doi.org/10.1016/B978-044452787-5.00032-9

Eyre, T. (1976). Wear Characteristics of Materials. *Tribology International, 10*, 203-212.

Fayyaz, A., Muhamad, N., & Sulong, A. (2018). Investigation on feedstock preparation for microcemented carbide injection molding. *Powder Metallurgy Progress, 18*(2), 96-102. doi:http://dx.doi.org/10.1515/pmp-2018-0010

Ferdinandov, N., & Gospodinov, D. (2020). Hardfacing of metal-cutting tools by arc welding in vacuum. *Journal of Achivments in Materials and Manufacturing Engineering, 99*(2), 49-56. doi:https://doi.org/10.5604/01.3001.0014.1775

Franke, S. (2019). *Gießerei Lexikon 2019 (In German)* (1 ed.). Schiele & Schön.

Gallo, S., Alam, N., & O'Donnell, R. (2013). In Situ Synthesis of TiC-Fe Composite Overlays from Low Cost TiO_2 Precursors Using Plasma Transferred Arc Deposition. *J. Therm. Spray Technol., 23*, 551-556. doi:https://doi.org/10.1007/s11666-013-0052-3

García-Vázquez, F., Hernández-García, H., Vargas-Arista, B., Aguirre, A., & Granda-Gutiérrez, E. (2014). Influence of Cr and Nb on the Overlay Deposited on D2 Steel by Plasma Transferred Arc Process. *Materials Science Forum 793*, 11-16. doi:10.4028/www.scientific.net/msf.793.11

GOST 23.201-78 Standard. (1987). Products Wear Resistance Assurance, Gas Abrasive Wear Testing of Materials and Coatings with Centrifugal Accelerator. Moscow, Russia: Publishing House of Standards.

International Organization for Standardization. (2018). ISO 6507-1. Geneva, Switzerland: International Organization for Standardization.

Jones, M., Horlock, A., Shipway, P., McCarthney, D., & Wood, J. (2001). A comparison of the abrasive wear behaviour of HVOF sprayed titanium carbide- and titanium boride-based cermet coatings. *Wear, 251*, 1009–1016.

Juhani, K. (2009). Reactive Sintered Chromium and Titanium Carbide-Based Cermets: PhD Thesis. Tallinn: Tallinn University of Technology.

Karaoglanli, A., Oge, M., Doleker, K., & Hotamis, M. (2017). Comparison of tribological properties of HVOF sprayed coatings with different composition. *Surface & Coatings Technology, 318*, 299-308. doi:http://dx.doi.org/10.1016/j.surfcoat.2017.02.021

Kennametal Inc. (2013). *Plasma Transfer Arc Machine. Stellite™ Professional Surfacing Overview.* Retrieved 12 07, 2020, from http://www.interweld.com.au/images/PTA_Literature.pdf

Khalili, A., Goodarzi, M., Mojtahedi, M., & Torkamany, M. J. (2016). Solidification microstructure of in-situ laser-synthesized Fe-TiC hard coating. *Surface & Coatings Technology, 307*, 747-752.

Kim, Y.-I., An, G., Lee, W., Jang, J., Park, B.-G., Jung, Y.-G., Koc, S.-H. (2017). In-situ fabrication of TiC-Fe$_3$Al cermet. *Ceramics International*, *43*, 5907-5913. doi:http://dx.doi.org/10.1016/j.ceramint.2017.01.078

Kulu, P., Veinthal, R., Saarna, M., & Tarbe, R. (2007). Surface fatigue processes at impact wear of powder materials. *Wear* (**263**), 463-471. doi:doi:10.1016/j.wear.2006.11.033

Kulu P., Tarbe, R., Saarna, M., Surzenkov, A., Peetsalu, P., & Talviste, K. (2015). Wear resistance and selection of steels, hardmetals and hardfacings for abrasive wear conditions. *International Journal of Microstructure and Materials Properties*, **10**(2), 101-113. doi: https://doi.org/10.1504/IJMMP.2015.068718

Kumar Koli, D., Agnihotri, G., & Purohit, R. (2015). Advanced Aluminium Matrix Composites: The Critical Need of Automotive and Aerospace Engineering Fields. *Materials Today: Proceedings, 2*, 3032-3041. doi:doi: 10.1016/j.matpr.2015.07.290

Kübarsepp, J., & Juhani, K. (2020). Cermets with Fe-alloy binder: A review. *International Journal of Refractory Metals & Hard Materials, 92*. doi:https://doi.org/10.1016/j.ijrmhm.2020.105290

Laskowski, J. (2017). Increase of Lifetime and Screening Results by Advanced Hardfacing Technologies. Rome. doi:http://doi.org/10.11159/mmme17.141

Lazić, V., Arsić, D., Mutavdžić, M., Nikolić, R., Meško, J., Radović, L., & Ilić, N. (2018). Review of the hard-facing technology application for reparation of the given parts in various branches of industry. *Sciendo, 1*(1), 279-285. doi:http://doi.org/10.2478/mape-2018-0035

Liang, X., Shang, J., Chen, Y., Zhou, Z., Zhang, Z., & Xu, B. (2018). Influence of ceramic particles and process parameters on residual stress of flame-sprayed Fe-based coatings. *Surface and Coatings Technology, 354*, 10-17. doi:https://doi.org/10.1016/j.surfcoat.2018.08.069

Limin, C., Walter, L., Peter, E., Klaus, D., Hans W., D., & Dieter, K. (2000). Fundamentals of liquid phase sintering for modern cermets and functionally graded cemented carbonitrides (FGCC). *Refractory Metals & Hard Materials*(**18**), 307-322. Retrieved from https://publik.tuwien.ac.at/files/publik_291459.pdf

Liu, H., & Huang, J. (2005). Reactive thermal spraying of TiC-Fe composite coating by using asphalt as a carbonaceous precursor. *J. Mater. Sci., **40***, 4149–4151. doi:https://doi.org/10.1007/s10853-005-2564-9

Liu, X.-B., & Gu, Y.-J. (2006). Plasma jet clad γ/Cr_7C_3 composite coating on steel. *Materials Letters, **60***, 577-580. doi:10.1016/j.matlet.2005.09.04

Liu, Y.-F., Xia, Z.-Y., Han, J.-M., Zhang, G.-L., & Yang, S.-Z. (2006). Microstructure and wear behavior of $(Cr,Fe)_7C_3$ reinforced composite coating produced by plasma transferred arc weld-surfacing process. *Surface & Coatings Technology, **201***, 863-867. doi:10.1016/j.surfcoat.2005.12.048

Lombardi, J., Hoffman, R., Waters, J., Popovich, D., Souvignier, C., & Boggavarapu, S. (1997). Issues Associated with EFF & FDM Ceramic Filled Feedstock Formulation. *Proceedings Solid Freeform Fabrication Symposium* (pp. 457-464). Austin: University of Texas at Austin.

Mercado Rojas, J., Wolfe, T., Fleck, B., & Qureshi, A. (2018). Plasma transferred arc additive manufacturing of Nickel metal matrix composites. *Manufacturing Letters, **18***, 31-34. doi:https://doi.org/10.1016/j.mfglet.2018.10.001

Mitsubishi Materials. (2020). *Cutting Tool Materials*. Retrieved 11 2020, 22, from http://www.mitsubishicarbide.net/contents/mht/enuk/html/product/technical_information/information/sessaku.html

Mohapatra, J., Nayak, S., & Mahapatra, M. (2020). Mechanical and tribology properties of Al-4.5%Cu-5%TiC metal matrix composites for light-weight structures. *International Journal of Lightweight Materials and Manufacture, **3***, 120-126. doi:https://doi.org/10.1016/j.ijlmm.2019.09.004

Narayanasamy, P., Selvakumar, N., & Balasundar, P. (2018). Effect of weight percentage of TiC on their tribological properties of magnesium composites. *Materials Today: Proceedings, **5***, 6570-6578.

Noria Corporation. (2018). *Common Causes of Machine Failures*. Retrieved 12 13, 2020, from https://www.machinerylubrication.com/Read/29331/machine-failure-causes

Ozerov, M., Klimova, M., Vyazmin, A., Stepanov, N., & Zherebtsov, S. (2017). Orientation relationship in a Ti/TiB metal-matrix composite. *Materials Letters, **186***, 168-170. doi:http://dx.doi.org/10.1016/j.matlet.2016.09.124

Postle Industries, Inc. (2020). *Guidelines For Applying Hardfacing Alloys.* Retrieved 12 05, 2020, from http://hardfacetechnologies.com/postle_hft_btsp/pdfs/guidelines-for-applying-hardfacing-alloys.pdf

Pradeep, C., Ramesh, A., & Durga Prasad, B. (2010). A Review Paper on Hardfacing Processes and Materials. *International Journal of Engineering Science and Technology, **2***(11), 6507-6510.

Qu, X., Wang, F., Shi, C., Zhao, N., Liu, E., He, C., & He, F. (2018). In situ synthesis of a gamma-Al_2O_3 whisker reinforced aluminium matrix composite by cold pressing and sintering. *Materials Science & Engineering, A **709***, 223-231. doi:http://dx.doi.org/10.1016/j.msea.2017.10.063

Rao, V., Ramanaiah, N., & Sarcar, M. (2016). Tribological properties of Aluminium Metal Matrix Composites (AA7075 Reinforced with Titanium Carbide (TiC) Particles). *International Journal of Advanced Science and Technology, **88***, 13-26. doi:http://dx.doi.org/10.14257/ijast.2016.88.02

Rawal, S. (2001). *Metal-Matrix Composites for Space Applications*. Retrieved 11 19, 2020, from https://www.tms.org/pubs/journals/JOM/0104/Rawal-0104.html

Saha, M., & Das, S. (2016). A Review on Different Cladding Techniques Employed to Resist Corrosion. *Journal of the Association of Engineers, 86*(1 & 2), 51-63.

Sarjas, H. (2016). *Novel Synthesized and Milled Carbide-based Composite Powders for HVOF Spray:* PhD Thesis. Tallinn: Tallinn University of Technology.

Sarjas, H., Kulu, P., Juhani, K., & Vuoristo, P. (2014, 16th–18th of June). Novel WC-Co spray powders and HVOF sprayed coatings on their bases. *Proceedings of the 28th International Conference on Surface Modification Technologies*, 35-42.

Sarjas, H., Kulu, P., Juhani, K., Viljus, M., Matikainen, V., & Vuoristo, P. (2016). Wear resistance of HVOF sprayed coatings from mechanically activated thermally synthesized Cr_3C_2–Ni spray powder. *Materials Engineering, 2*(65), 101-106.

Sexton, C. (2015). *Hardfacing: traditional versus laser.* Bishopstown: Melbourne Business Park. Retrieved from https://laserage.eu/wp-content/uploads/2017/03/Hardfacing-Traditional-vs-Laser-LaserAge-Ltd-1.pdf

Shih, S. A. (2015). Towards and Interactive Learning Approch in Cybersecurity Education. *Proceedings of the 2015 Information Security Curruculum Development Conference* (p. 11). New York: SCM.

Simson, T., Kulu, P., Surženkov, A., Ciuplys, A., Viljus, M., & Zaldarys, G. (2018). Comparison of Plasma Transferred Arc and Submerged Arc Welded Abrasive Wear Resistant Composite Hardfacings. *Materials Science (Medžiagotyra), 24*(2), 172-176. doi:http://dx.doi.org/10.5755/j01.ms.24.2.19121

SteelBenchmarker™. (2020, 12 30). *Price History: Tables and Charts.* Retrieved 01 02, 2021, from http://steelbenchmarker.com/files/history.pdf

Sun, X., Yang, J., & Chen, S. (2019). Microstructure evolution and mechanical properties of in-situ bimodal TiC-Fe coatings prepared by reactive plasma spraying. *Ceram. Int., 45*, 5848–5857. doi:https://doi.org/10.1016/j.ceramint.2018.12.051

Surzhenkov, A., Antnov, M., Goljandin, D., Vilgo, T., Mikli, V., Viljus, M., Kulu, P. (2013). Sliding wear of TiC-NiMo and Cr_3C_2-Ni cermet particles reinforced FeCrSiB matrix HVOF sprayed coatings. *Estonian Journal of Engineering, 19*(3), 203-211. doi:doi: 10.3176/eng.2013.3.03

Surzhenkov, A., Goljandin, D., Traksmaa, R., Viljus, M., Talviste, K., Aruniit, A., Kulu, P. (2015). High Temperature Erosion Wear of Cermet Particles Reinforced Self-Fluxing Alloy HVOF Sprayed Coatings. *Materials Science (Medžiagotyra), 21*(3), 386-390. doi:dx.doi.org/10.5755/j01.ms.21.3.7617

Zhang, Z., Chen, Y., Zhang, Y., Gao, K., Zuo, L., Qi, Y., & Wei, Y. (2017). Tribology characteristics of ex-situ and in-situ tungsten carbide particles reinforced iron matrix composites produced by spark plasma sintering. *Journal of Alloys and Compounds,704*, 260-268. doi:http://dx.doi.org/10.1016/j.jallcom.2017.02.003

Zikin, A., Antonov, M., Hussainova, I., Katona, L., & Gavrilovic, A. (2013). High temperature wear of cermet particle reinforced NiCrBSi hardfacings. *Tribology International, 68*, 45-55. doi:http://dx.doi.org/10.1016/j.triboint.2012.08.013

Zikin, A., Hussainova, I., Katsich, C., Badisch, E., & Tomastik, C. (2012). Advanced chromium carbide-based hardfacings. *Surface & Coatings Technology, 206*, 4270–4278. doi:https://doi.org/10.1016/j.surfcoat.2012.04.039

Zikin, A., Ilo, S., Hussainova, I., Katsich, C., & Badisch, E. (2012). Plasma Transferred ARC (PTA) Hardfacing of Recycled Hardmetal Reinforced Nickel-matrix Surface Composites. *Materials Science (Medžiagotyra), 18*(1), 12-17. doi:http://dx.doi.org/10.5755/j01.ms.18.1.1334

The Welding Insitute, TWI. (2020). *What Is Hardfacing?* Retrieved 27 11, 2020, from https://www.twi-global.com/technical-knowledge/faqs/faq-what-is-hardfacing

Wang, H., Yan, X., Zhang, H., Gee, M., Zhao, C., Liu, X., & Song, X. (2019). Oxidation-dominated wear behaviors of carbide-based cermets: A comparison between WC-WB-Co and Cr_3C_2-NiCr coatings. *Ceramics International, 45*, 21293-21307. doi:https://doi.org/10.1016/j.ceramint.2019.07.113

Wang, Z.-T., Zhou, X.-H., & Zhao, G.-G. (2008). Microstructure and formation mechanism of in-situ TiC-TiB_2/Fe composite coating. *Trans. Nonferrous Met. Soc. China, 18*, 831-835.

Wang, X., Song, S., Qu, S., & Zou, Z. (2007). Characterization of in situ synthesized TiC particle reinforced Fe-based composite coatings produced by multi-pass overlapping GTAW melting process. *Surface & Coatings Technology, 201*, 5899-5905.

Vashishtha, N., Khatirkar, R., & Sapate, S. (2017). Tribological behaviour of HVOF sprayed WC-12Co, WC-10Co-4Cr and Cr_3C_2–25NiCr coatings. *Tribology International, 105*, 55-68. doi:http://dx.doi.org/10.1016/j.triboint.2016.09.025

Wu, F., Chen, T., Wang, H., & Liu, D. (2017). Effect of Mo on Microstructures and Wear Properties of In Situ Synthesized Ti(C,N)/Ni-Based Composite Coatings by Laser Cladding. *Materials, 10*(1047). doi:https://doi.org/10.3390/ma10091047

Young, D. (2016). Chapter 9 - Corrosion by Carbon. In *High Temperature Oxidation and Corrosion of Metals (Second Edition)* (pp. 431-439). Sydney: Elsevier. doi:https://doi.org/10.1016/B978-0-08-100101-1.00009-1

Yu, H., Zhang, W., Ji, X., Song, Z., Li, X., & Xu, B. (2017). In-situ synthesis of TiC/Ti composite coating by high frequency induction cladding. *Journal of Alloys and Compounds, 701*, 244-255.

Yuan, Y., & Zhuguo, L. (2014). Effects of rod carbide size, content, loading and sliding distance on the friction and wear behaviors of $(Cr,Fe)_7C_3$-reinforced α-Fe based composite coating produced via PTA welding process. *Surface & Coatings Technology, 248*, 9-22. doi:http://dx.doi.org/10.1016/j.surfcoat.2014.03.029

Yung, D., Zikin, A., Hussainova, I., Danninger, H., Badisch, E., & Gavrilovic, A. (2017). Tribological performances of ZrC-Ni and TiC-Ni cermet reinforced PTA hardfacings at elevated temperatures. *Surface & Coatings Technology, 309*, 497-505. doi:http://dx.doi.org/10.1016/j.surfcoat.2016.11.099

Acknowledgements

List of figures

List of tables

Abstract

Abrasive Wear Resistant Composite Hardfacings with *ex-situ* and *in-situ* Synthesized Carbide Reinforcement

Half of all the cases of faulty machine behavior are attributed to the mechanical wear of their parts. The abrasive wear is its most common form, which often occurs in the fields such as the automotive industry, oil extraction, aviation, recycling of materials, civil and marine engineering. In order to lessen wear effects, working surfaces are being protected (new part) or restored (used part) by means of deposition of a specially designed coating/hardfacing.

Two widely applied deposition techniques were the principal focus of this work: high velocity oxy fuel spraying (HVOFS) and plasma transferred arc welding (PTAW).

Regarding the feedstock materials, the constantly increasing price of tungsten carbide (WC) stimulates the search for cheaper alternatives, for example titanium carbide (TiC) and chromium carbide (Cr_3C_2). In particular, TiC- and Cr_3C_2-based cermets are commonly used as a replacement of expensive WC-based materials.

The aim of this work was to propose new composite coatings and hardfacings manufactured by HVOFS or PTAW, which contain Ti and Cr carbide-based reinforcement synthesized *ex-situ* (by mechanically activated synthesis, MAS) and *in-situ* (during the deposition process). Technological route with the *in-situ* synthesis of carbide reinforcement was hypothesized to become a shorter and cheaper alternative to MAS. Stainless steel (SS) AISI 316L was mainly used as matrix forming constituent.

The phase analysis, morphology and flowability of experimental powder compositions were studied to clarify their influence on the hardness and wear resistance of the produced coatings and hardfacings. Similarly, the phase content, hardness and wear properties of the deposited coatings and hardfacings were studied.

The *in-situ* synthesis of carbide reinforcement was successfully achieved in the Ti- and Cr- contained compositions both using HVOFS and PTAW deposition methods. HVOFS coatings with the *ex-situ* manufactured reinforcement possessed rather homogeneous structure (except for hardfacing with Cr_3C_2-Ni reinforcement, whose interparticle cohesion and overall thickness was very low) or distinctive lamellar structure (with *in-situ* synthesized reinforcement).

PTAW hardfacings with the *ex-situ* synthesized reinforcement generally exhibited homogeneous low-porosity structure, unlike their counterparts with the *in-situ* formed carbides. These hardfacings were found to have less homogeneous microstructure characterized by the presence of significant pores and, in the case of using TiO_2 as a carbide precursor, by low presence of the hard phase.

In the abrasive rubber wheel wear (ARWW) test, most of the experimental compositions (HVOFS coatings and PTAW hardfacings) showed better (1.1–6.4 times) wear resistance than the reference steel Hardox 400. In the abrasive-erosive wear (AEW) under low impact angle (30°), most of the PTAW hardfacings exhibited similar or slightly higher wear resistance (20%) as compared to the reference material, while under normal impact angle (90°), one PTAW hardfacing with the *in-situ* synthesized Cr-based carbide demonstrated the closest (0.7 times) to the Hardox 400 wear resistant capacity.

HVOFS coatings with the *ex-situ* added reinforcement (MAS) compared to analogous coatings with the *in-situ* synthesized reinforcement showed about 4–5 times higher wear resistance in abrasion and demonstrated nearly equal results in erosion wear. The difference in the wear resistance of PTAW hardfacings with the *ex-situ* MAS

reinforcement and the *in-situ* synthesized reinforcement was 3–4 times in abrasion wear in favour of the hardfacings with the *ex-situ* synthesized reinforcement (Table 5.1) and in the erosion wear 2–6 times in favor of the hardfacings with the *in-situ* synthesized reinforcement.

Under abrasion conditions, the HVOFS coatings and PTAW hardfacings were comparable and demonstrated high applicability potential. Under erosion conditions (30°, 90°), PTAW hardfacings outperformed HVOFS coatings by 1.5–3 times, which shows that the latter are not suitable for such wear conditions.

Lühikokkuvõte
Abrasiivkulumiskindlad komposiitpinded *ex-situ* ja *in-situ* sünteesitud karbiidse kõvafaasiga

Enamikel juhtudel on masinate rivist väljalangemise põhjuseks masinaosade mehaaniline kulumine, eelkõige liug- ja abrasiivkulumine, mis leiab aset autodes, naftakeemiaseadmeis, materjalide ringluses, lennunduses, ehitus- ja meretehnikas. Vähendamas kulumise mõju läbi uute toodete tugevdamise või kulunud masinaosade taastamise, kasutatakse laialdaselt spetsiaalselt disainitud kõvapindeid.

Käesoleva töö fookuses on pindamisel laia kasutamist leidnud hapnik-kiirleekpihustus (HVOFS) ja plasmapealesulatus (PTAW), pindepulbritest aga eksperimentaalsed *ex-situ* ja *in-situ* sünteesitud kõvafaasiga segud.

Pinnatehnikas on kulumiskindlate pinnete korral enamlevinumaiks volframkarbiidi (WC) baasil pindepulbrid. Samas volframi kui WC-baasil pindepulbri põhikomponendi hind on pidevalt kasvamas, mis tingib otsima alternatiive, näiteks titaankarbiidi (TiC) ja kroomkarbiidi (Cr_3C_2) baasil materjale. Täna on titaan- ja kroomkarbiidikermised asendamas teatud valdkondades WC-baasil kõvasulameid.

Käesoleva töö eesmärgiks oli pakkuda komposiitpindeid, mis on saadud HVOFS ja PTAW teel ja mis sisaldavad titaan- ja kroomkarbiide. Viimased on saadud kas *ex-situ* sünteesi (mehaaniliselt aktiveeritud süntees, MAS) ja *in-situ* sünteesi teel (pihustusprotsessis süntees). Karbiidse kõvafaasi *in-situ* süntees pindamisprotsessis oleks alternatiiv tööstuslikele ja MAS tehnoloogiatele. Maatriksmaterjalina kasutati roostevaba terast (SS) AISI 316L.

Uuriti erinevate eksperimentaalpulbersegude koostist, osakeste morfoloogiat ja pulbrite voolavust, selgitamaks nende mõju sünteesile ja saadavate pinnete kõvadusele ning kulumiskindlusele. Samuti uuriti saadud pulberpinnete faasilist koostist, kõvadust ja abrasiivkulumiskindlust.

Pindamise käigus kõvafaasi *in-situ* sünteesi tulemusena õnnestus saada pinded karbiidide sisaldusega kuni 30 mahu%, kasutades kiirleekpihustamist või plasmasulatust. Pihustuspinnetest *ex-situ* sünteesitud kõvafaasiga pihustuspinded olid struktuurilt homogeensed (v.a Cr_3C_2 pinded – olid kehva kohesiooni ja väikese paksusega), *ex-situ* sünteesitud kõvafaasiga pinnetele oli omane lamelaarstruktuur. Sulatuspinnetest *ex-situ* sünteesitud kermisfaasiga sulatuspinded omasid homogeense, madala poorsusega struktuuri erinevalt *in-situ* formeerunud kõvafaasiga pinnetest. TiO_2 prekursorina kasutades oli ka pinnetele omane väike kõvafaasi hulk.

Abrasioonkulumise (ARWW) tingimustes enamik eksperimentaalseid pihustus- ja sulatuspindeid (nii *ex-situ* ja *in-situ* sünteesitud kõvafaasiga) omasid suuremat kulumiskindlust (1.1-6.4 korda) võrreldes etalonmaterjali – Hardox 400 terasega. Erosioonkulumise (AEW) tingimustes väikestel kohtumisnurkadel (30º) oli parimate pinnete kulumiskindlus teras Hardox 400 tasemel (0.7-1.2 korda), suurtel kohtumisnurkadel (90º) aga mitmeid kordi madalam.

Kokkuvõttes kiirleekpihustus- ja plasmapealesulatuspinded MAS kõvafaasiga näitasid kõrget potentsiaali tööks abrasioonkulumise tingimustes; erosioonkulumise tingimustes tööks uuritud eksperimentaalpinded ei ole sobivad.

Appendix 1

Production of Thermal Spray Cr₃C₂-Ni Powders by Mechanically Activated Synthesis

Dmytro TKACHIVSKYI[1,a*], Kristjan JUHANI[1], Andrei SURŽENKOV[1],
Priit KULU[1], Mart VILJUS[1], Rainer TRAKSMAA[1], Vytenis JANKAUSKAS[2],
Rimtautas LEIŠYS[3]

[1]Department of Mechanical and Industrial Engineering, Tallinn University of Technology,
Ehitajate tee 5, 19086 Tallinn, Estonia

[2]Institute of Power and Transport Machinery Engineering, Aleksandras Stulginskis University,
Studentu gatvia 15, 53362 Akademija, Kaunas district, Lithuania

[3]UAB "Dangų inžinerijos centras", Jegainės gatvia 6, 52494 Kaunas, Lithuania

dmtkac@ttu.ee

Abstract. The aim of this research was to optimize the mechanically activated synthesis (MAS) technology of the Cr_3C_2-Ni powder intended for thermal spraying. The MAS production route included ball milling for 72 h (ball-to-powder ratio 20:1) and sintering under 1075 °C in vacuum for 4 h. Sintered compact was crushed, classified by sieving to obtain the fraction suitable for thermal spraying (20–45 μm). The morphology and the phase composition of the powder were analyzed by a scanning electron microscope (SEM) and X-ray diffraction (XRD). The optimal Cr:C ratio found was 7:1. The powder had an equiaxial or a slightly elongated lamellar shape, Cr_3C_2 carbides in a single powder particle had an elongated shape. The principal phases in the optimized powder were Cr_3C_2, Cr_7C_3 and Ni(Cr) solid solution. Coatings from the manufactured powder were produced by the high velocity oxy-fuel (HVOF) spraying. The abrasive wear tests were carried out according to standard ASTM G65. The wear tests showed that the sprayed coatings from the experimental powder exhibited about five times higher wear rate at abrasive wear conditions than the coatings from the reference commercial powder.

Introduction

The cost of powder feedstock materials intended for thermal spray applications contributes up to 75% of the whole cost of the final coating [1, 2]. This problem is especially pronounced in the case of carbide-metal (cermet) composite powders [3], such as those based on WC or Cr_3C_2. Despite this, chromium carbide-based coatings produced by the thermal spraying of powder have become more widespread, as they demonstrate good wear resistance under various wear conditions [4–6].

Disintegrator milling is widely used in production process of thermal spray powders [1, 3, 7–10]. However, avoiding disintegrator milling can shorten the production process and lower its cost [11].

This study addresses the production of spray Cr_3C_2-20% Ni powder via only mechanically activated synthesis (MAS) [12–14] and insignificant manual crushing. Focus is on powder morphology, phase composition and abrasive wear resistance of the high velocity oxy-fuel (HVOF) sprayed coatings from this powder.

Experimental

Powder production and characterization. For the production of composite spray powders by mechanically activated synthesis (MAS), pure chromium (99.5% Cr) with an average grain size 6.65 μm (Pacific Particulate Materials Ltd.), nickel (99.7% Ni) with an average grain size 2.4 μm (Pacific Particulate Materials Ltd.) and carbon black (99.8% C) with an average grain size 6.45 μm (Timrex KS6) powders were used. On the basis of the preliminary experiments, two compositions

(P21 and P23) of experimental powders were produced (Table 1). The chromium-to-carbon atomic ratio in the mixtures was chosen to be 6:1 and 7:1, respectively. The commercial thermal spray powder Cr_3C_2-25% NiCr (Amperit 588.074, H.C. Stark) was used as the reference material.

Table 1. Chemical composition of powders

Powder code	Composition [wt%]			
	Ni	Cr	C	Cr_3C_2
P21	20	68.5	11.5	-
P23	20	69.3	10.7	-
Amperit	20	5	-	75

The manufacturing process of the experimental powders by the MAS route is described in detail in [3]. The mechanical activation and milling of initial powders of chromium, carbon and nickel were carried out in a conventional ball mill with WC-Co hardmetal lining and WC-Co balls (balls-to-powder ratio 20:1). Isopropyl alcohol was used as milling media. The milling time was 72 h. After milling, the plasticizer was added to the powder (3 wt% of paraffin; 60 wt% of dissolvent). Synthesizing of chromium carbide was completed in a conventional sintering furnace in vacuum (temperature graph in Fig. 1. After sintering, powder compacts were manually crushed and classified by sieving.
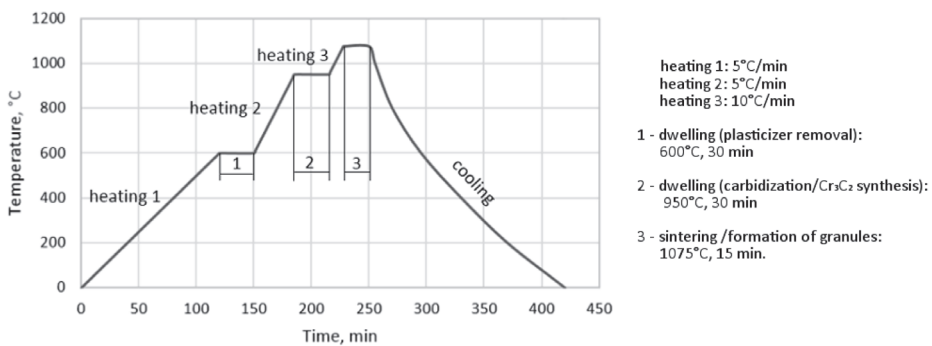
Fig. 1. Sintering curve of experimental MAS powders

The phase composition of the powder after sintering was assessed by the X-ray diffraction (XRD) method with Cu Kα radiation (AXS D5005, Bruker) with a step of 0.04°. Particle shape and morphology were estimated using a scanning electron microscope (SEM) EVO MA-15 (Carl Zeiss). The flowability and apparent density of the produced powders were studied using a Hall flowmeter.

Coating deposition and evaluation. Prepared powders were deposited onto a substrate using a high velocity oxy-fuel spraying (HVOFS) system Hipojet 2700 (Metallizing Equipment Co. Pvt. Ltd., India), equipped with a gravity based powder feeder using propane pressurized to 6 bar as fuel, and combustion pressure and oxygen pressure of 6 bar. Consumption rate of propane was 1.1 dm^3/s and consumption rate of oxygen was 4.2 dm^3/s. The spraying distance was 200 mm. To estimate wear resistance of coatings, abrasive wear test equipment was set according to the standard ASTM G65. The load was 130 N, linear velocity was 2.4 m/s, silica sand of the grain size 0.2–0.3 mm with feeding rate of 300–400 g/min was used. The weight loss of the tested samples was measured after each minute of testing.

Results and Discussion

Characterization of spray powder. Experimental powders possessed particles of irregular flake-like shape, while particles of the commercial powder exhibited round near-spherical shape (Fig. 2) due to the different production technology (gas atomization and sintering [15]). The flowability of

the experimental powder could not be assessed as the powder did not flow freely through the flowmeter. The flowability of commercial powder was taken as 43.6 ± 0.7 s, as it was measured in previous studies [9]. The unsatisfactory flowability of the experimental powders may be explained by the irregular shape of the particles. The apparent densities of experimental powders were in the range 1.2–1.8 g/cm^3 against 2.3–3.0 g/cm^3 of the commercial powder.
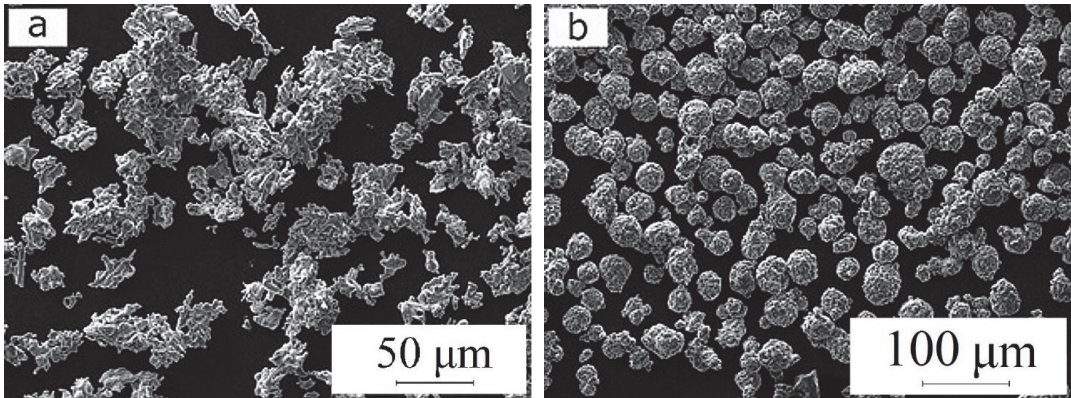
Fig. 2. Morphology of powders: (a) experimental (P23) Cr$_3$C$_2$-20% Ni
and (b) commercial

The structures of the experimental graphite-free and the commercial powder are presented in Fig. 3. The shape of experimental powder particles tends to be elongated, and they contain carbide grains of longitudinal shape (Fig. 3a), while carbides in reference powder particles exhibit more equiaxial shape (Fig. 3b). Due to lower sintering temperature and shorter time during mechanical activated synthesis, chromium carbide does not grow noticeably in vacuum [12].
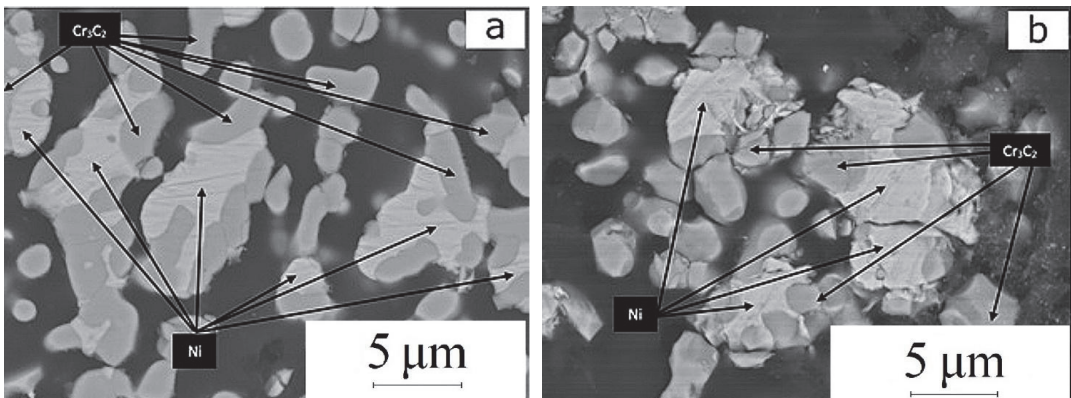
Fig. 3. Particle structure of (a) experimental graphite-free Cr$_3$C$_2$-20% Ni powder (P23)
and (b) commercial powder (Amperit)

Particle size distribution of experimental powders is shown in Fig. 4. The fraction of 20–45 μm commonly used for thermal spray feedstocks shows the largest share: about 37% of P21 and 40% of P23.

XRD results of experimental powders revealed three main phases: Cr$_3$C$_2$, Cr$_7$C$_3$, Ni present in the graphite-free (P23) powder and four main phases: Cr$_3$C$_2$, Cr$_{23}$C$_6$, nickel chromium carbide (Cr$_{2.965}$Ni$_{0.035}$C$_2$) and Ni present in the graphite-containing (P21) powder. The residual content of the carbon in the P21 powder was 3.7 wt% (Fig. 5), while no carbon black was found in the powder
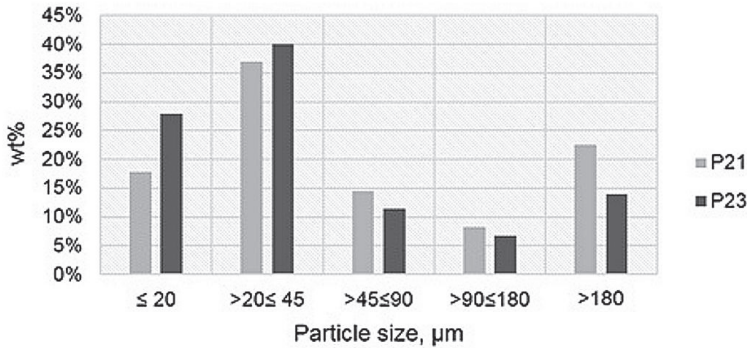
Fig. 4. Particle size distribution in experimental powders P21 (Cr:C – 6:1) and P23 (Cr:C – 7:1)

P23. Considering carbon to have a detrimental effect on the wear resistance of the HVOFS coating, it was decided to use only the powder P23 for spraying.
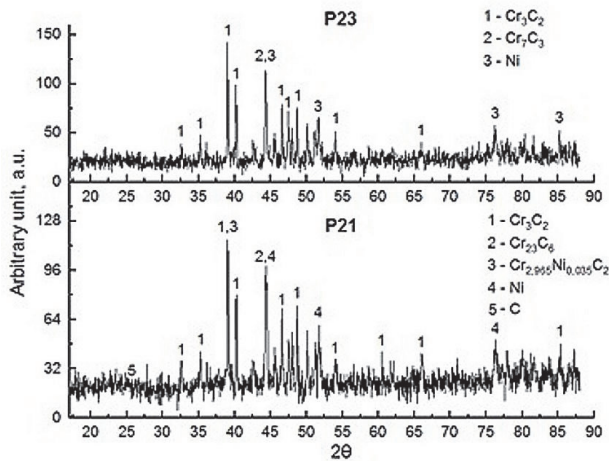
Fig. 5. XRD patterns of experimental graphite-free (P23) and graphite-containing (P21) powders

Deposition of coatings. Due to its intrinsically low flowability a low deposition efficiency of the experimental powder was observed. As a result, the thickness of the coating from the experimental powder was approximately 30 μm, while the thickness of the coating from the reference commercial powder was approximately 300 μm. Moreover, an insufficient cohesion of the experimental powder particles was observed when attempting to prepare a cross-section for the microstructural studies. Due to low adhesion, the cross-section of the coating from the experimental powder could not be polished to a required condition.

As followed from the XRD results of coating surface, four main phases: Cr_3C_2, Cr_7C_3, WC and $W_2Fe_{21}C_6$ were found in the commercial coating and three main phases: Cr_3C_2, WC and $B_{13}C_2$ were found in the experimental coating (Fig. 6). The presence of tungsten may be due to the contamination from both milling attritor and balls, which are made of WC-Co hardmetal.

Abrasive wear of coatings. The results of the adopted ASTM G65 wear test are depicted in Fig. 7. As shown in the figure, the experimental coating exhibited much higher wear rate. Considering results of relative wear resistance of Amperit to steel C45 from [3], the relative wear resistance of Cr_3C_2-20% Ni to steel C45 is theoretically calculated as 1.6. Figure 8 indicates cracks between the deposited Cr_3C_2 particles and regions of depleted Ni reinforcement. A higher wear of the experimental coating is thus caused by a low cohesion between particles, mentioned earlier, what led to spallation of the deposited powder particles from the coating.
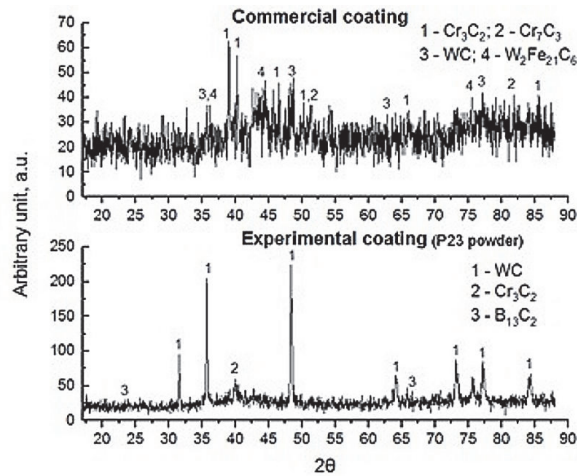
Fig. 6. XRD patterns of coatings from experimental and commercial powders
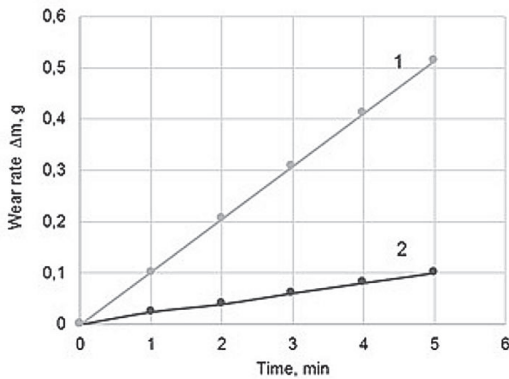
Fig. 7. Influence of testing time on the wear rate of coatings: 1 – experimental (P23), 2 – commercial
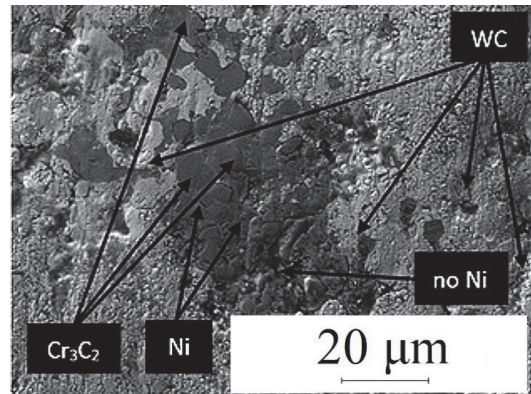
Fig. 8. SEM image of worn out surface of experimental coating

Conclusions

1. Experimental powders are characterized by an irregular shape of particles. To avoid residual graphite in agglomerates, an optimal Cr:C ratio should be around 7:1. XRD results of the experimental powder used for spraying (P23) indicate the presence of three main phases Cr_3C_2, Cr_7C_3, and Ni.

2. Due to low flowability of the experimental powder, the application of powder at HVOF spraying for producing coatings with required thickness is complicated. To improve the technological properties, powder particles with a more spherical shape should be produced.

3. Deposited particles in the coating from the experimental powder exhibit a low cohesion, what significantly increases the wear rate of the coating.

Acknowledgements

References

[1] H. Sarjas, P. Kulu, K. Juhani, P. Vuoristo, Novel WC-Co spray powders and HVOF sprayed coatings on their bases, Proc. 28th Int. Conf. on Surface Modification Technologies (SMT28), Tampere, Finland, 16th–18th of June 2014, 35–42.

[2] Europeans Chemical Agency, Functional Chrome Plating: analysis of alternatives, Non-confidential report, Lanexx Deutschland GmbH (2015) 98.

[3] H. Sarjas, P. Kulu, K. Juhani, M. Viljus, V. Matikainen, P. Vuoristo, Wear resistance of HVOF sprayed coatings from mechanically activated thermally synthesized Cr_3C_2–Ni spray powder, P. Est. Acad. Sci. 65 (2016) 101–106.

[4] M.M.M. Sarcar, K. Suman, S. Kamaluddin, Tribological and corrosion behavior of HVOF sprayed WC-Co, NiCrBSi and Cr_3C_2-NiCr coatings and analysis using design of experiments, Mater. Today: Proc. 2 (2015) 2654–2665.

[5] M.A. Aavareh, A. Sarhan, B.B. Razak, W.J. Basirun, The tribological and electrochemical behavior of HVOF-sprayed Cr_3C_2–NiCr ceramic coating on carbon steel, Ceram. Int. 41 (2015) 5387–5396.

[6] V. Matikainen, G. Bolelli, H. Koivuluoto, P. Sassatelli, L. Lusvarghi, P. Vuoristo, Sliding wear behaviour of HVOF and HVAF sprayed Cr_3C_2-based coatings, Wear 388–389 (2017) 57–71.

[7] A. Surzhenkov, A. Vallikivi, V. Mikli, M. Viljus, T. Vilgo, P. Kulu, Wear resistant self-fluxing alloy based TiC-NiMo and C_2C_3-Ni hardmetal particles reinforced composite coatings. Proc. 2nd Int. Conf. Manufacturing Engineering & Management 2012, 5–7 December 2012, Prešov, Slovak Republic, 33–36.

[8] P. Kulu, H. Käerdi, A. Surzenkov, R. Tarbe, R. Veinthal, D. Goljandin, A. Zikin, Recycled hardmetal-based powder composite coatings: Optimization of composition, structure and properties. Int. J. Mater. Prod. Tech. 49 (2014) 180–202.

[9] H. Sarjas, A. Surzhenkov, K. Juhani, M. Antonov, E. Adoberg, P. Kulu, M. Viljus, Abrasive-erosive wear of thermally sprayed coatings from experimental and commercial Cr_3C_2-based powders, J. Therm. Spray Tech. 26 (2017) 2020–2029.

[10] S. Tkachenko, K. Dvořák, D. Jech, K. Slámečka, L. Klakurkova, D. Paloušek, L. Čelko, Wear of grinding rotors with thermally-sprayed coatings in a high-speed mill, Wear 412–413 (2018) 49–59.

[11] T. Sahraoui, N.-E. Fenineche, G. Montavon, C. Coddet, Alternative to chromium: characteristics and wear behavior of HVOF coatings for gas turbine shafts repair (heavy-duty), J. Mat. Proc. Tec. 152 (2004) 43–55.

[12] J. Pirso, M. Viljus, S. Letunovits, K. Juhani, Reactive carburizing sintering—A novel production method for high quality chromium carbide-nickel cermets, Int. J. Refract. Met. H. 412–413 (2006) 263–270.

[13] K. Juhani, J. Pirso, M. Viljus, S. Letunovits, Two-body dry abrasive wear of Cr_3C_2-Ni cermets, Proc.Est. Acad. Sci. 4 (2006) 368–376.

[14] K. Juhani, Reactive Sintered Chromium and Titanium Carbide-Based Cermets, PhD thesis, TUT Press, Tallinn, 2009.

[15] J. Dunkley, Atomization, in: ASM Handbook, volume 7, Powder Metal Technologies and Applications, ASM International, Materials Park, 1998, pp. 35–52.

Appendix 2

Publication II

R.Bendikiene, A. Ciuplys, S. M. Jankus, A. Surzhenkov, **D. Tkachivskyi**, K. Juhani, M. Viljus, R. Traksmaa, M. Antonov, P. Kulu, Study of submerged and plasma arc welded composite hardfacings with a novel Cr_3C_2–Ni reinforcement, *Proceedings of the Estonian Academy of Sciences*, 2019, **68**, 150-157.

Study of submerged and plasma arc welded composite hardfacings with a novel Cr$_3$C$_2$–Ni reinforcement

Regita Bendikiene[a*], Antanas Ciuplys[a], Simonas Mindaugas Jankus[a], Andrei Surzhenkov[b*], Dmytro Tkachivskyi[b], Kristjan Juhani[b], Mart Viljus[b], Rainer Traksmaa[b], Maksim Antonov[b], and Priit Kulu[b]

[a] Department of Production Engineering, Faculty of Mechanical Engineering and Design, Kaunas University of Technology, Studentu gatve 56, 51424 Kaunas, Lithuania
[b] Department of Mechanical and Industrial Engineering, Tallinn University of Technology, Ehitajate tee 5, 19086 Tallinn, Estonia

Abstract. This paper studies possible uses of Cr$_3$C$_2$–Ni cermet prepared via mechanically activated synthesis as reinforcement in submerged arc welded (SAW) and plasma transferred arc welded (PTAW) Fe- and Ni-based hardfacings. The microstructure and phase composition of the hardfacings were analysed by scanning electron microscopy and X-ray diffraction, respectively. Vickers hardness (HV30) was measured and two-body (ASTM G132) and three-body (ASTM G65) abrasive wear were tested. Cermet particles were found to be entirely dissolved in the SAW hardfacings, while in the PTAW hardfacings they were partially retained. The main phases in the Fe-based hardfacings were γ-Fe and α-Fe along with Cr$_7$C$_3$ in the PTAW hardfacing. The Ni-based SAW and PTAW hardfacings were mostly comprised of different carbides (Cr$_3$C$_2$, CrC, NiC$_{0.22}$). Addition of cermet particles increased the hardness of the hardfacings 1.1–3.3 times, the effect being more pronounced in the Fe-based hardfacings and PTAW hardfacings. Under two-body abrasive wear conditions, composite hardfacings exhibited 1.2–7.8 times lower wear and under three-body abrasive wear conditions 1.4–9.4 times lower wear than the unreinforced hardfacings. The wear resistance of the PTAW hardfacings was improved considerably, while the effect of the matrix alloy was insignificant. Microcutting was the major wear mechanism under both two-body and three-body abrasive wear conditions, accompanied by microploughing in the SAW hardfacings in the former case and by the pull-out of carbide particles in the PTAW hardfacings in the latter case. The principle of the wear mechanism remained unaltered in the presence of cermet particles, but the wear was less severe.

Key words: composite hardfacing, cermet reinforcement, submerged arc welding, plasma transferred arc welding, abrasive wear.

1. INTRODUCTION

Despite their obvious advantages, for example high hardness and high melting point, the most frequently used reinforcements in cladded composite hardfacings such as tungsten carbide (WC) [1–4] and WC-based hardmetals [5–7], as well as titanium carbide [2,8–10]

exhibit certain limitations. For example, WC and WC-based hardmetals are prone to degradation above 500 °C with the formation of a brittle WO$_3$ layer [11,12]. The price of both tungsten and cobalt has fluctuated to a large extent over decades; moreover, cobalt has been classified as a toxic metal [13]. As to TiC, several authors have reported its uneven distribution in a hard-facing [8,9] due to different densities of the molten metal matrix and titanium carbide [14], which may deteriorate the mechanical properties of the hard-

* Corresponding authors, andrei.surzenkov@taltech.ee,
  regita.bendikiene@ktu.lt

facing [9]. Therefore, alternative reinforcement materials are required.

Relatively few studies have focused on separately synthesized chromium carbide (Cr_3C_2) or a Cr_3C_2-based cermet as reinforcement candidates and on their influence on the wear resistance of hardfacings. Nurminen et al. [2] found that despite a high dissolution rate of Cr_3C_2 in the Ni-based alloy, the Cr_3C_2 reinforced hardfacing exhibits the lowest wear among the studied Ni- and Co-based hardfacings reinforced with tungsten, chromium, and vanadium carbides. According to Goswami et al. [15], addition of chromium carbide to a Ni–Cr alloy hardfacing reduces its wear rate remarkably as compared to the analogous hardfacing from the Stellite 6 alloy. In [16–18] it was shown that addition of approximately 30 wt% Cr_3C_2 particles to a Ni-based alloy improves their wear resistance by 1.5–1.7 times. Luo et al. [19] reported that the relative abrasive wear resistance of a chromium carbide reinforced Ni_3Al hardfacing is up to six times higher than that of the Stellite 12 alloy. Janicki [20] obtained up to three times higher erosion wear resistance with the introduction of porous chromium carbide to the nickel-based laser-clad matrix. Zikin et al. [11] demonstrated that Cr_3C_2-based cermet reinforcement is more favourable than Cr_3C_2 due to its lower dissolution rate.

One of the obstacles associated with the application of carbide-based cermets in hardfacings is their relatively high price [21]. One of the ways to lower it is to synthesize the carbide phase in situ during the sintering process [22–24]. To raise the reactivity of the feedstock powders, several researchers have proposed mechanical activation by high-energy ball milling [23,25,26]. The production of Cr_3C_2-based powders for thermal spraying by such a technology was recently reported in [21,27]; however, their perspective as a reinforcement phase in cladded hardfacings is still unclear.

The present research concentrates on the Ni- and Fe-based composite hardfacings with a novel Cr_3C_2–Ni cermet reinforcement. The influence of the cladding technology and of the matrix alloy on the micro-structure, hardness, and two- and three-body abrasive wear is studied.

2. EXPERIMENTAL

2.1. Preparation of the reinforcement

Mechanically activated synthesis (MAS) of Cr_3C_2–Ni powder reinforcement described in detail in [21] was used. To obtain the Cr_3C_2–Ni (80 wt% Cr_3C_2, 20 wt% Ni) cermet powder, powders of pure Cr (99.5 wt%; average particle size 6.65 µm) and pure Ni (99.7 wt%; average particle size 2.4 µm), supplied by Pacific Particulate Materials Ltd., as well as pure carbon black (99.7 wt%; average particle size 6.45 µm), supplied by Imerys SA, were milled in the conventional ball mill with hardmetal balls (ball-to-powder ratio 20 : 1) in isopropanol during 72 h, then plasticized and sintered in vacuum at 1100 °C to obtain bulk compacts. The sintered agglomerates were manually crushed and the powder fraction suitable as reinforcement (size range 90–300 µm) was sieved.

2.2. Deposition of hardfacings

Two deposition technologies – submerged arc welding (SAW) and plasma transferred arc welding (PTAW) – were used to prepare the hardfacings. The deposition parameters are provided in Table 1. For SAW, the consumable Ø1.2 mm wire electrode (wt%: 0.1 C, <0.03 Si, 0.35–0.6 Mn, <0.15 Cr, <0.3 Ni, bal. Fe) and flux ОЦК-45 (wt%: 38–44 SiO_2, 38–44 MnO, <2.5 MgO, 6–9 CaF_2, <6.5 CaO, <2 Fe_2O_3, <0.15 S, < 0.15 P) were applied. For PTAW, the Ø3.2 mm non-consumable bulk electrode WT 20 (wt%: 98.0 W, 2.0 ThO_2) was used. The normalized structural steel S355 (wt%: 0.22 C, 1.60 Mn, 0.05 Si, 0.05 P, 0.05 S, bal. Fe) was used as the substrate steel in all the cases. Table 2 shows the designation and the chemical composition of the hard-facings. In the composite hardfacings, the rate of the matrix and reinforcement in the hardfacings was adjusted to be 60 : 40 wt%. Prior to the PTAW process, the

Table 1. Deposition equipment and parameters

Process	Equipment (manufacturer)	Current, A	Voltage, V	Oscillation frequency, Hz	Traverse speed, mm/s	Gas consumption, L/s
SAW	Integra 350 Professional (Miller)	180	22–24	–	4	–
PTAW	GAP 3001 DC (Castolin Eutectic®)	95	22–24	0.6	1	Plasma gas (Ar) – 1.5 Shield gas (Ar) – 6.5 Carrier gas (Varigon®*) – 3.75 (reinforcement), 2.75 (matrix)

* 95% Ar + 5% H_2.

Table 2. Designation and chemical composition of the hardfacings

Designation	Deposition technology	Matrix composition, wt%	Reinforcement composition
SAW-SS	SAW	99.9 stainless steel* + 0.1 wire electrode	–
SAW-Ni	SAW	99.9 Ni alloy** + 0.1 wire electrode	–
SAW-SS+CrC	SAW	99.9 stainless steel + 0.1 wire electrode	Cr_3C_2–Ni***
SAW-Ni+CrC	SAW	99.9 Ni alloy + 0.1 wire electrode	Cr_3C_2–Ni
PTAW-SS	PTAW	Stainless steel	–
PTAW-Ni	PTAW	Ni alloy	–
PTAW-SS+CrC	PTAW	Stainless steel	Cr_3C_2–Ni
PTAW-Ni-CrC	PTAW	Ni alloy	Cr_3C_2–Ni

  * Austenitic stainless steel EN-X3CrNiMo17-13-3; powder grade Castolin 16316 (wt%: 0.03 C, 17.5 Cr, 13 Ni, 2.7 Mo, bal. Fe).
 ** Ni-based self-fluxing alloy; powder grade Castolin 16221 (wt%: 0.2 C, 4 Cr, 1 B, 2.5 Si, max. 2 Fe, 1 Al, bal. Ni).
*** Experimental cermet powder, produced by the MAS route.

powders were dried at 50 °C for 5 h, while no drying of powders was applied in the SAW process.

2.3. Microstructure studies

The microstructure of the obtained hardfacings was studied using a scanning electron microscope (SEM) EVO MA-15 (Carl Zeiss, Germany), equipped with an energy dispersive spectroscopy (EDS) device. An X-ray diffraction (XRD) device AXS D5005 (Bruker, Germany), equipped with a Cu Kα radiation source, was used to study the phase composition of the hardfacings (measuring step 0.04°).

2.4. Hardness measurements

Vickers surface hardness (HV30) of the surface of the hardfacings was measured by using the Vickers hardness tester Indentec 5030KV (Zwick/Roell, Germany) at the load 294.3 N (30 kgf) and the dwell time 10 s. Ten measurements were made at each hardfacing, and the average hardness value was calculated.

2.5. Wear tests

The data on the applied wear tests are given in Table 3. The size of the tested specimens was 6 mm × 20 mm ×

10 mm and 50 mm × 25 mm × 10 mm for the two-body and three-body wear tests, respectively. Three specimens of each hardfacing type were tested, and the average volumetric wear was determined. Worn surfaces of the hardfacings were studied with SEM EVO MA-15 (Carl Zeiss) and FEI Quantra FEG (Bruker Quantax) to find out the wear mechanisms.

3. RESULTS AND DISCUSSION

3.1. Microstructure analysis

Unreinforced hardfacings had microstructures, typical for welded Fe- and Ni-based hardfacings reported elsewhere [7,11]. Therefore, they are not analysed here. Particles of the Cr_3C_2–Ni reinforcement were entirely dissolved in the SAW hardfacings (Fig. 1a,c), while in the PTAW hardfacings, cermet particles remained integral (Fig. 1b,d). The reason was most probably the higher welding current during the SAW process, which according to the Joule–Lenz law, would lead to a higher heat input to the hardfacing and, consequently, to a higher dissolution rate. Apart from that, the amount of the retained Cr_3C_2–Ni reinforcement was much lower in the Fe-based hardfacing, which is intrinsic to the Fe-based hardfacings [2].

Table 3. Parameters of the wear tests

Test type	Standard designation	Force, N	Speed of rotation, L/s	Linear speed, m/s	Duration, s	Abrasive type	Abrasive size, mm	Other parameters
Two-body	ASTM G132	5	1.05	0.4	3600	Al_2O_3	0.08–0.1	Emery paper was changed after each 300 s
Three-body	ASTM G65, procedure A	130	3.6	2.4	1800	SiO_2	0.2–0.3	Abrasive mass flow rate $(5.0–6.7) \times 10^{-2}$ kg/s
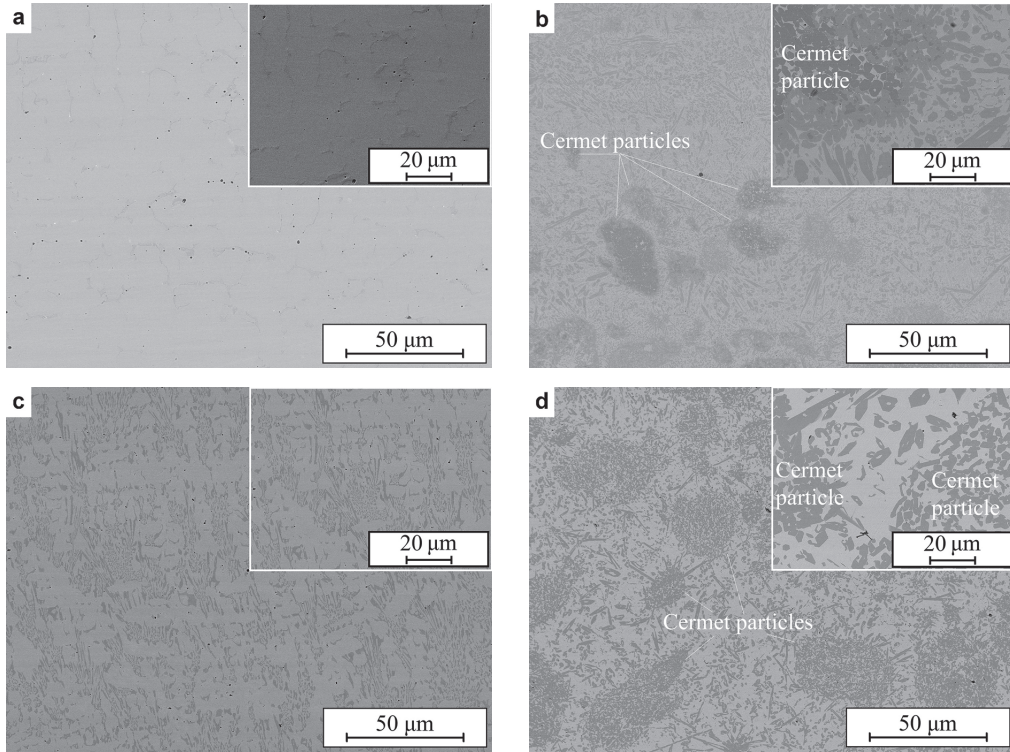
Fig. 1. Microstructure of the hardfacings: a – SAW-SS+CrC, b – PTAW-SS+CrC, c – SAW-Ni+CrC, d – PTAW-Ni+CrC.

3.2. Phase composition

Almost no differences were found between the unreinforced Fe- and Ni-based SAW and PTAW hardfacings. For this reason, the phase composition of these hardfacings is not analysed here. The principal phases in the SAW-SS+CrC hardfacing were solid solution of Cr in α-Fe and, on a smaller scale, Ni-rich retained austenite (γ-Fe) and a small amount of secondary carbide Cr_3C, while Cr_7C_3 and austenite (γ-Fe) prevailed in the microstructure of the PTAW-SS+CrC hardfacing accompanied by the solid solution of Fe(Cr) (Fig. 2a). The relatively small amount of secondary carbides could be explained by the dissolution of carbon in the retained austenite.

The SAW-Ni+CrC hardfacing comprised mostly different chromium carbides (CrC, Cr_3C_2) and, on a minor scale, γ-Fe (Fig. 2b). The PTAW Ni+CrC hardfacing contained mostly primary Cr_3C_2 carbide and nickel-based secondary carbide $NiC_{0.22}$, accompanied by minor amounts of Cr_3Si and Cr_2B (not indicated in the XRD chart).
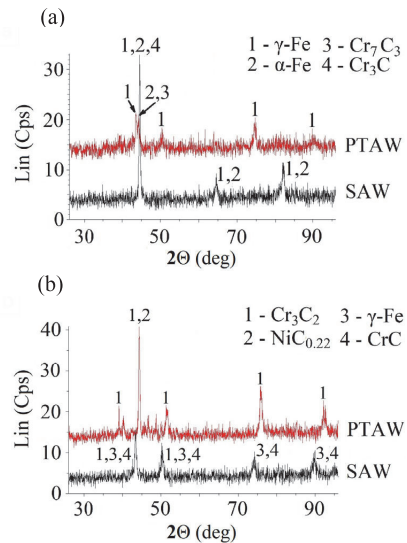
Fig. 2. XRD charts of the hardfacings: a – SS-type hardfacings, b – Ni-type hardfacings.

3.3. Hardness studies

Addition of Cr_3C_2–Ni particles increased the average hardness of the hardfacings by 1.1–3.3 times. A larger growth was observed in the case of the stainless steel matrix hardfacings and PTAW hardfacings (Fig. 3). The latter may be explained by the presence of retained cermet particles in the matrix. A larger increase of the hardness of SS-CrC type hardfacings is the result of the relatively low initial hardness of unreinforced hardfacings made of stainless steel.

3.4. Wear of the hardfacings

The results of the wear tests generally correlated with those of hardness. Under the two-body abrasive wear conditions, the composite SAW hardfacings exhibited 1.2–1.8 times lower wear, and composite PTAW hard-facings, 6.7–7.8 times lower wear than the respective unreinforced hardfacings (Fig. 4). Analogously, under the three-body abrasion wear conditions addition of Cr_3C_2–Ni particles to the Ni- or Fe-based alloy led to 1.4–1.8 times lower wear of the SAW hardfacings and 9.2–9.4 times lower wear of the PTAW hardfacings (Fig. 5).

The increase of wear resistance was more pronounced in the case of Fe-based hardfacings and PTAW hardfacings. A larger enhancement of the wear resistance of the latter may be explained by the retention of Cr_3C_2–Ni particles in the hardfacings. The relatively lower wear of the SS-CrC type hardfacings, stress-induced martensitic transformation of the retained austenite, which happens during the wear test [28], may be suggested as the most probable cause.

As the SS-CrC type hardfacings exhibited the lowest overall wear, they were used in the analysis of the wear mechanisms (Fig. 6). Under the two-body abrasive wear,

Fig. 4. Two-body abrasive wear of hardfacings.

Fig. 5. Three-body abrasive wear of hardfacings.

the wear mechanism of the SAW hardfacing was a combination of microcutting and microploughing (Fig. 6a). In the case of the PTAW hardfacing, microcutting became dominant and the grooves left by abrasive particles became shallower (Fig. 6b). Material loss due to the spalling of flat fragments became insignificant as well. A better wear resistance of the PTAW SS-CrC hard-facings may be explained by a larger amount of primary as well as secondary carbides. Under the three-body abrasive wear conditions, microcutting was the common wear mechanism of both the SAW (Fig. 6c) and the PTAW hardfacing (Fig. 6d). However, the depth and the length of the grooves were obviously larger in the SAW hardfacing, as cermet reinforcement tackled the movement of free abrasive and its penetration inside the matrix in the PTAW hardfacing. Loss of carbide particles from the cermet reinforcement was also observed, although the cermet particles themselves remained holistic, which is a sign of their good integration with the matrix.

Fig. 3. Vickers macrohardness of the hardfacings.
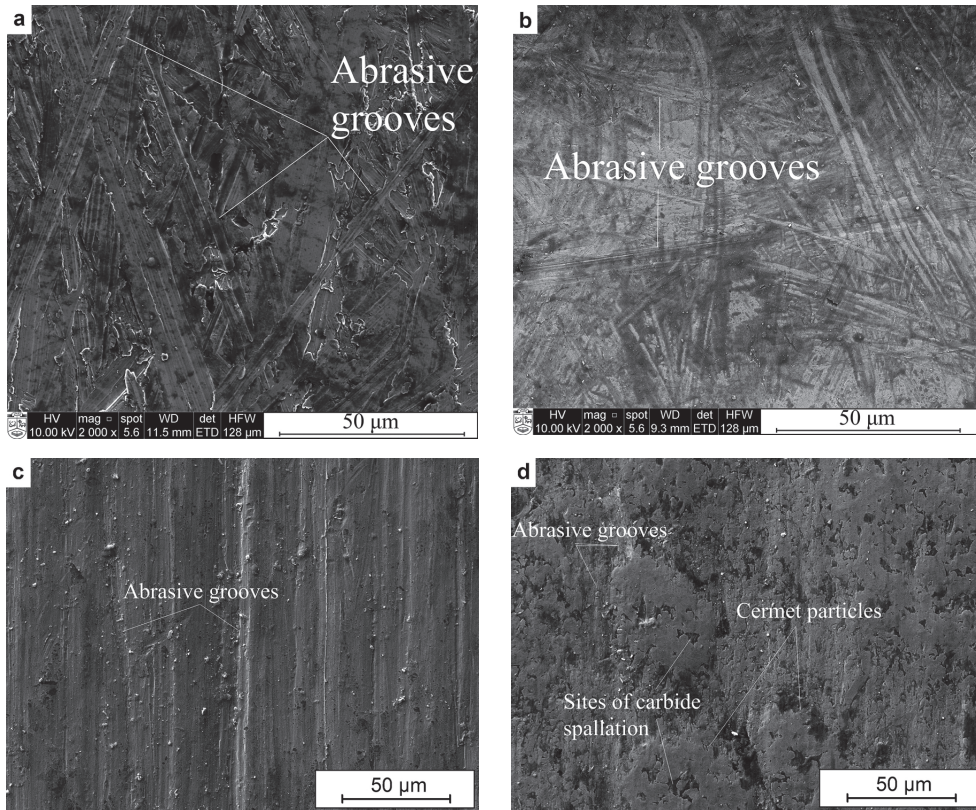
Fig. 6. Worn surfaces of the hardfacings: a – SAW SS-CrC, two-body abrasive wear; b – PTAW SS-CrC, two-body abrasive wear; c – SAW SS-CrC, three-body abrasive wear; d – PTAW SS-CrC three-body abrasive wear.

4. CONCLUSIONS

- It is possible to efficiently use Cr_3C_2–Ni cermet produced by mechanically activated synthesis (MAS) as a reinforcement in composite welded hardfacings, although it is more feasible in the plasma transferred arc welding (PTAW) process than in the submerged arc welding (SAW) process.
- The dissolution rate of Cr_3C_2–Ni particles was higher in the Fe-based hardfacing than in the Ni-based one, and the re-precipitation rate of secondary carbides was the lowest in the Fe-based SAW hardfacing.
- Reinforcement by Cr_3C_2–Ni cermet particles led to 1.1–3.3 times higher hardness as compared with the unreinforced coating; this effect was more pronounced in the case of PTAW hardfacings and hardfacings with a Fe-based matrix.
- Addition of Cr_3C_2–Ni cermet particles improved the wear resistance of the hardfacings both under two- and three-body abrasive wear conditions by 1.2–9.4 times; this effect was greater in the case of PTAW

hardfacings, as well as under the three-body abrasive wear conditions, while the influence of the matrix alloy was insignificant.
- Retention of primary Cr_3C_2–Ni particles led to the formation of a harder and stronger structure, which was more resistant to wear.

REFERENCES

1. Gassmann, R. C. Laser cladding with (WC+W$_2$C)/Co–Cr–C and (WC+W$_2$C)/Ni–B–Si composites for enhanced abrasive wear resistance. *Mater. Sci. Technol*, 1996, **12**, 691–696.
2. Nurminen, J., Näkki, J., and Vuoristo, P. Microstructure and properties of hard and wear resistant MMC coatings deposited by laser cladding. *Int. J. Refract. Met. H. Mater.*, 2009, **27**, 472–478.
3. Surzhenkov, A., Baroninš, J., Viljus, M., Traksmaa, R., and Kulu, P. Sliding wear of composite stainless steel hardfacing under room and elevated temperature. *Sol. St. Phen.*, 2017, **267**, 195–200.
4. Sui, Y., Yang, F., Qin, G., Ao, Z., Liu, Y., and Wang, Y. Microstructure and wear resistance of laser-cladded Ni-based composite coatings on downhole tools. *J. Mater. Process. Technol*, 2018, **252**, 217–224.
5. Wang, P-Z., Qu, J-X., and Shao, H-S. Cemented carbide reinforced nickel-based alloy coating by laser cladding and the wear characteristics. *Mater. Design*, 1996, **17**, 289–296.
6. Bendikiene, R., Ciuplys, A., and Kavaliauskiene, L. Preparation and wear behaviour of steel turning tools surfaced using the submerged arc welding technique. *Proc. Estonian Acad. Sci.*, 2016, **65**, 117–122.
7. Bendikiene, R., Ciuplys, A., and Pupelis, E. Research on possibilities to replace industrial wear plates by surfaced coatings using waste materials. *Int. J. Surf. Sci. Eng.*, 2016, **10**, 330–338.
8. Liu, J., Wang, L., and Li, H. Reactive plasma cladding of TiC/Fe cermet coating using asphalt as a carbonaceous precursor. *Appl. Surf. Sci.*, 2009, **255**, 4921–4925.
9. Emamian, A., Alimardani, M., and Khajepour, A. Correlation between temperature distribution and in situ formed microstructure of Fe–TiC deposited on carbon steel using laser cladding. *Appl. Surf. Sci.*, 2012, **258**, 9025–9031.
10. Sahoo, C. K. and Masanta, M. Microstructure and mechanical properties of TiC-Ni coating on AISI304 steel produced by TIG cladding process. *J. Mater. Process. Technol.*, 2017, **240**, 126–137.
11. Zikin, A., Hussainova, I., Katsich, C., Badisch, E., and Tomastik, C. Advanced chromium carbide-based hardfacings. *Surf. Coat. Technol.*, 2012, **206**, 4270–4278.
12. Humphry-Baker, S. A. and Lee, W. E. Tungsten carbide is more oxidation resistant than tungsten when processed to full density. *Scr. Mater.*, 2016, **116**, 67–70.
13. Kolnes, M. *Cobalt- and Nickel-free Titanium and Chromium Carbide-based Cermets*. PhD thesis. TTÜ Press, Tallinn, 2018.
14. Pelletier, J. M., Jobez, S., Saif, Q., Kirat, P., and Vannes, A. B. Laser surface alloying: mechanism of formation and improvement of surface properties. *J. Mater. Eng.*, 1991, **13**, 281–290.
15. Goswami, G. L., Kumar, S., Galun, R., and Mordike, B. L. Laser cladding of nickel based carbide dispersion

16. Huang, Z., Hou, Q., and Wang, P. Microstructure and properties of Cr$_3$C$_2$-modified nickel-based alloy coating deposited by plasma transferred arc process. *Surf. Coat. Tech.*, 2008, **202**, 2993–2999.
17. Zhang, D-W., Lei, T. C., and Li, F-J. Laser cladding of stainless steel with Ni–Cr$_3$C$_2$ for improved wear performance. *Wear*, 2001, **251**, 1372–1376.
18. Verdi, D., Garrido, M. A., Munez, C. J., and Poza, P. Cr$_3$C$_2$ incorporation into an Inconel 625 laser cladded coating: effects on matrix microstructure, mechanical properties and local scratch resistance. *Mater. Design*, 2015, **67**, 20–27.
19. Luo, H-L., Gong, K., Li, S-P., Cao, X., Zhang, X-C., Feng, D., and Li, C-H. Abrasive wear comparison of Cr$_3$C$_2$/Ni$_3$Al composite and Stellite 12 alloy cladding. *J. Iron Steel Res. Int.*, 2007, **14**(4), 15–20.
20. Janicki, D. Laser cladding of Inconel 625-based composite coatings reinforced by porous chromium carbide particles. *Opt. Laser Technol.*, 2017, **94**, 6–14.
21. Sarjas, H., Juhani, K., Viljus, M., Matikainen, V., and Vuoristo, P. Wear resistance of HVOF sprayed from mechanically activated thermally synthesized Cr$_3$C$_2$–Ni powder. *Proc. Estonian Acad. Sci.*, 2016, **65**, 101–106.
22. Wei, C., Song, X., Zhao, S., Zhang, L., and Liu, W. In-situ synthesis of WC–Co composite powder and densification by sinter-HIP. *Int. J. Refract. Met. H.*, 2010, **28**, 567–571.
23. Jõeleht, M., Pirso, J., Juhani, K., Viljus, M., and Traksmaa, R. The formation of reaction sintered (Ti, Mo)C–Ni cermet from nanocrystalline powders. *Int. J. Refract. Met. H.*, 2014, **43**, 284–290.
24. Zhou, W., Zheng, Y., Zhao, Y., Zhang, G., Dong, Z., and Xiong, W. Fabrication of Ti(C,N)-based cermets by in-situ carbothermal reduction of MoO$_3$ and subsequent liquid sintering. *J. Am. Ceram. Soc.*, 2017, **100**, 1578–1587.
25. Ren, R., Yang, Z., and Shaw, L. L. A novel process for synthesizing nanostructured carbides: mechanically activated synthesis. In *22nd Annual Conference on Composites, Advanced Ceramics, Materials, and Structures: B: Ceramic Engineering and Science Proceedings* (Bray, D., ed.). John Wiley & Sons, Inc., Hoboken, New York, 1998, 461–468.
26. Chicardi, E., Gotor, F. J., Medri, V., Guicciardi, S., Lascano, S., and Córdoba, J. M. Hot-pressing of (Ti, Mt)(C, N)–Co–Mo$_2$C (Mt = Ta, Nb) powdered cermets synthesized by a mechanically induced self-sustaining reaction. *Chem. Eng. J.*, 2016, **292**, 51–61.
27. Sarjas, H., Surzhenkov, A., Juhani, K., Antonov, M., Adoberg, E., Kulu, P., et al. Abrasive-erosive wear of thermally sprayed coatings from experimental and commercial Cr$_3$C$_2$-based powders. *J. Therm. Spray Technol.*, 2017, **26**, 2020–2029.
28. Colaço, R. and Vilar, R. On the influence of the retained austenite in the abrasive wear behaviour of a laser surface melted tool steel. *Wear*, 2005, **258**, 225–231.

alloys for hardfacing applications. *Laser. Eng.*, 2003, **13**, 35–44.

Uudse Cr₃C₂–Ni armatuuriga räbustikaar- ja plasmakaarpealekeevitatud komposiitkõvapinnete uuring

Regita Bendikiene, Antanas Ciuplys, Simonas Mindaugas Jankus, Andrei Surzhenkov, Dmytro Tkachivskyi, Kristjan Juhani, Mart Viljus, Rainer Traksmaa, Maksim Antonov ja Priit Kulu

On uuritud mehaaniliselt aktiveeritud termosünteesi abil saadud Cr_3C_2–Ni kermise kasutamise võimalikkust armatuurina räbustikaar- (SAW) ja plasmakaarpealekeevitatud (PTAW) raud- ning nikkelmaatriksiga kõvapinnetes. Mikrostruktuuriuuringud näitasid, et kõvafaasi osakesed olid täielikult lahustunud SAW-pinnetes, kuid osaliselt säilinud PTAW-pinnetes. Põhilised faasid olid γ-Fe ja α-Fe koos Cr_7C_3-ga (PTAW-pinne) raudmaatriksiga pinnetes ning Cr_3C_2, CrC ja $NiC_{0,22}$ nikkelmaatriksiga pinnetes. Kermise kõvafaasina lisamine suurendas pinde kõvadust 1,1–3,3 korda, seejuures kõvaduse tõus oli suurim raudmaatriksiga PTAW-pinde korral. Fikseeritud abrasiiviga abrasiivkulumise tingimustes näitasid komposiitpinded armeerimata pinnetega võrreldes 1,2–7,8 korda paremat kulumiskindlust, fikseerimata abrasiiviga abrasiivkulumise tingimustes 1,4–9,4 korda paremat kulumiskindlust. PTAW-pinnete kulumiskindlus paranes rohkem, kusjuures erineva maatriksi mõju oli vähe märgatav. Kulumismehhanismidest oli mikrolõikamine põhiline kulumismehhanism mõlemat tüüpi abrasiivkulumise tingimustes, sellele lisandus mikrovagude teke ja karbiidiosakeste väljarebimine uuritud pinnetes. Kermiseosakeste lisamine ei muutnud oluliselt kulumismehhanisme.

Appendix 3

Article

HVOF Sprayed Fe-Based Wear-Resistant Coatings with Carbide Reinforcement, Synthesized In Situ and by Mechanically Activated Synthesis

Dmytro Tkachivskyi [1,*], Kristjan Juhani [1], Andrei Surženkov [1], Priit Kulu [1], Tomáš Tesař [2], Radek Mušálek [2], František Lukáč [2], Jakub Antoš [3], Marek Vostřák [3], Maksim Antonov [1] and Dmitri Goljandin [1]

[1] Department of Mechanical and Industrial Engineering, Tallinn University of Technology, Ehitajate tee 5, 19086 Tallinn, Estonia; kristjan.juhani@taltech.ee (K.J.); andrei.surzenkov@taltech.ee (A.S.); priit.kulu@taltech.ee (P.K.); maksim.antonov@taltech.ee (M.A.); dmitri.goljandin@taltech.ee (D.G.)
[2] Institute of Plasma Physics of the Czech Academy of Science, Za Slovankou 1782/3, 182 00 Prague, Czech Republic; tesar@ipp.cas.cz (T.T.); musalek@ipp.cas.cz (R.M.); lukac@ipp.cas.cz (F.L.)
[3] Research and Testing Institute Plzen, Tylova 1581/46, 301 00 Pilsen, Czech Republic; antos@vzuplzen.cz (J.A.); vostrak@vzuplzen.cz (M.V.)
* Correspondence: dmytro.tkachivskyi@taltech.ee

check for
updates

Abstract: The aims of this study were: (1) to produce composite coatings by high velocity oxy fuel (HVOF) spraying with steel matrix reinforced by cermets (a) Cr_3C_2–20%Ni and (b) TiC–20%NiMo, manufactured by mechanically activated synthesis (MAS); (2) to synthesize in situ a carbide reinforcement for iron matrix from a mixture of titanium and carbon during HVOF reactive thermal spraying (RTS); (3) to compare the wear resistance of produced coatings. As a reference, HVOF sprayed coatings from commercial Cr_3C_2–25%NiCr (Amperit 588.074) and AISI 316L were utilized. Study of microstructure revealed the inhomogeneity of the Cr-based MAS coating; the Ti-based MAS coating had typical carbide granular structure, and the Ti-based RTS coating possessed elongated structures of TiC. The X-ray diffraction revealed two main phases in the Cr-based MAS coating: Cr_3C_2 and austenite, and two phases in the Ti-based coatings: TiC and austenite. Among the studied coatings, the Cr-based MAS coating demonstrated the highest low-force hardness (490 HV0.3). During the abrasive rubber wheel test (ASTM G65), the Ti-based MAS coating showed the best wear resistance, followed by Cr_3C_2–25%NiCr and Ti-based RTS coating. In the abrasive–erosive test (GOST 23.201-78), the Ti-based MAS coating was 44% better than Cr_3C_2–25%NiCr coating. The Ti-based RTS coating was 11% more wear resistant than the reference Cr_3C_2–25%NiCr coating.

Keywords: mechanically activated synthesis; in situ synthesis; powder; TiC–NiMo; Cr_3C_2–Ni; coating; thermal spray; abrasive wear

1. Introduction

Transition metal carbide-based cermet coatings obtained by thermal spraying are deservedly appreciated in the industry for their superb durability. Particularly, good resistance to erosion is required in cyclone dust collectors used in the recycling industry or in hydroelectric valves of water dams. Similarly, the oil and building industries use equipment like slush-pump piston rods or concrete mixer screw conveyors, which need to stay resistant to abrasive wear [1]. However, the relatively high production costs of the feedstock cermet powders still limit their broader application [2,3]. One of the reasons is the high expenditures for the transition metals used for their production. For example,

the extraction of pure titanium from the ore, despite its abundance on Earth, remains complex, time consuming and relatively expensive [4].

At the same time, one of the first intermediate products in the pure Ti production, titanium dioxide (TiO_2) with purity up to 97% [5], has been reported to be successfully utilized for titanium carbide (TiC) synthesis via carbothermal reduction [6]. This drastically decreases the overall span of production and its cost. Another argument in favor of using TiO_2 as precursor powder for TiC synthesis is derived from the chemical reactivity of pure titanium. In study [7], aiming to synthesize TiC from elemental Ti and C powders, a tremendous amount of heat was reported to be released due to the exothermic nature of reaction. However, the information about the synthesis of TiC from TiO_2 during the manufacturing of bulk cermets remains relatively restricted [8,9]. Moreover, to the authors' best knowledge, no information about the application of TiO_2 for the production of TiC-based cermet powders for thermal spraying is available.

Another way to lower the final cost of a feedstock cermet powder or a thermally sprayed cermet coating would be to apply preliminary reactive sintering [10] using titanium dioxide powder as a precursor for spray powder production. Alternatively, the in situ synthesis of the carbide phase [11] during the deposition of the coating is considered. Multiple studies reported the successful in situ synthesis of TiC in coatings, using induction cladding [12], laser remelting [13], as well as various welding [14–16] and thermal spray [17,18] methods. The authors of this study [19] successfully achieved the in situ formation of TiC reinforcement inside of iron matrix using the selective laser melting technique. Similarly, in this research, stainless steel (AISI 316L) was added to all experimental compositions in order to form an iron matrix in the high velocity oxy fuel (HVOF) sprayed coatings. The HVOF spraying technique was comprised due to the high density of produced coatings, as well as their good adhesion with substrate and cohesion between particle splats. It is also shown by several researchers that Ti-based wear-resistant coatings produced by this method can possess remarkable hardness [20] and excellent abrasive–erosive wear resistance [21]. However, there is still a lack of comparative data about the thermally sprayed coatings with the ex situ added TiC-based and the in situ-synthesized reinforcement.

The present study addresses HVOF sprayed composite stainless steel-based coatings with the TiC-based and Cr_3C_2-based cermet reinforcement, synthesized via mechanically activated synthesis (MAS) [22], as well as composite coatings with the in situ synthesized TiC reinforcement. The focus is on using TiO_2 as non-flammable precursor powder for carboreduction; the shortening of the coating production process by using raw powders as an alternative feedstock materials; and comparing the wear resistance of coatings developed by different technological routes. The microstructure, hardness and abrasive wear resistance of the coatings are analyzed.

2. Materials and Methods

2.1. Powder Production and Characterization

Chemical compositions of raw powders for (MAS and reactive thermal spraying (RTS)) TiC-based and (MAS) Cr_3C_2-based [23] cermet powders are presented in Table 1. The chemical composition of reference Cr_3C_2-based cermet powder (Amperit 588.074, H.C. Starck) is included. For developing TiC–20%NiMo powder, the optimal ratio for carburization TiO_2:C was found to be 4:1 as well as the amount of NiMo binder and Ni:Mo ratio (2:1) [24]. The constituent powders were subjected to high energy milling in a conventional ball mill with WC–Co hardmetal lining and WC–Co balls (balls-to-powder ratio 20:1) for 72 h. Isopropyl alcohol was used as wetting agent. Then, the plasticizer was added to the powder (4 wt.% of paraffin; 120 wt.% of wetting agent due to low wetting of TiO_2) and the mixture was dried for 4 h. Reactive sintering in vacuum for another 4 h followed, where TiO_2 was carbothermally reduced according to the following equation:

$$TiO_{2(s)} + 3C_{(s)} = TiC_{(s)} + 2\,CO_{(g)} \tag{1}$$
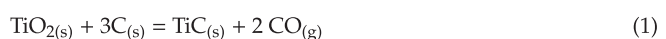
TiC grains grew from nano scale to micro scale particles of precursor powder (TiO$_2$) during the reactive sintering process, which is explained in detail in [25].

Table 1. Chemical composition and the amounts of constituents in the spraying powders.

Composition	Constituents and Their Amount, (wt.%)	Grade	Manufacturer	Average Particle Size (Range), (μm)	Chemical Composition, (wt.%)
MAS (TiC–20%NiMo)	64 TiO$_2$	Pretiox CG 100	Precheza a.s.	0.02	100 TiO$_2$
	16 C	7782-42-5	Imerys SA (Timrex KS6)	6.45	99.8 C, 0.1 moisture, 0.06 ash, bal. residuals
	13.3 Ni	Ni-7262	Pacific Particulate Materials Ltd.	2.4	99.7 Ni, 0.14 O, 0.14 C, bal. residuals
	6.7 Mo	Mo-7164	Pacific Particulate Materials Ltd.	2.32	99.8 Mo, 0.05 O, 0.0003 Fe, bal. residuals
MAS (Cr$_3$C$_2$–20%Ni)	69.3 Cr	Cr-6995	Pacific Particulate Materials Ltd.	6.65	99.5 Cr, 0.38 O, 0.01 Fe, bal. residuals
	10.7 C	7782-42-5	Imerys SA (Timrex KS6)	6.45	99.8 C, 0.1 moisture, 0.06 ash, bal. residuals
	20 Ni	Ni-7262	Pacific Particulate Materials Ltd.	2.4	99.7 Ni, 0.14 O, 0.14 C, bal. residuals
Cr$_3$C$_2$–25%NiCr	-	Amperit 588.074	H.C. Starck	15–45	Base Cr, 18–22 Ni, 0.6 O, 9–11 C, 0.5 Fe
RTS (Ti + C) + AISI 316L	32.8 Ti	HFTi-1 99.5%	Baoji Ziyu Metal Materials CO., Ltd.	20–90	98.8 Ti, 1.2 Al
	8.2 C [1]	-	-	20–90	100 C
	59 AISI 316L	16316	Castolin Eutectic®	20–90	Base Fe, 0.03 C, 17.5 Cr, 13 Ni, 2.7 Mo

[1] Obtained by disintegrator milling of graphite in Tallinn University of Technology.

Sprayed feedstock powders were prepared by the mechanical mixture of either the produced MAS-powders or the elementary Ti and C powders (for the in situ synthesis of TiC) with the stainless steel powder. MAS-powders and the in situ synthesized TiC were intended to serve as the reinforcement and the stainless steel as the matrix in the sprayed coatings. The proportions of the reinforcement and matrix powders, given in Table 2, were adjusted to provide the reinforcement/matrix ratio of (40:60 vol.%), which was found to be optimal [26]. The flowability of experimental powders was measured using a manual Hall flowmeter funnel (ASTM B213) [27].

Table 2. Reinforcement to matrix ratio of the experimental powders.

Composition	MAS (Cr$_3$C$_2$–20%Ni):AISI 316L	MAS (TiC–20%NiMo):AISI 316L	Ti:C: AISI 316L
Ratio, (vol.%)	50:50	56:44	32.8:8.2:59

The phase composition of the experimental powders was investigated by the X-Ray diffraction (XRD) method with Cu Kα radiation (D8 Discover, Burker, Bremen, Germany) with 0.025° step and a 1 s period. Particle morphology was assessed using a scanning electron microscope (SEM) EVO MA-15 (Carl Zeiss, Oberkochen, Germany) equipped with energy dispersive X-ray spectroscopy (EDS) detector XFlash® 5010. The analyzed powders were embedded in EpoFix epoxy resin and cross-sections were prepared using a standardized metallographic procedure.

2.2. Coating Deposition

Prepared powders were sprayed using HVOF spraying system HP/HVOF Tafa JP-5000® (Praxair Inc., Danbury, CT, USA). The substrate material with dimensions of 50 × 25 × 10 mm^3 was hot-rolled

S235 steel (wt.%: 0.19–0.23 C, 1.40 Mn, 0.0035 P, 0.035 S, 0.55 Cu, 0.012 Ni, bal. Fe). Spraying parameters for each experimental powder composition are presented in Table 3.

Table 3. Spraying parameters.

Composition	Oxygen Flow Rate, (L/min)	Kerosene Flow Rate, (L/h)	Powder Feed Rate, (g/min)	Carrier Gas Flow Rate, (L/min)	Spraying Distance, (mm)	Number of Passes
MAS (TiC–20%NiMo) + AISI 316L	870	28	60	5	380	14
RTS (Ti + C) + AISI 316L	870	28	60	5	380	6
MAS (Cr3C2–20%Ni) + AISI 316L	872	27	68	5	380	12
Cr3C2–25%NiCr (Amperit)	872	27	68	5	380	12
AISI 316L	900	24	100	5	360	7

2.3. Microstructure Studies

The polished cross-sections of specimens with sprayed coatings were studied with the SEM EVO MA-15 (Carl Zeiss, Oberkochen, Germany). The phase composition of coatings was investigated by the X-Ray diffraction (XRD) method with Cu Kα radiation (D8 Discover, Bruker, Bremen, Germany) with a 0.025° step and 1 s period.

2.4. Study of Hardness

Vickers low-force hardness on the surface and at the cross-sections was measured according to the standard ISO 6507-1 "Metallic materials—Vickers hardness test" [28], using a Nexus 4505 hardness tester (Innovatest, Maastricht, The Netherlands). The surface hardness of coatings was measured by indentation at 9.8 N (1 kgf) load, except for the MAS (Cr_3C_2–20%Ni) + AISI 316L, where the load of 2.94 N (0.3 kgf) was chosen due to the small thickness of the coating. The cross-section hardness of all coatings was measured at a load of 2.94 N (0.3 kgf). Dwell time was 10 s. For each material, ten measurements were made and an average value of hardness was evaluated. Standard deviation was calculated according to the following formula:

$$S = \sqrt{\frac{\Sigma(x - \overline{x})^2}{N - 1}}, \tag{2}$$

where S is the standard deviation, x is each value in the data set, $\overline{x}$ is a mean of all values in the data set, and N is a number of values in the data set.

2.5. Abrasive Wear Study

In order to evaluate the wear resistance of the coatings during the abrasive rubber wheel wear (ARRW), the test equipment was set according to the standard ASTM G65 "Standard Test Method for Measuring Abrasion Using the Dry Sand/Rubber Wheel Apparatus" (procedure E) [29]. Before testing, all samples were ultrasonically cleaned in acetone. Run in was done immediately before testing and overall 4 samples of each type of coating were tested. The average volume wear was calculated on the basis of the weight loss and the theoretical density of the coatings. The standard deviation was calculated according to Equation (2). The abrasive–erosive wear (AEW) was conducted according to the standard GOST 23.201-78 "Gas abrasive wear testing of materials and coatings with centrifugal

accelerator" [30]. Each testing batch comprised of 3 samples of the same coating. The average volume wear and standard deviation were calculated, using the same principle as in the abrasive wear test. The relative volumetric wear resistance ε_v was calculated with regard to reference wear-resistant bulk steel Hardox 400 (SSAB) by the following equation:

$$\varepsilon_v = I_v / I_v^{\,H\,400},$$ (3)

where I_v is the volumetric wear rate of the coating; $I_v^{\,H\,400}$ is the volumetric wear rate of steel Hardox 400.

The test parameters are shown in Table 4. The wear mechanisms of the worn surfaces were assessed by SEM TM1000 (Hitachi High-Technologies Europe GmbH, Mannheim, Germany).

Table 4. Parameters of the abrasive wear tests.

Wear Test	Load, (N)	Linear Speed, (m/s)	Impact Angle, (°)	Wheel Diameter, (mm)	Number of Wheel Revolutions	Testing Temp., (°C)	Abrasive Type and Size, (mm)	Abrasive Amount, (kg)	Abrasive Feed Rate, (g/s)	Duration of the Test, (s)
ARWW	130	2.4	–	227	1007	20	Silica, 0.2–0.3	1.85	5–6.5	300
AEW	–	40 [1]	30	–	–	20	Silica, 0.2–0.3	2 + 6 [2]	6.94	2400

[1] Velocity of abrasive particles; [2] Run-in—2 kg, regular test—6 kg.

3. Results and Discussion

3.1. Characterization of Spray Powders

Due to the irregular shape of the particles, the flowability of both single MAS and elementary powders could not be measured. However, feedstock powder mixtures that contained spherical stainless steel (AISI 316L) particles exhibited a satisfactory flowability (Table 5).

Table 5. Flowability of the experimental compositions and reference powders.

Composition	Flowability, s
MAS (TiC–20%NiMo) + AISI 316L	31.9 ± 0.3
RTS (Ti + C) + AISI 316L	49.2 ± 1.0
MAS (Cr_3C_2–20%Ni) + AISI 316L	55.7 ± 2.2
Cr_3C_2–25%NiCr (Amperit)	37.3 ± 0.2
AISI 316L	15.2 ± 0.1

Figure 1 shows the particle structures of the experimental powder mixtures and reference powder before thermoreaction. Experimental powders manufactured by the MAS method possessed particles of angular shape. In the particles of MAS (TiC–20%NiMo), the amount of cracks was higher than in the MAS (Cr_3C_2–20%Ni), which is a sign of a higher intrinsic brittleness of the TiC–NiMo cermets, as reported earlier in [31]. The average TiC grain size was also larger due to the higher sintering temperature: 1400 °C for TiC–20%NiMo [25] and 1075 °C for Cr_3C_2–20%Ni [23]. Particles of pure titanium (Figure 1b) exhibited an angular-like profile similar to TiC–20%NiMo particles, which, without adding mediators such as stainless steel, decreased its flowability remarkably. Particles of commercial Cr_3C_2–25%NiCr composition were found to be nearly round shaped with the presence of some porosity (Figure 1d).
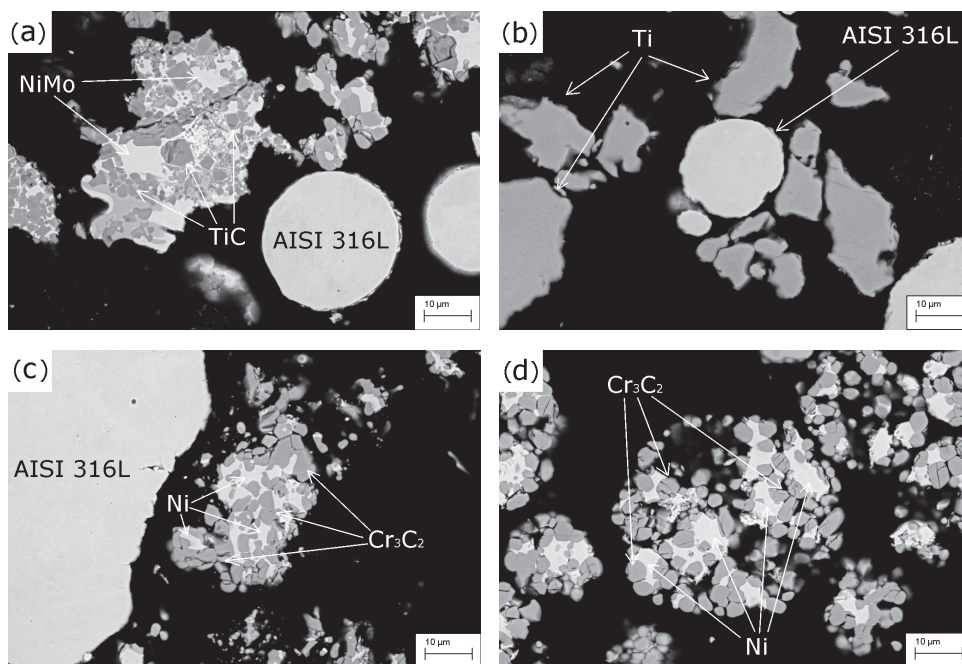
Figure 1. Particle structure of: (**a**) MAS (TiC–20%NiMo) + AISI 316L; (**b**) Ti + C + AISI 316L; (**c**) MAS (Cr_3C_2–20%Ni) + AISI 316L; and (**d**) Cr_3C_2–25%NiCr (Amperit).

Results of the XRD analysis of the experimental MAS powders are shown in Figure 2. Two main phases were revealed in each composition: chromium carbide (Cr_3C_2) and austenite (γ-Fe) in the Cr-based cermet powder and titanium carbide (TiC) and austenite (γ-Fe) in the Ti-based cermet powder. Additionally, metallic Ni was found in both compositions together with an insignificant amount of C in the Cr-based composition. The analysis of the XRD result of the agglomerated mixture of Ti, C and stainless steel is not presented. Unlike the MAS powders, it was not exposed to any kind of treatment at all; therefore, no phase transformation of its constituents is expected.
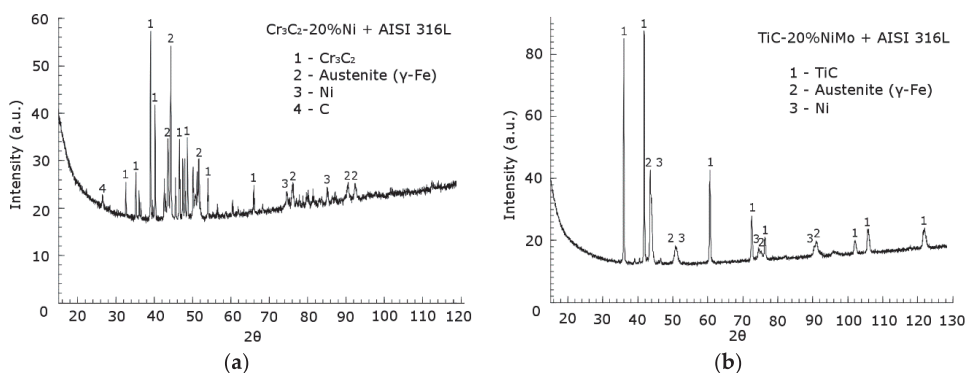
Figure 2. XRD patterns of experimental MAS powders: (**a**) Cr-based powder; (**b**) Ti-based powder.

3.2. Deposition of Coatings

In the deposition process of experimental Cr-based composition, stainless steel particles demonstrated a low melting ability, which, in turn, decreased its matrix-forming potential. This resulted in inhomogeneous structure of the coating, as well as low cohesion between the splats and the relatively small thickness of the coating (Figure 3a,b). Particles of pure stainless steel melted better; however, separate splats could still be clearly distinguished (Figure 3c). In Figure 3d, the SEM image of a surface depicts an abundance of unmelted stainless steel particles. This might be caused by the average size of the stainless steel particles (20–90 μm), which, as compared to cermets, may require more heat for complete melting. As expected, Cr_3C_2–25%NiCr coating obtained from commercial powder had a good homogeneity and dense carbide structure (Figure 3e,f). Due to its good flowability and, therefore, the absence of stainless steel in this powder, all carbide particles were properly melted.
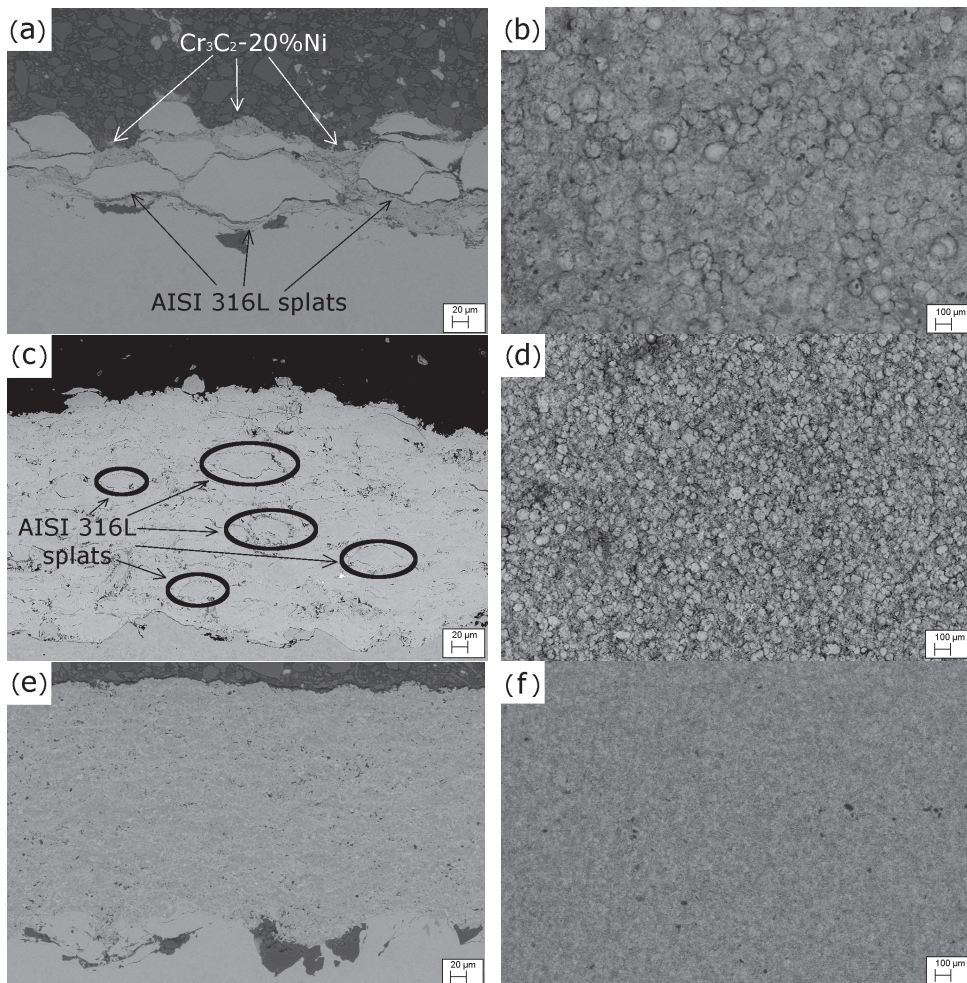
Figure 3. Microstructure (left column) and surface images (right column) of high velocity oxy fuel (HVOF) sprayed coatings: (**a**,**b**) MAS (Cr_3C_2–20%Ni) + AISI 316L; (**c**,**d**) AISI 316L (commercial); (**e**,**f**) Cr_3C_2–25%NiCr (Amperit).

Coatings produced from the Ti-based MAS powder and the RTS mixture of Ti, C and stainless steel (Figure 4) exhibited much better homogeneity and fewer unmolten particles than those of the Cr-based MAS powder. This effect can be the result of the difference in spraying parameters (Table 3). Some porosity was observed on the surface of the coatings (Figure 4b,d). The Ti-based MAS coating possessed a lamellar structure while the RTS coating consisted of swirled alternating layers of the iron-based matrix and TiC reinforcement with minor cracks. Nevertheless, the complete melting of stainless steel particles was not achieved in either of the coatings. The distribution of constituents in the TiC reinforcement of the Ti-based coatings is shown in Figure 5.
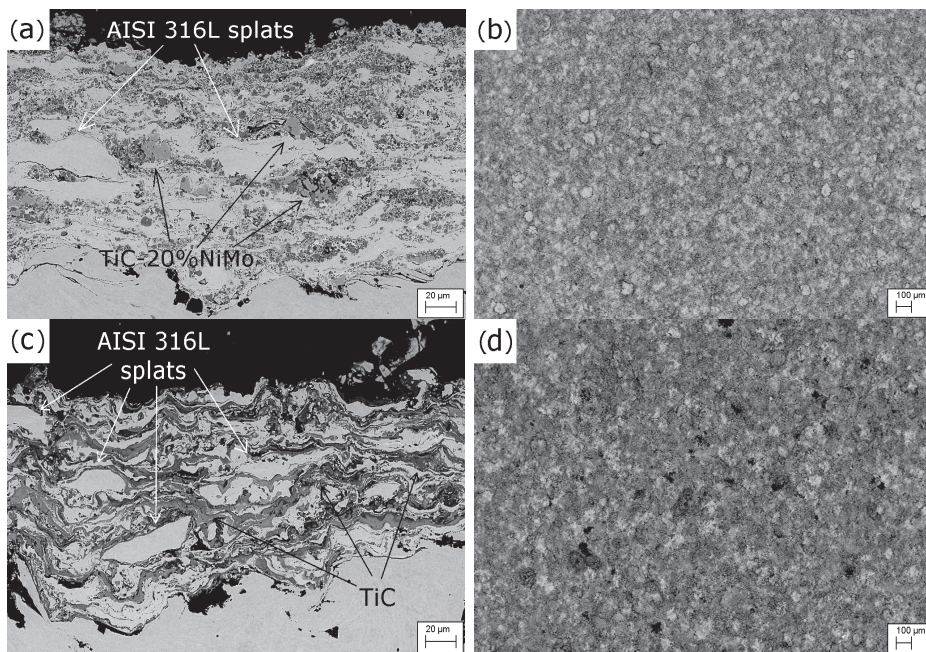
Figure 4. Microstructure (left column) and surface images (right column) of Ti-based HVOF sprayed coatings: (**a**,**b**) MAS (TiC–20%NiMo) + AISI 316L; (**c**,**d**) RTS (Ti + C) + AISI 316L.
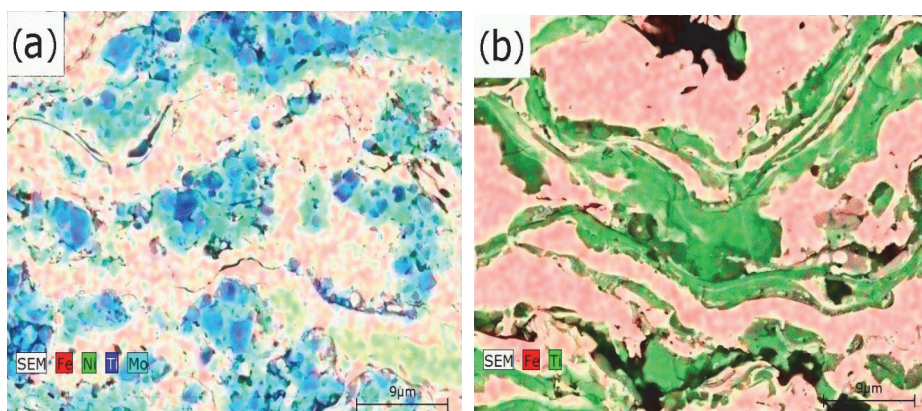
Figure 5. EDS maps of Ti-based coatings: (**a**) MAS (TiC–20%NiMo) + AISI 316L; (**b**) RTS (Ti + C) + AISI 316L.

Phase compositions of the experiment coatings, as evaluated by XRD, are presented in Table 6. The analysis has revealed the presence of two main phases in each coating. They were either TiC or Cr_3C_2 and austenite (γ-Fe). The Cr_3C_2 phase did not change to Cr_7C_3 after spraying, however, a small amount (~4.4 wt.%) of Cr_2O_3 was found in the Cr-based MAS coating. The α-Ti phase could be formed due to the excessive burning out of carbon, meant for bonding with Ti. XRD diffractograms of the experimental coatings are shown in Figure 6.
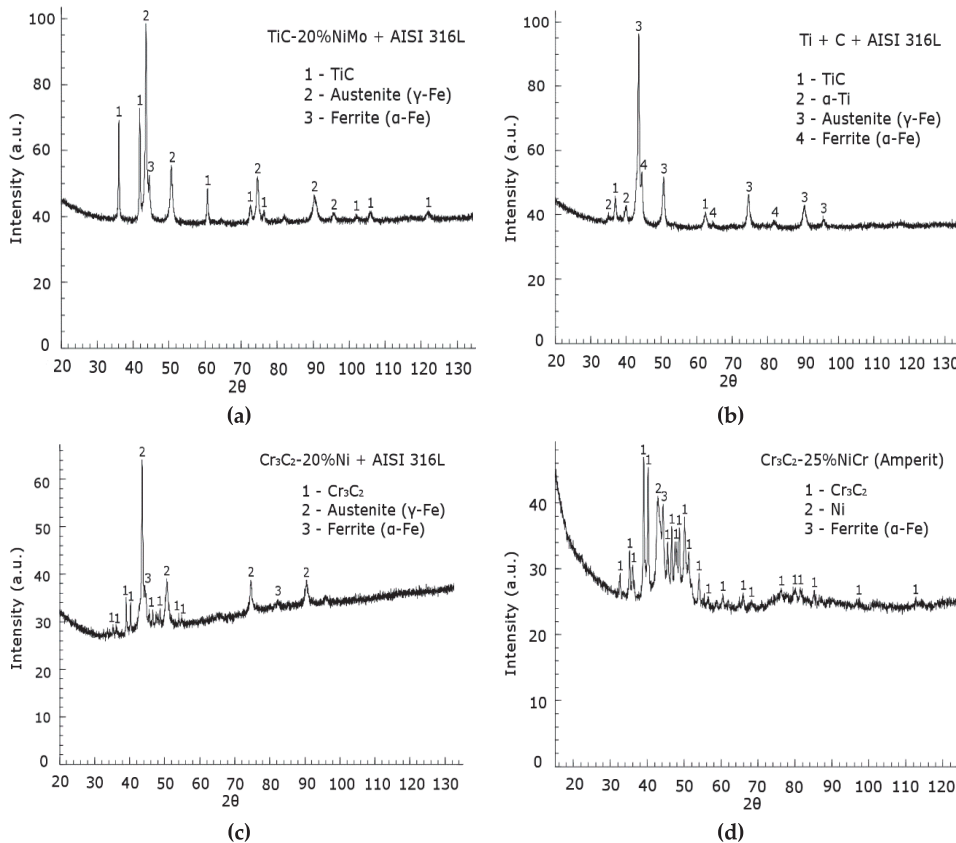
Figure 6. XRD patterns of the HVOF sprayed coatings. (**a**) Ti-based MAS coating; (**b**) Ti-based RTS coating; (**c**) Cr-based MAS coating; (**d**) Reference coating (Amperit).

Table 6. Phase composition of the HVOF sprayed coatings.

Type of Coating	TiC, (wt.%)	α-Ti, (wt.%)	Cr_3C_2, (wt.%)	Ni, (wt.%)	γ-Fe, (wt.%)	α-Fe, (wt.%)
MAS (TiC–20%NiMo) + AISI 316L	37.8	–	–	–	53.2	9
RTS (Ti + C) + AISI 316L	27	12.8	–	–	47.6	12.6
MAS (Cr_3C_2–20%Ni) + AISI 316L	–	–	36.1	–	44.8	14.6
Cr_3C_2–25%NiCr (Amperit)	–	–	58.2	41.8	–	–
AISI 316L	–	–	–	–	88.8	11.2

3.3. Hardness of the Coatings

MAS (Cr_3C_2–20%Ni) + AISI 316L coating demonstrated the highest surface hardness among the experimental coatings, while the cross-sectional hardness among developed coatings was highest in the MAS (TiC–20%NiMo) + AISI 316L coating (Table 7).

Table 7. Thickness and hardness of the HVOF sprayed coatings.

Type of Coating	Thickness, (μm)	Vickers Hardness HV, (GPa)		
		Surface		Cross-Section
		HV1	HV0.3	HV0.3
MAS (TiC–20%NiMo) + AISI 316L	120	4.5 ± 1.0	-	4.5 ± 1.3
RTS (Ti + C) + AISI 316L	90	4.0 ± 0.6	-	3.3 ± 0.7
MAS (Cr_3C_2–20%Ni) + AISI 316L	55	-	4.9 ± 1.1	2.6 ± 0.8
Cr_3C_2–25%NiCr (Amperit)	263	8.8 ± 1.0	8.2 ± 2.1	9.2 ± 1.6
AISI 316L	203	3.2 ± 0.4	2.7 ± 1.2	3.1 ± 0.7

3.4. Abrasive Wear

Figure 7 presents the data of the abrasive rubber wheel wear (ARWW) test according to ASTM G65 standard. Experimental MAS (TiC–20%NiMo) + AISI 316L coating exhibited a slightly lower wear rate than the commercial Cr_3C_2–25%NiCr coating. Both experimental Ti-based coatings showed better results than Hardox 400 steel, whose wear rate data were taken from [32].
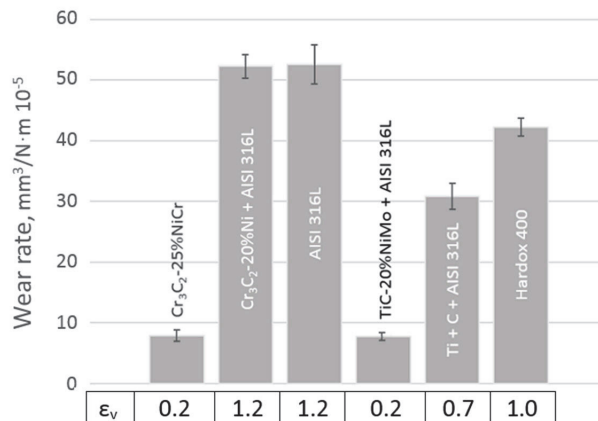
Figure 7. Wear rates and relative volumetric wear resistance (ε_V) of HVOF sprayed coatings to Hardox 400 steel at ARWW.

As can be seen from Figure 7 below, the presence of a carbide phase in the coatings with iron matrix increases their wear resistance, except for the coating with the MAS (Cr_3C_2–20%Ni) reinforcement. The relatively low cohesion between the latter and the stainless steel matrix is the most probable reason for the relatively low wear resistance of the corresponding coating.

Somewhat surprising are the nearly equal wear rates of the MAS (TiC–20%NiMo) + AISI 316L and the reference Cr_3C_2–25%NiCr coating. To further explore this phenomenon, wear mechanisms of the coatings under abrasive sliding wear (ARWW) (Figure 8) and abrasive–erosive wear (AEW) with low impact angle ($\alpha = 30°$) (Figure 9) were evaluated. The common wear mechanism for the performed tests (ARWW and AEW) was microcutting. In the case of plastic materials (AISI 316L, Hardox 400), numerous grooves with metallic chips were found on the surface. Additionally, these reference

materials were subjected to forming surface pits via material depletion, but were crack-free without visible material fracturing (Figure 10e,f).

For the Cr-based coatings (MAS (Cr_3C_2–20%Ni) + AISI 316L; Cr_3C_2–25%NiCr (Amperit)), the wear mechanism was a combination of the microcutting of the softer metallic matrix and the microchipping of brittle carbide reinforcement. The abrasive, seemingly, had been depleting the surrounding metallic matrix and the consequent peeling of carbide particles occured (Figures 8c,d and 9c,d). These coatings were observed to have additional microcracking and spalling. In the composite Ti-based coatings (MAS and RTS), the wear was similar to that of the Cr-based MAS coating. The wear of the steel matrix was more intense compared to the carbide reinforcement (Figure 8a,b). In some parts, carbide clusters were depleted, delaminated (Figure 8b) or formed surface pits (Figure 9a,b).
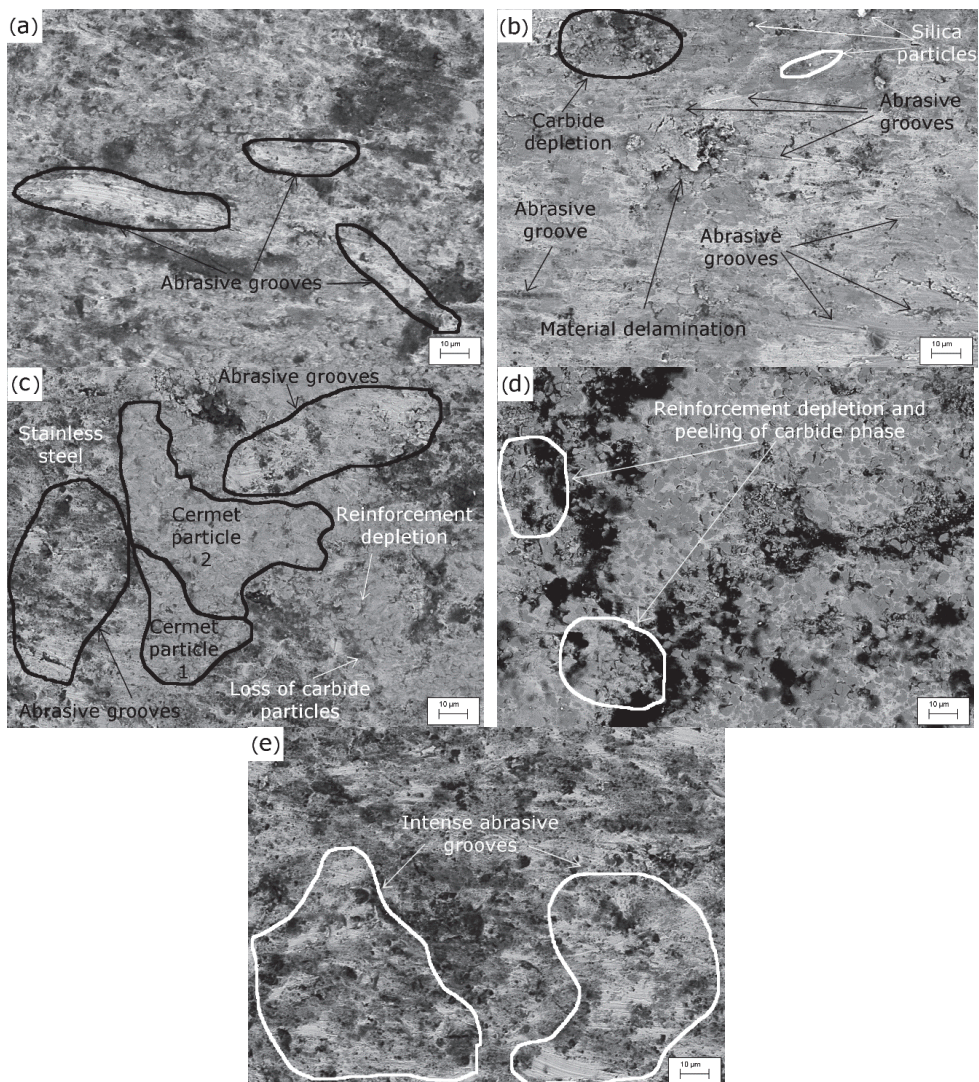
Figure 8. Topography of the wear surfaces after ARWW: (**a**) MAS (TiC–20%NiMo) + AISI 316L; (**b**) RTS (Ti + C) + AISI 316L; (**c**) MAS (Cr_3C_2–20%Ni) + AISI 316L; (**d**) Cr_3C_2–25%NiCr (Amperit); (**e**) AISI 316L.

Silica abrasive residues were observed on the surface of experimental coating RTS (Ti + C) + AISI 316L (Figure 8b). These defects may have emerged due to the domination in the composition of iron solid solutions, which gives the coating ductile properties.
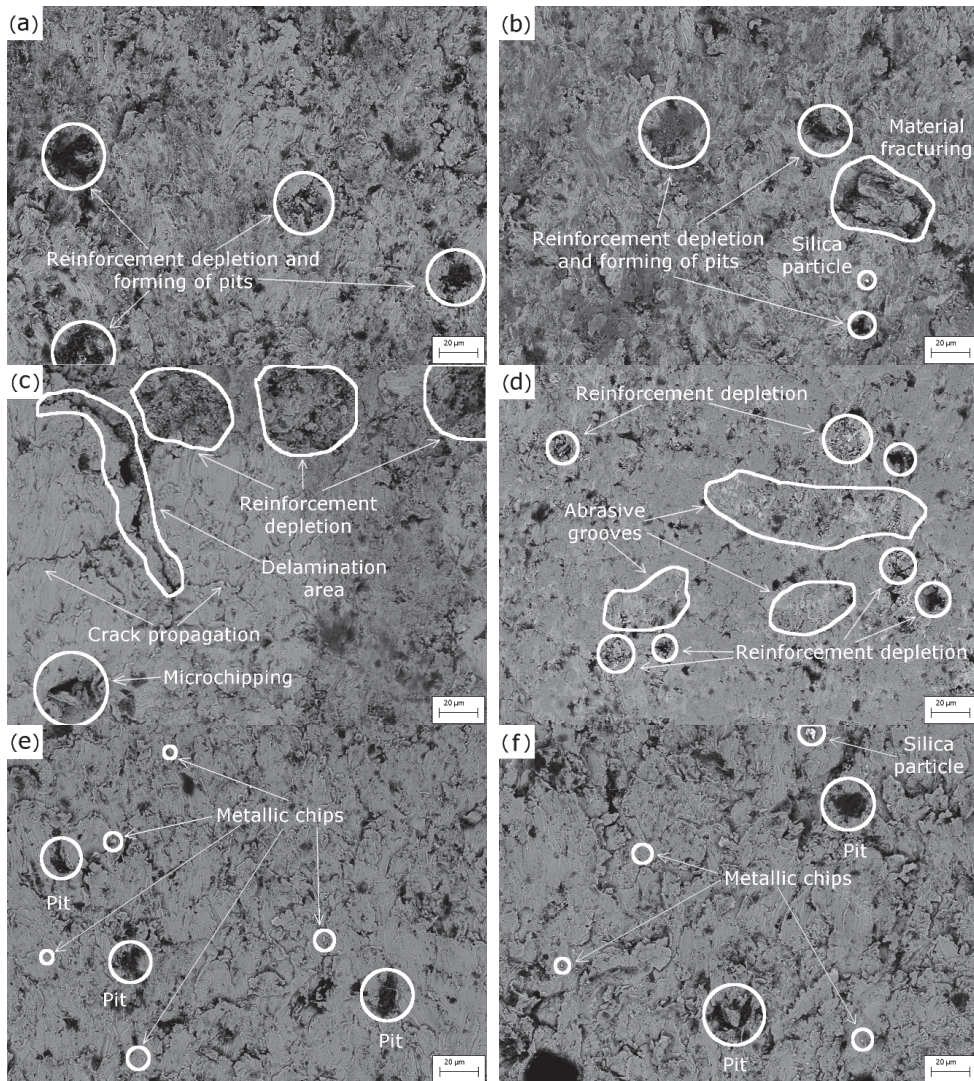
Figure 9. The topography of the wear surfaces after AEW: (**a**) MAS (TiC–20%NiMo) + AISI 316L; (**b**) RTS (Ti + C) + AISI 316L; (**c**) MAS (Cr_3C_2–20%Ni) + AISI 316L; (**d**) Cr_3C_2–25%NiCr (Amperit); (**e**) AISI 316L; (**f**) Hardox 400.
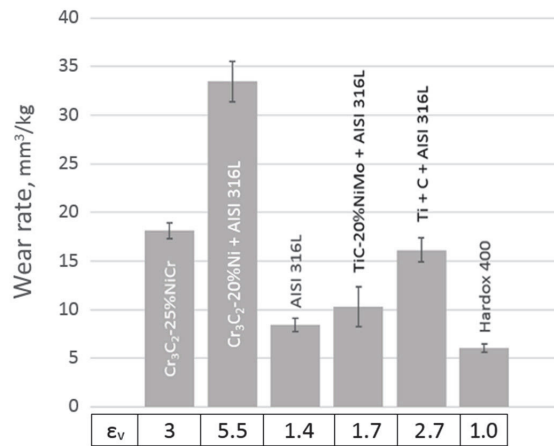
Figure 10. Wear rates and relative volumetric wear resistance (ε_V) to the Hardox 400 steel of HVOF sprayed coatings at AEW.

Resistance of the developed materials to abrasive–erosive wear is shown in Figure 10. During the run-in test with 2 kg of silica, Hardox 400 steel showed almost two times less material loss than during a regular test with 6 kg of abrasive. This means that silica particles embedded in the surface of the tested samples due to intrinsically softer structure of metals [33]. On the SEM images, silica residues were observed on the tested surfaces even after regular testing (Figure 10f). Therefore, the plasticity of Hardox 400 steel and AISI 316L sprayed coating allowed them to exhibit the lowest loss of material. As for carbide-containing coatings, generally they possess higher brittleness under impact erosion than their metallic counterparts. In this study, each experimental coating contained roughly 40 wt.% of carbide phase, except for the RTS coating (Table 6). As a result, the coatings did not demonstrate competitive wear resistance in the abrasive–erosive testing. However, due to the presence of steel matrix, both Ti-based coatings outperformed the commercial Cr_3C_2–25%NiCr (Amperit) coating by 44% (MAS) and 11% (RTS). MAS (Cr_3C_2–20%Ni) + AISI 316L coating exhibited the lowest wear resistance due to its weak intersplat cohesion and low coating thickness.

4. Conclusions

1. HVOF sprayed wear-resistant composite coatings were designed from cermet powders produced by mechanically activated synthesis (MAS) and from the agglomerated mixture of elemental powders.

2. Carbide phase formation was achieved by the carbothermal reduction of TiO_2 via MAS and by in situ synthesis during the deposition of the agglomerated mixture via reactive thermal spray (RTS) of (Ti + C) + AISI 316L. The Ti-based MAS coating showed homogeneous and fine-grained microstructure.

3. Developed Ti-based coatings (MAS and RTS) were demonstrated to be superior to Cr_3C_2–25%NiCr coating performance in the abrasive–erosive test. However, the abrasive–erosive wear resistance of the developed materials can be enhanced even further by increasing the presence of metal matrix in the composite. Compared to the Ti-based RTS coating, the Ti-based MAS coating is more applicable to abrasive rubber wheel wear due to containing 10% more of the hard carbide phase. Its performance was slightly better than that of the reference Cr_3C_2–25%NiCr coating. Cr-based MAS coating did not exhibit satisfactory wear resistance due to its inhomogeneous microstructure.

References

1. Davis, E.J. Introduction to Applications for Thermal Spray Processing. In *Handbook of Thermal Spray Technology*; Davis, J.R., Ed.; ASM International: Geauga County, OH, USA, 2004; p. 172.

2. Sarjas, H.; Kulu, P.; Juhani, K.; Vuoristo, P. Vuoristo, Novel WC-Co Spray Powders and HVOF Sprayed Coatings on Their Basis. In Proceedings of the 28th International Conference on Surface Modification Technologies, Tampere, Finland, 16–18 June 2014.

3. Sarjas, H.; Kulu, P.; Juhani, K.; Viljus, M.; Matikainen, V.; Vuoristo, P. Wear resistance of HVOF sprayed coatings from mechanically activated thermally synthesized Cr_3C_2–Ni spray powder. *Proc. Est. Acad. Sci.* **2016**, *65*, 101. [CrossRef]

4. Bordbar, H.; Yousefi, A.A.; Abedini, H. Production of titanium tetrachloride ($TiCl_4$) from titanium ores: A review. *Polyolefins J.* **2017**, *4*, 150–169.

5. Kang, J.; Okabe, T.H. Removal of Iron from Titanium Ore through Selective Chlorination Using Magnesium Chloride. *Mater. Trans.* **2013**, *54*, 1444–1453. [CrossRef]

6. Woo, Y.-C.; Kang, H.-J.; Kim, D.J. Formation of TiC particle during carbothermal reduction of TiO_2. *J. Eur. Ceram. Soc.* **2007**, *27*, 719–722. [CrossRef]

7. Rahimi-Vahedi, A.; Adeli, M.; Saghafian, H. Formation of Fe-TiC composite clad layers on steel using the combustion synthesis process. *Surf. Coat. Technol.* **2018**, *347*, 217–224. [CrossRef]

8. Terry, B.S.; Chinyamakobvu, O.S. In situ production of Fe-Tic composites by reactions in liquid iron alloys. *J. Mater. Sci. Lett.* **1991**, *10*, 628–629. [CrossRef]

9. Nuilek, K.; Memongkol, N.; Niyomwas, S. The Effect of TiO_2 on Synthesizing Fe-TiC Composites. In Proceedings of the 4th Thailand Materials Science and Technology Conference, Bangkok, Thailand, 31 March–1 April 2006.

10. Sarjas, H.; Surzhenkov, A.; Juhani, K.; Antonov, M.; Adoberg, E.; Kulu, P.; Viljus, M.; Traksmaa, R.; Matikainen, V.; Vuoristo, P. Abrasive-Erosive Wear of Thermally Sprayed Coatings from Experimental and Commercial Cr_3C_2-Based Powders. *J. Therm. Spray Technol.* **2017**, *26*, 2020–2029. [CrossRef]

11. Zhang, G.; Zheng, Y.; Zhou, W.; Zhao, Y.; Zhang, J.; Ke, Z.; Yu, L. Microstructure and mechanical properties of Ti(C,N)-based cermets fabricated by in situ carbothermal reduction of TiO_2 and subsequent liquid phase sintering. *Ceram. Int.* **2018**, *44*, 3092–3098. [CrossRef]

12. Yu, H.; Zhang, W.; Wang, H.; Ji, X.; Song, Z.; Li, X.; Xu, B. In-situ synthesis of TiC/Ti composite coating by high frequency induction cladding. *J. Alloy Compd.* **2017**, *701*, 244–255. [CrossRef]

13. Khalili, A.; Goodarzi, M.; Mojtahedi, M.; Torkamany, M.J. Solidification microstructure of in-situ laser-synthesized Fe-TiC hard coating. *Surf. Coat. Technol.* **2016**, *307*, 747–752. [CrossRef]

14. Wang, X.; Song, S.; Qu, S.; Zou, Z. Characterization of in situ synthesized TiC particle reinforced Fe-based composite coatings produced by multi-pass overlapping GTAW melting process. *Surf. Coat. Technol.* **2007**, *201*, 5899–5905. [CrossRef]

15. Emamian, A.; Corbin, S.F.; Khajepour, A. Tribology characteristics of in-situ laser deposition of Fe-TiC. *Surf. Coat. Technol.* **2012**, *206*, 4495–4501. [CrossRef]

16. Gallo, S.C.; Alam, N.; O'Donnell, R. In Situ Synthesis of TiC-Fe Composite Overlays from Low Cost TiO_2 Precursors Using Plasma Transferred Arc Deposition. *J. Therm. Spray Technol.* **2013**, *23*, 551–556. [CrossRef]

17. Liu, H.; Huang, J. Reactive thermal spraying of TiC-Fe composite coating by using asphalt as a carbonaceous precursor. *J. Mater. Sci.* **2005**, *40*, 4149–4151. [CrossRef]

18. Sun, X.; Huang, J.; Yang, J.; Chen, S. Microstructure evolution and mechanical properties of in-situ bimodal TiC-Fe coatings prepared by reactive plasma spraying. *Ceram. Int.* **2019**, *45*, 5848–5857. [CrossRef]

19. Almangour, B.; Grzesiak, D.; Yang, J.-M. In-situ formation of novel TiC-particle-reinforced 316L stainless steel bulk-form composites by selective laser melting. *J. Alloy. Compd.* **2017**, *706*, 409–418. [CrossRef]

20. Bolelli, G.; Colella, A.; Lusvarghi, L.; Morelli, S.; Puddu, P.; Righetti, E.; Sassatelli, P.; Testa, V. TiC-NiCr thermal spray coatings as an alternative to WC-CoCr and Cr_3C_2-NiCr. *Wear* **2020**, 203273. [CrossRef]

21. Surzhenkov, A.; Goljandin, D.; Traksmaa, R.; Viljus, M.; Talviste, K.; Aruniit, A.; Latokartano, J.; Kulu, P. High Temperature Erosion Wear of Cermet Particles Reinforced Self-Fluxing Alloy HVOF Sprayed Coatings. *Mater. Sci. (Medžiagotyra)* **2015**, *21*, 386–390. [CrossRef]

22. Pirso, J.; Viljus, M.; Letunovits, S.; Juhani, K. Reactive carburizing sintering—A novel production method for high quality chromium carbide–nickel cermets. *Int. J. Refract. Met. Hard Mater.* **2006**, *24*, 263–270. [CrossRef]

23. Tkachivskyi, D.; Juhani, K.; Surzhenkov, A.; Kulu, P.; Viljus, M.; Traksmaa, R.; Jankauskas, V.; Leišys, R. Production of Thermal Spray Cr_3C_2-Ni Powders by Mechanically Activated Synthesis. *Key Eng. Mater.* **2019**, *799*, 31–36. [CrossRef]

24. Pirso, J.; Viljus, M.; Juhani, K.; Kuningas, M. Three-body abrasive wear of TiC-NiMo cermets. *Tribol. Int.* **2010**, *43*, 340–346. [CrossRef]

25. Jõeleht, M.; Pirso, J.; Juhani, K.; Viljus, M.; Traksmaa, R. The formation of reactive sintered (Ti, Mo)C-Ni cermet from nanocrystalline powders. *Int. J. Refract. Met. Hard Mater.* **2014**, *43*, 284–290. [CrossRef]

26. Kulu, P.; Pihl, T. Selection Criteria for Wear Resistant Powder Coatings Under Extreme Erosive Wear Conditions. *J. Therm. Spray Technol.* **2002**, *11*, 517–522. [CrossRef]

27. ASTM International. *ASTM B213-20, Standard Test Methods for Flow Rate of Metal Powders Using the Hall Flowmeter Funnel*; ASTM International: West Conshohocken, PA, USA, 2020.

28. ISO 6507-1. *Metallic Materials—Vickers Hardness Test 2018*; International Organization for Standardization: Geneva, Switzerland, 2018.

29. ASTM International. *ASTM G65-16e1, Standard Test Method for Measuring Abrasion Using the Dry Sand/Rubber Wheel Apparatus*; ASTM International: West Conshohocken, PA, USA, 2016.

30. GOST 23.201-78 Standard. *Products Wear Resistance Assurance, Gas Abrasive Wear Testing of Materials and Coatings with Centrifugal Accelerato*; Publishing House of Standards: Moscow, Russia, 1987. (In Russian)

31. Pirso, J.; Viljus, M.; Letunovitš, S.; Juhani, K.; Joost, R. Three-body abrasive wear of cermets. *Wear* **2011**, *271*, 2868–2878. [CrossRef]

32. Antonov, M.; Veinthal, R.; Yung, D.-L.; Katušin, D.; Hussainova, I. Mapping of impact-abrasive wear performance of WC-Co cemented carbides. *Wear* **2015**, *332*, 971–978. [CrossRef]

33. Antonov, M.; Pirso, J.; Vallikivi, A.; Goljandin, D.; Hussainova, I. The effect of fine erodent retained on the surface during erosion of metals, ceramics, plastic, rubber and hardmetal. *Wear* **2016**, *354–355*, 53–68. [CrossRef]

Appendix 4

Comparative Study of Plasma Cladded Fe-Based Composite Hardfacings with *In Situ* Synthesized Cr and Ti Carbide Reinforcement

Dmytro Tkachivskyi[a *], Mart Viljus[b], Rainer Traksmaa[c], Maksim Antonov[d], Andrei Surzhenkov[e], Kristjan Juhani[f] and Priit Kulu[g]

Department of Mechanical and Industrial Engineering, Tallinn University of Technology, Ehitajate tee 5, 19086 Tallinn, Estonia

[a]dmytro.tkachivskyi@taltech.ee, [b]mart.viljus@taltech.ee, [c]rainer.traksmaa@taltech.ee, [d]maksim.antonov@taltech.ee, [e]andrei.surzenkov@taltech.ee, [f]kristjan.juhani@taltech.ee, [g]priit.kulu@taltech.ee

Keywords: PTA; cladding; Fe-based hardfacing; *in-situ* synthesis; carbide reinforcement.

Abstract. This study aimed to compare the X3CrNiMo17-13-3 stainless steel based plasma transferred arc (PTA) cladded hardfacings, reinforced with the *in-situ* synthesized Cr and Ti carbides. Carbon black and either pure Cr, pure Ti, or TiO_2 were utilized as reinforcement precursors (the respective hardfacings are further referred to as Cr+C, Ti+C and TiO_2+C). The pre-placed mixtures of matrix and reinforcement precursor powders were remelted by the plasma transferred arc, applying the preliminarily optimized process parameters (95 A, 22 – 24 V, 0.2 mm/s). As a reference, the unreinforced stainless steel hardfacing was used. The carbide reinforcement was successfully *in-situ* synthesized in all the hardfacings. The $Cr + C$ hardfacing exhibited the largest average hardness (556 ± 29 HV1), while the $TiO_2 + C$ hardfacing had the largest average Young's modulus (156.3 ± 19.7 GPa). The $Cr + C$ and $Ti + C$ hardfacings demonstrated the 2.3 and 2.1 times higher resistance to abrasive wear than the reference hardfacing. The $TiO_2 + C$ hardfacing showed 1.5 times lower wear resistance than the reference hardfacing presumably due to a lack of the reinforcement and a lower strain hardening ability.

Introduction

The *in-situ* synthesis of reinforcement of a metal matrix composite (MMC) has multiple advantages over its *ex-situ* addition, such as higher mechanical properties of the MMC, reinforcement's better thermodynamic stability, etc. [1]. Among the other matrix-reinforcement combinations, Fe-based matrix with the *in-situ* synthesized TiC has probably been studied most intensively. The reasons are a good performance-to-price ratio of the obtained MMCs [2], as well as strong carbide forming ability of titanium [3], impossibility of formation of mixed Ti-Fe carbides [3,4] with lower hardness, than pure TiC, stability of TiC in a Fe-based melt [4], as well as a relatively good wettability of TiC by the molten iron [5].

In the case of the Fe-based surface MMCs (hardfacings), pure Ti [3] and ferrotitanium (FeTi; [6]) are most frequently utilized for the *in-situ* synthesis of TiC. However, both have certain disadvantages. Pure Ti is more prone to oxidation during hardfacing deposition, moreover, it is more expensive [7]. In its turn, the content of Ti in FeTi is relatively low, what doesn't allow to obtain a high content of TiC in the resultant hardfacing [8]. However, the information about the potential substitutes, such as ilmenite ($FeTiO_3$; [9]) and especially titanium dioxide (TiO_2; [10]) still remains limited.

Apart from that, the general disadvantage of TiC as a reinforcement in the Fe-based hardfacings is its relatively low density (4.94 g/cm^3), as a result of which TiC tends to segregate in the upper part of the hardfacing [7]. Thus some properties of such a MMC hardfacing, such as resistance to wear, are going to decrease during the service life of the hardfaced component. At the same time, despite chromium carbides, such as Cr_3C_2, Cr_7C_3, etc., exhibit a similar density to Fe-based alloys, only few studies [11,12] about their *in-situ* synthesis in a Fe-based composite hardfacing may be found.

For deposition of composite hardfacings with the *in-situ* synthesized reinforcement, various welding technologies, such as laser welding [7-9,12], tungsten inert gas (TIG) welding [13-15], and plasma transferred arc welding (PTAW) [10,16,17] are applied most extensively. Among these, the PTAW technology exhibits lower production cost and higher production rates to be compared with laser welding [18,19], as well as lower distortion of the substrate to be compared with TIG welding [20]. Typical applications of the PTAW technology include valve seats, buckets of wheel excavators, agricultural equipment, compressor blades of a plane engine, etc. [19].

The present research aims to compare the PTAW Fe-based composite hardfacings with the TiC reinforcement, *in-situ* synthesized from Ti and TiO_2 precursors, as well as the PTAW Fe-based hardfacings, reinforced by the *in-situ* synthesized Cr and Ti carbides.

Experimental

Deposition of Hardfacings. The data of the feedstock powders are given in Table 1. The feedstock powders were mixed in the proportions, given in Table 2, along with paraffine and pre-placed on the preliminarily sand-blasted and degreased substrates ($35 \times 25 \times 10$ mm), made from the normalized steel S235 (wt.%: $0.19 - 0.23$ C, 1.40 Mn, 0.0035 P, 0.035 S, 0.55 Cu, 0.012 Ni, bal. Fe) and dried at the room temperature during 24 hours. The approximate thickness of the pre-placed layers after drying was 1.5 mm.

After it, the pre-fabricated specimens were heated at 300 °C for 6 hours. Instantly after this, the powder mixtures were remelted by the plasma transferred arc, using the PTAW device EuTronic Gap 3001 DC (Castolin Eutectics®). The same preliminarily optimized remelting parameters (95 A, $22 - 24$ V, 0.2 mm/s, plasma gas (Ar) flow – 0.025 dm^3/s, shield gas (Ar) flow – 0.108 dm^3/s) were applied for all the powder mixtures. During the remelting process, graphite plates were utilized to prevent the splashing of the melt off the substrate. As a reference, the hardfacing from the matrix material (stainless steel X3CrNiMo17-13-3) was deposited, applying the same deposition parameters, as during remelting, except for the powder feed rate (0.085 g/s) and the carrier gas (Ar+H_2) flow (0.0625 dm^3/s).

Table 1. Chemical composition of the feedstock powders

Powder	Type	Manufacturer	Particle size [μm]	Chemical composition [wt%]
Stainless steel	Matrix	Castolin Eutectics®	$10 - 45$	0.03 C, 17.5 Cr, 13 Ni, 2.7 Mo, bal. Fe
Carbon black	Reinforcement precursor	Imerys SA	$5.5 - 7$	99.8 C, 0.1 moisture, 0.06 ash, bal. residuals
Cr	Reinforcement precursor	Pacific Particulate Materials Ltd.	$5 - 10$	99.5 Cr, 0.38 O, 0.01 Fe, bal. residuals
Ti	Reinforcement precursor	Baoji Ziyu Metal Materials CO., LTD	$60 - 80$	98.8 Ti, 1.2 Al
TiO_2	Reinforcement precursor	Tronox Holdings Plc.	$0.1 - 0.3$	100 TiO_2

Table 2. Designations and feedstock compositions of the hardfacings

Designation	Feedstock powder [wt.%]				
	Stainless steel	Carbon black	Cr	Ti	TiO_2
SS	100	–	–	–	–
Cr + C	60	8	32	–	–
Ti + C	50	10	–	40	–
TiO_2 + C	50	10	–	–	40

Microstructure Studies. The polished cross-sections of the hardfacings were studied under the scanning electron microscope (SEM) Evo MA-15 (Carl Zeiss, Germany). In order to later get a more reliable picture of the relationship between the microstructure and the wear performance, the machined samples were used for the microstructure studies. The final thickness of the machined SS, Cr + C and Ti + C samples was about 0.75 mm. The one of the machined TiO_2 + C sample was about 0.5 mm. The phase composition of the hardfacings was determined, utilizing the X-ray diffraction (XRD) device SmartLab SE, equipped with the D/teX Ultra 250 1D detector (Rigaku, Japan), equipped with the Cu Kα radiation source (2Θ range 25 – 100°, measurement step 0.01°, speed of measurement 5°/min).

Study of Mechanical Properties. Vickers hardness (applying the standard ISO 6507-1:2018) and the Young's modulus (applying the Oliver-Pharr indentation method [21]) were measured, using the parameters, shown in Table 3. The average Vickers hardness of each hardfacing was calculated on the basis of ten measurements and the average Young's modulus – on the basis of six measurements.

Table 3. Parameters of Vickers hardness and Young's modulus measurements

Parameter	Desig-nation	Device	Load [N (kgf)]	Load application speed [N/s]	Indentation depth [μm]	Dwell time [s]
Hardness	HV1 (H)	Indentec 5030 SKV (Zwick, Germany)	9.8 (1)	10	N/a[1]	10
Young's modulus	E	Z2.5 (Zwick, Germany)	100 (10.2)	1	50	10

[1] Not applicable.

Abrasive Wear Studies. The abrasive wear resistance was determined according to the standard ASTM G65 (modified procedure D), applying the block-on-ring (rubber wheel) scheme (the test parameters are specified in Table 4). Prior to testing and instantly after it the preliminarily machined samples were ultrasonically cleaned in acetone for 300 s. Each type of hardfacings was tested three times, and the average volume loss was calculated.

Table 4. Parameters of the abrasive wear test

Sample size [mm]	Load [N]	Linear speed [m/s]	Wheel diameter [mm]	Abrasive type	Abrasive size [mm]	Abrasive feed rate [g/s]	Duration of the test [s]
25×10×5	22.6	1	80	Quartz sand	0.2–0.3	5.0–6.5	600

Results and Discussion

Microstructure Studies. The Cr + C hardfacing exhibited a eutectic structure with the elongated carbide grains, evenly distributed in the iron-based matrix (Fig. 1 a). In contrast, the distribution of the *in-situ* synthesized carbide reinforcement in the Ti + C hardfacing was uneven, as large carbide-free pockets were observed in the microstructure of the hardfacing (Fig. 1 b). Moreover, large gas pores could be seen, as well. The formation of the carbide-free areas was most probably caused by the insufficient carbon content in the molten pool [22]. In its turn, this may have been caused by the burnout of carbon during cladding, what is indirectly confirmed by the presence of pores. The TiO_2 + C hardfacing, *vice-a-versa*, had a pore-free microstructure, comprised of large grains with a tiny amount of secondary phases, precipitated at the grain boundaries (Fig. 1 c). The EDS analysis of the latter showed that these were the Ti- and Mo-based carbides. However, the overall amount of the carbide phases in the TiO_2 + C hardfacing was remarkably lower than that in the Ti + C hardfacing.

In order to finally confirm or to disconfirm a large-scale *in-situ* formation of the carbide phase in the TiO_2 + C hardfacing, the microstructure of the unmachined side of the sample was studied. The microstructure observations and the EDS analysis proved the occurrence of the small-size (mostly < 1 μm) *in-situ* synthesized Ti- and Mo-based carbides in the subsurface zone of the hardfacing (Fig. 1 d). As the average size of the carbide reinforcement in the TiO_2 + C hardfacing was smaller, than in the Ti + C one, the *in-situ* synthesized carbide particles would more easily float upwards in

the melt [7], what caused their segregation in a relatively thin zone in the upper part of the hardfacing. Therefore it may be currently suggested that the principle amount of the *in-situ* synthesized carbide particles in the $TiO_2 + C$ hardfacing was removed during machining.

The absence of porosity $TiO_2 + C$ hardfacing could be explained by the melt viscosity reducing action of TiO_2 [23], what allowed the gas bubbles to escape before the solidification of the melt.
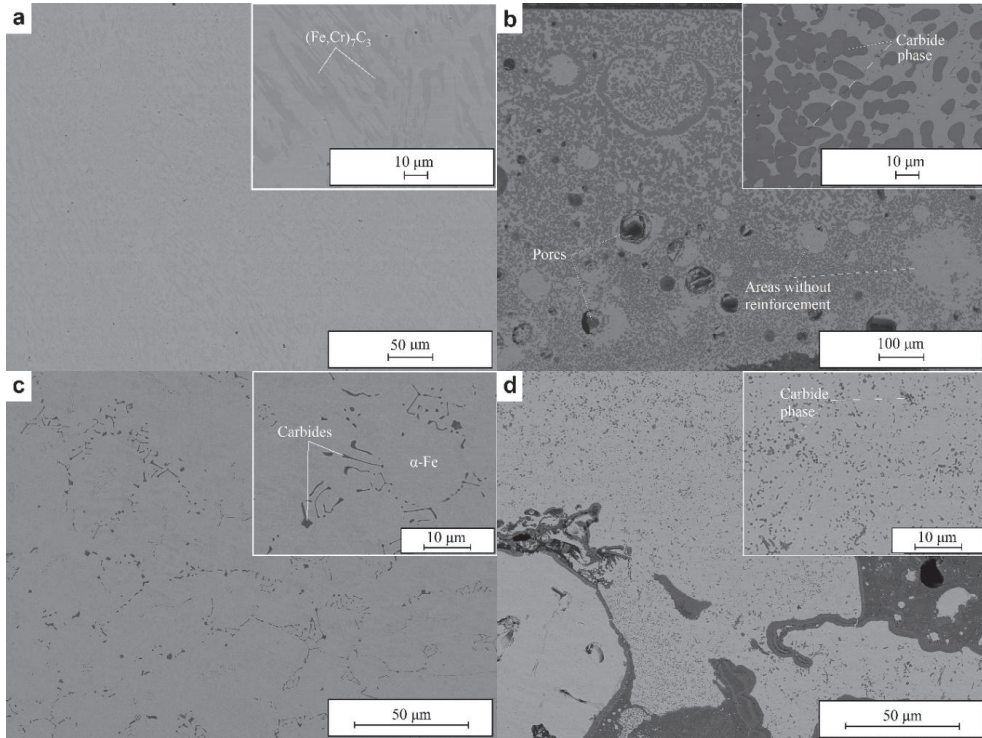
Fig. 1. Microstrucrure of the hardfacings: a – Cr + C; b – Ti + C; c – $TiO_2 + C$ (machined); d – $TiO_2 + C$ (unmachined side)

The *in-situ* synthesis of $(Fe,Cr)_7C_3$ (19.8 wt.%), as well as TiC (9.9 wt.%) and $(Ti,Mo)C$ (9.6 wt.%) was proven by the XRD analysis in the Cr+C and Ti+C hardfacings, respectively (the approximate reinforcement volume contents were 23.5 vol.% and 27.5 vol.%, respectively). The matrix of the Cr + C hardfacing was mostly austenitic, while the matrix of the Ti + C hardfacing was ferritic-austenitic. At the same time, no carbide phases were detected in the $TiO_2 + C$ hardfacing, neither was the presence of Ti. The microstructure of the hardfacing comprised of α-Fe, Ni(Cr,Mo) and Fe(Mo) solid solutions.

The formation of ferrite in the Ti+C hardfacing could be explained by a more complete reaction of the precursor elements (titanium and carbon) to be compared with chromium and carbon in the Cr+C hardfacing. The Gibbs energy of formation of TiC is much lower to be compared with that of $(Fe,Cr)_7C_3$ [24], thus the process of formation of TiC would be more intensive. In its turn, that would lead to the more intensive decarburization of the Fe-rich melt to be compared with the formation of $(Fe,Cr)_7C_3$. A relatively high remaining carbon content in the steel matrix of the Cr+C hardfacing would favour the formation of the retained austenite [25], and, vice-a-versa, the relatively low carbon content in the steel matrix would promote the formation of ferrite, what occurred in the Ti+C hardfacing.

Mechanical properties. The Cr + C hardfacing exhibited the highest average hardness (556 ± 29 HV1), which was 3.5 times higher than that of the reference SS hardfacing (Fig. 2). The relatively large deviation of hardness values of the Ti+C coating may be explained by the presence of reinforcement-free pockets, as discussed before.

The Cr + C and TiO$_2$ + C hardfacings, as well as Ti+C and SS hardfacings had the similar values of the Young's modulus, with one of the TiO$_2$ + C hardfacing (156.3 ± 19.7 GPa) being the largest (1.22 times higher than Young's modulus of the SS hardfacing) (Fig. 3). This indicates that the stiffness of the Cr + C and TiO$_2$ + C hardfacings was higher than that of Ti + C and SS ones.
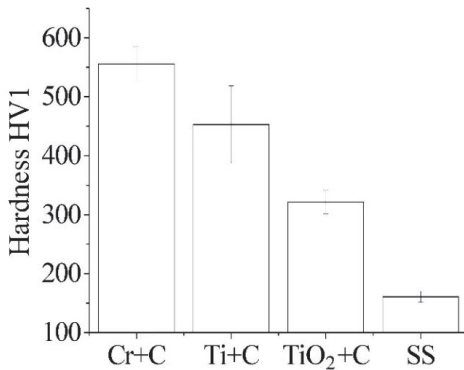
Fig. 2. Hardness of the hardfacings   Fig. 3. Young's modulus of the hardfacings
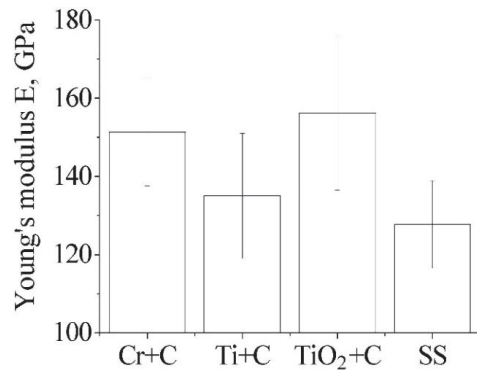
Abrasive Wear. Generally, the wear of the composite hardfacings correlated well with their H/E ratios [26], which are shown in Fig. 4. The Cr + C and Ti + C hardfacings exhibited similar average resistance to abrasive wear, which was respectively 2.3 and 2.1 times higher than that of the reference SS hardfacing. At the same time, the TiO$_2$ + C hardfacing exhibited 1.5 times higher wear, than the reference hardfacing, despite the higher hardness (Fig. 5). The last phenomenon may be explained by the strain hardening of the stainless steel during the wear test, what leads to the lessening of the wear rate during the test [27].
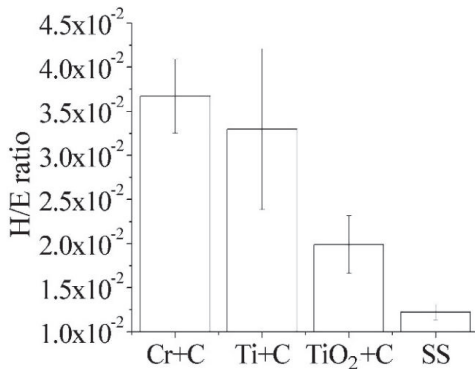
Fig. 4. H/E ratio of the hardfacings   Fig. 5. Abrasive wear of the hardfacings
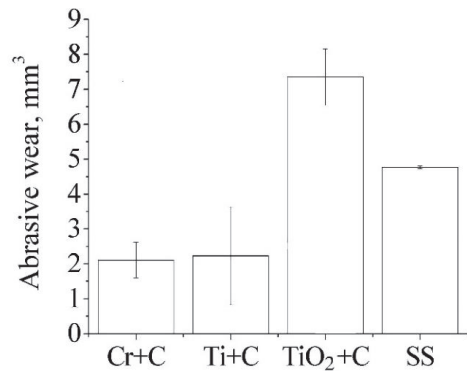
The principle wear mechanism of all the studied hardfacings was a combination of microcutting and microploughing (Fig. 6). However, the grooves, left by the abrasive particles, were much shallower in the case of the Cr + C and Ti + C hardfacings, thus in their case the wear was less intensive, what correlates well with the corresponding wear rates (Fig. 5).

Summary

1. The stainless steel-based hardfacing, reinforced with the *in-situ* synthesized Cr-based carbides exhibited the highest hardness, as well as the highest resistance to abrasive wear among the studied hardfacings (respectively 5.6 times higher and 2.3 times higher than the corresponding parameters of the reference).
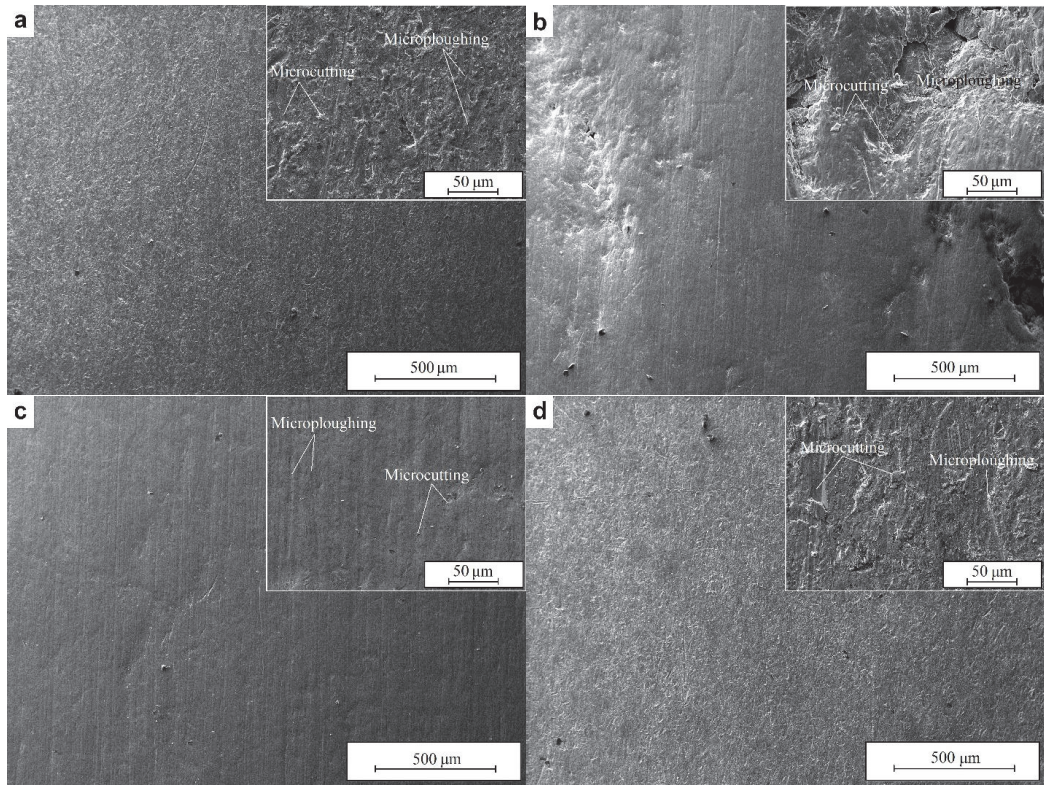
Fig. 6. Worn surfaces of the hardfacings: a – SS; b – Cr + C; c – Ti + C; d – TiO$_2$ + C

2. In the present case the application of the pure Ti as a reinforcement precursor turned out to be more beneficial to be compared with TiO$_2$ due to a more favourable distribution of the *in-situ* synthesized reinforcement.

3. The *in-situ* formation of the carbide reinforcement didn't change the wear mechanism (a combination of microcutting and –ploughing), but made it less severe.

References

[1]   S.C. Tong, Z.Y. Ma, Microstructural and mechanical characteristics of in situ metal matrix composites, Mat. Sci. Eng. R 29 (2000) 49-113.

[2]   T. Mojisola, M.M. Ramakokohvu, J. Raethel, P.A. Olubambi, W.R. Matizamhuka, In-situ synthesis and characterization of Fe-TiC based cermet produced from enhanced carbothermally reduced ilmenite, Int. J. Refract. Met. H. Mater. 78 (2019) 92-99.

[3]   X.H. Wang, Z.D. Zou, S.Y. Qu, L. Song, Microstructure and properties of the TiC/Fe-based alloy hardfacing layers, J. Mater. Sci. 40 (2005) 3629-3633.

[4]   S. Ariely, J. Shen, M. Bamberger, F. Dausiger, H. Hugel. Laser surface alloying of steel with TiC, Surf. Coat. Technol. 45 (1991) 403-408.

[5]   R.J. Li, Ceramic-metal Composite, second ed., Metallurgical Industry Press, Beijing, 2005.

[6]   X. Sun, J. Huang, J. Yang, S. Chen, Microstructure evolution and mechanical properties of in-situ bimodal TiC-Fe coatings prepared by reactive plasma spraying, Ceram. Int. 45 (2019) 5848-5857.

[7]   X.H. Wang, S.Y. Qu, B.S. Du, Z.D. Zou, In situ synthesized TiC particles reinforced Fe based composite coating produced by laser cladding, Mater. Sci. Technol. 25 (2009) 388-392.

[8]   X. Wang, M. Zhang, S. Qu, Development and characterization of (Ti,Mo)C carbides reinforced Fe-based surface composite coating produced by laser cladding, Opt. Lasers Eng. 48 (2010) 893-898.

[9]   A. Khalili, M. Mojtahedi, M. Goodarzi, M.J. Torkamani, Synthesis of Fe-TiC hard coating from ilmenite via laser cladding, Iranian J. Mater. Sci. Eng. 16 (2019) 75-86.

[10] S. Corujeira Gallo, N. Alam, R. O'Donnel, In situ synthesis of TiC-Fe composite overlays from low cost TiO2 precursors using plasma transferred arc deposition, J. Therm. Spray Technol. 23 (2014) 551-556.

[11] L. Niu, Y. Xu, H. Wu, W. Wang, Preparation of in situ (Fe,Cr)7C3/Fe composite coating by centrifugal casting, Surf. Eng. 27 (2011) 587-590.

[12] A. Singh, N.B. Dahotre, Laser in-situ synthesis of mixed carbide coating on steel, J. Mater. Sci. 39 (2004) 4553-4560.

[13] S.L. Song, W.H. Zhang, Z.D. Zou, S.Y. Qu. In situ formation TiC particles reinforced Fe-based alloy composite coating by GTAW, Tran. China Weld. Inst. 27 (2006) 39.

[14] X. Wang, Z. Zou, S. Song, S. Qu. Microstructure and wear properties of in-situ TiC/FeCrBSi composite coating prepared by gas tungsten arc welding, Wear 260 (2006) 705-710.

[15] F. Sadeghi, H. Nafaji, A. Abbasi. The effect of Ta substitution for Nb on the microstructure and wear resistance of an Fe-Cr-C hardfacing alloy, Surf. Coat. Tech. 324 (2017) 85-91.

[16] W. Xibao, W. Xiaofeng, S. Zhongquan. The composite Fe–Ti–B–C coatings by PTA powder surfacing process, Surf. Coat. Tech. 192 (2005) 257-262.

[17] P. Zhang, X. Wang, L. Guo, L. Cai, H. Sun. Characterization of in situ synthesized TiB2 reinforcements in iron-based composite coating, Appl. Surf. Sci. 258 (2011) 1592-1598.

[18] A. Gebert, B. Bouaifi, Surface Protection by Means of Build-Up Welding, in: F.-W. Bach, K. Möhwald, A. Laarmann, T. Wenz, Modern Surface Technology, Wiley VCH Verlag GmbH & Co. KGaa, Weinheim, 2006, pp. 263-296.

[19] L. Łatka, P. Biskup. Development in PTA surface modifications – A Review, Adv. Mater. Sci. 20 (2020) 39-53.

[20] W. Wu, L.Y. Hwu, D.Y. Lin, J.L. Lee, The relationship between alloying elements and retained austenite in martensitic stainless steel welds, Scripta Mater. 42 (2000) 1071-1076.

[21] W.C. Oliver, G.M. Pharr, Measurement of hardness and elastic modulus by instrumented indentation: Advances in understanding and refinements to methodology, J. Mater. Res. 19 (2004) 3-20.

[22] M. Cheng, Q. Zhuang, N. Lin, Y. He, Improvement in microstructure and mechanical properties of Ti(C,N)-Fe cermets with the carbon additions, J. Alloy Compd. 701 (2017) 408-415.

[23] J.L. Liao, J. Li, X.D. Wang, Z.T. Zhang, Influence of TiO2 and basicity on viscosity of Ti bearing slag, Ironmak. Steelmak. 39 (2012) 133-139.

[24] S.R. Shatynski. The thermochemistry of transition metal carbides, Oxid. Met. 13 (1979) 105-118.

[25] G. Krauss, Principles of Heat Treatment of Steel, ASM International, Materials Park, 1980.

[26] A. Leyland, A. Matthews, On the significance of the H/E ratio in wear control: a nanocomposite coating approach to optimized tribological behaviour, Wear. 246 (2000) 1-11.

[27] O.A. Zambrano, E.C. Muños, S.A. Rodríguez, J.J. Coronado, Running-in period for the abrasive wear of austenitic steels, Wear. 452-453 (2020) 203298.

Curriculum vitae

Personal data

Name:	Dmytro Tkachivskyi
Date of birth:	08.11.1988
Place of birth:	Ivano-Frankivsk, Ukraine
Citizenship:	Ukraine

Contact data

E-mail:	dmtkac@ttu.ee

Education

2017–2021	Tallinn University of Technology – PhD
2015–2017	MSC, Tallinn University of Technology, Mechatronics
2005–2011	BSC, IFNTUNG (Ukraine), Automation
2002–2005	High school, Physics and Technical Lyceum (Ukraine)

Language competence

English	Fluent
Russian	Fluent
Italian	Basic Skills
Ukrainian	Native Speaker

Professional employment

2012–2013	IF (Ukraine), Engineering enterprise "Tyco Electronics", Process engineer
2011–2012	IF (Ukraine), Engineering enterprise "Komel", Automation engineer

Elulookirjeldus

Isikuandmed

Nimi:	Dmytro Tkachivskyi
Sünniaeg:	08.11.1988
Sünnikoht:	Ivano-Frankivsk, Ukraina
Kodakondsus:	Ukraina

Kontaktandmed

E-post:	dmtkac@ttu.ee

Hariduskäik

2017–2021	Tallinna Tehnikaülikool – PhD
2015–2017	MSC, Tallinna Tehnikaülikool, Mehhatroonika
2005–2011	BSC, IFNTUNG (Ukraina), Automaatika
2002–2005	Keskharidus, Füüsika ja Tehnika Lütseum (Ukraina)

Keelteoskus

Inglise keel	Kõrgtase
Vene keel	Kõrgtase
Itaalia keel	Põhioskused
Ukraina keel	Emakeel

Teenistuskäik

2012–2013	IF (Ukraina), inseneriettevõte "Tyco Electronics", protsessiinsener
2011–2012	IF (Ukraina), inseneriettevõte "Komel", automaatikainsener